(NASA-CR-165426) TECHNOLOGY DEVELOPMENT FOR PHOSPHORIC ACID FUEL CELL POWERPLANT, PHASE 2 Final Technical Report (Energy Research Corp., Danbury, Conn.) 159 p HC A08/MF A01 CSCL 10A G3/44

N82-16462

Unclas 07576

DOE/NASA/0067-79-7
NASA CR-165426

TECHNOLOGY DEVELOPMENT FOR PHOSPHORIC ACID FUEL CELL POWERPLANT (PHASE II)

FINAL TECHNICAL REPORT

Larry Christner
ENERGY RESEARCH CORPORATION

December 1981

Prepared for
NATIONAL AERONAUTICS AND SPACE ADMINISTRATION
Lewis Research Center
Under Contract DEN3—67

For
U.S. DEPARTMENT OF ENERGY
Energy Technology
Division of Fossil Fuel Utilization

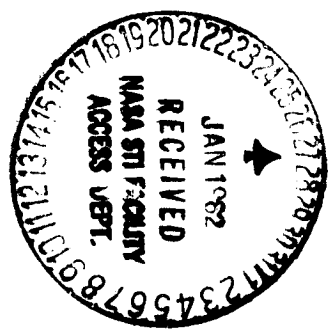

EXECUTIVE SUMMARY

The objective of this program (DEN3-67) was to develop cost effective phosphoric acid fuel cell technology for an on-site integrated energy system in the 100 kW to 1 MW range. This program was a follow on to NASA Contract No. EC-77-C-03-1404 where the initial bipolar plate scale-up to 12 in. x 17 in. was accomplished. Emphasis of DEN3-67 was placed on the development of corrosion resistant and more conductive materials and longer term testing of full-scale components. Significant progress was made under this program with improvements in:

- Cell performance up to 50 mV at 100 mA/cm^2 due to elimination of catalyst poisons from the cell materials,
- Decreased cell resistance that resulted in approximately 60 mV improvement at 100 mA/cm^2,
- Bipolar corrosion rate decreased tenfold compared with previous standard graphite/resin plates.

These improvements were primarily the result of heat-treating the bipolar plates to 900°C. This treatment converts the plate material from a resin/graphite composite to a glassy carbon/graphite composite.

Other achievements included:

- Long-term stack tests (3-cell, 350 cm^2 type, up to 10,000 hours and 5-cell, 1200 cm^2 type, 5,000 hours).
- Low platinum loaded electrode stack test (3-cell, 350 cm^2 type, 0.12 mg Pt/cm^2 anode and 0.25 mg Pt/cm^2 cathode) for 4,500 hours, with stability similar to the electrodes with standard loading (twice the amount).
- A selectively wet-proofed anode was developed and successfully tested for 4,000 hours.
- The ERC proprietary high bubble pressure matrix, MAT-1, was tested for 10,000 hours.
- Three 23-cell stacks (~2 kW capacity) using the best state-of-the-art full size components were tested to demonstrate the initial viability of these components for large stacks.

CONTRIBUTORS

Those who have contributed to the success of this program are acknowledged below:

J. Ahmad
B. Baker
L. Christner
M. Farooque
D. Kelley
M. Lambrech
C. Lee
H. Maru
D. Patel
S. Perkari
M. Puskar

TABLE OF CONTENTS

TABLE OF CONTENTS (continued)

TABLE OF CONTENTS (concluded)

LIST OF FIGURES

LIST OF FIGURES (continued)

LIST OF FIGURES (continued)

LIST OF FIGURES (concluded)

LIST OF TABLES

LIST OF TABLES (concluded)

TASK 1. COMPONENT DEVELOPMENT

The objective of this task was to design and fabricate components capable of long-term operation. Ease of manufacturing by cost effective techniques was used as the basic criteria for evaluating the fabrication methods pursued. The components that were studied are listed below:

- electrolyte matrix
- bipolar plate
- electrode backing paper
- cell edge and manifold seals
- acid inventory control member.

1.1 Matrix Development and Fabrication

Development of the SiC matrix as a replacement for the phenolic fiber matrix was initiated under the previous contract No. EC-77-C-03-1404*. A simple bar casting technique was identified as a viable method of manufacture. A few matrices were prepared using this technique but the process required further refinements and characterization. Improvements were sought in wickability, scale-up of the batch size, handleability, and sintering requirements. Additional characterization of the prepared matrices for potential degradation and available porosity was necessary to determine the acceptability of this type of material.

Characterization

Exposure of a matrix to 100% phosphoric acid at 205°C for up to six months showed no observable degradation. Post-test scanning electron micrographs (SEMs) showed no sign of

*Energy Research Corp., "Development of Phosphoric Acid Fuel Cell Technology", Final Report for Contract EC-77-C-03-1404, Sept. 1978.

corrosion or degradation of the SiC. Perhaps just as important an indicator is the fact that the acid remained clear during the entire six months. Previous experience with phosphoric acid has shown that even minute quantities of contaminants can cause the acid to discolor; so the lack of discoloration tends to indicate that there are no degradation products present.

The use of 1 μm particle size SiC from Carborundum was evaluated with the expectation that reducing the particle size from the standard 7 μm mean particle diameter would result in matrices of higher bubble pressure. The smaller particle size SiC, however, produced cracked, crumbly and totally unacceptable matrices. Since the smaller particle size has many more particles in a given volume of matrix, it also takes proportionately more binder to hold them together. It was necessary to add so much Dupont Polytetrafluoroethylene (TFE-30) to eliminate cracking, that the matrix lost its wicking ability. It had been expected that improvements in matrix formulation, casting and sintering techniques over the last two years would permit production of good quality matrices with 1 μm SiC at acceptable PTFE levels. Such was not the case. Matrices made with the standard 4% PTFE cracked and crumbled to such an extent that further work with 1 μm SiC was not considered worthwhile.

Silicon carbide matrices are not as porous as the phenolic fiber matrices used previously, averaging 51% and 70%, respectively. Mercury porosimetry tests of the SiC matrix indicated that 64% of the pores were between 1 μm and 4 μm, and 94% were less than 4 μm. The mean pore size was 1.8 μm. In phenolic fiber matrices, 40% of the pores were between 1 μm and 4 μm, and 90% were less than 4 μm. The mean pore size was 1.0 μm.

To learn more about what happens to a matrix at the microscopic level during sintering, samples of both sintered and

unsintered matrices were examined with a scanning electron microscope (SEM). Figure 1.1a shows an unsintered SiC matrix. The large, irregular particles are SiC and the smaller, spheroidal particles are PTFE. The PTFE can be seen clinging to the sides of the SiC and partially filling the gaps between particles. Since there is only 4 wt% PTFE in this particular sample, a cluster this large suggested a poor distribution. However, more detailed examination showed evenly distributed PTFE. Figures 1.1b, 1.1c and 1.1d show a similar matrix sintered at 350°C for 15 minutes. Figure 1.1b shows how the PTFE particles have flowed together to form elongated "puddles". In Figure 1.1c, taken elsewhere in the same sample, PTFE can be seen clinging to the sides of the SiC and bridging the gap between particles. Figure 1.1d is an enlargement of the center portion of Figure 1.1c. In the last three figures, it appears that, although the sintered PTFE did flow at the sintering temperature, the flow did n pro-duce large, nonwettable films of PTFE on the SiC particles.

Fabrication

Improving the cost effectiveness of the procedures for manufacturing matrices was achieved by eliminating a cleaning procedure for the 7 μm SiC powder and by developing a ball mill mixing technique for making large batches of SiC slurry.

Uncleaned, as-received Carborundum green 1000 grit SiC appears to be not only acceptable, but beneficial in matrices. SiC had routinely been cleaned to remove a very small, non-green fraction of the material. However, the cleaning step was time consuming and whatever small amount of impurities may be present in the non-green fraction, the difference in chemical makeup between clean and unclean SiC was not detectable by emission spectrophotometry. In addition to eliminating a step, the use of unclean SiC produced matrices that were mechanically strong,

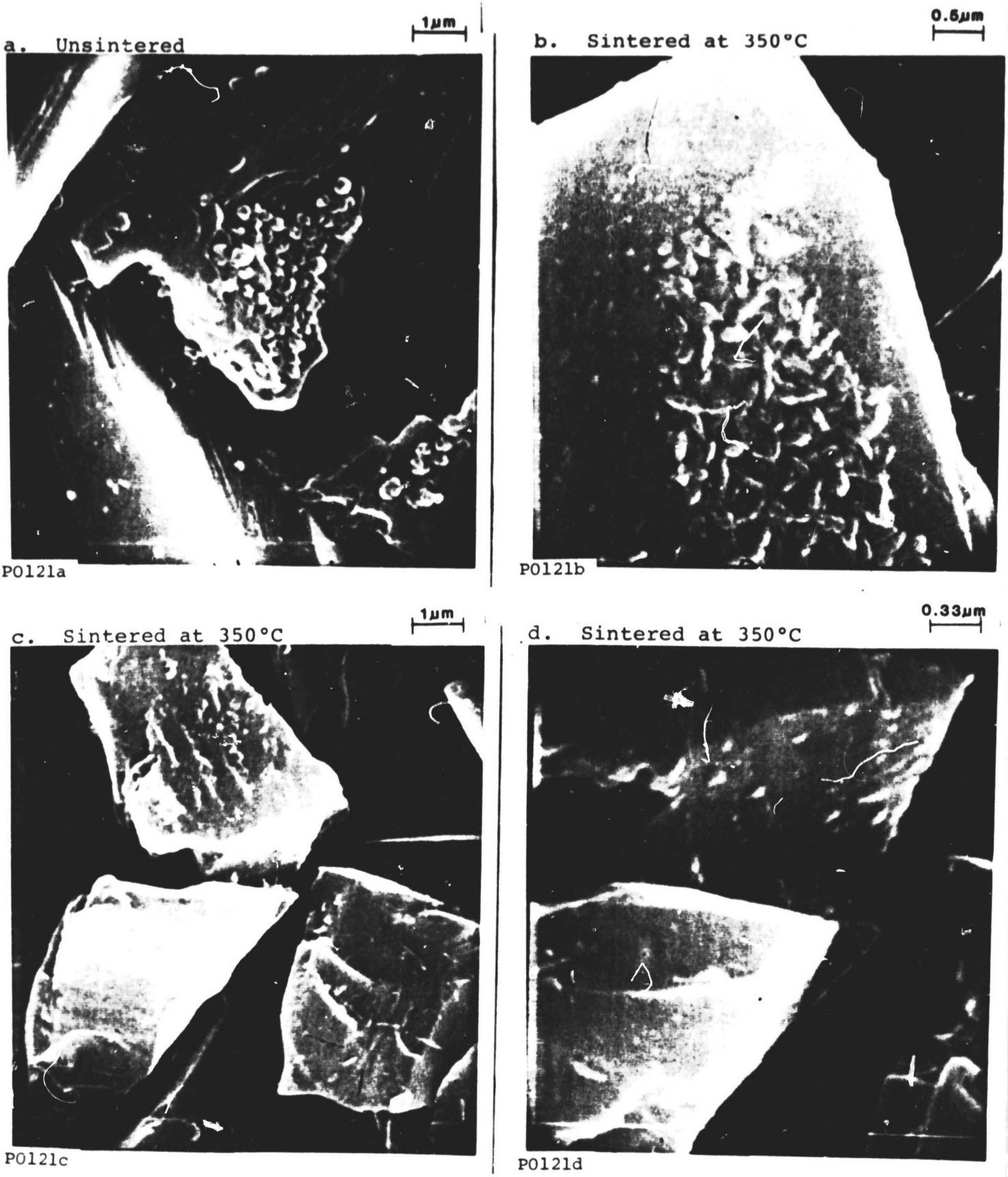

FIGURE 1.1 SEMS OF SiC MATRICES

had high bubble pressures, and were more porous and faster wicking than matrices made with "clean" SiC. The matrices are strong enough to be cut to shape with a steel rule die, a time-saving step introduced previously. Bubble pressures of these matrices were as high as 210 kPa. The average porosity was 62% compared with 51% for standard SiC matrices.

A matrix made with as-received SiC wicked faster than one made with "clean" SiC (Figure 1.2). The matrix performed very well in a number of 25 cm^2 test cells. A cell built specifically to test the matrix reached a peak performance of 678 mV at 200 mA/cm^2 IR-free and was still performing well at 1800 hours when terminated On the basis of all the tests conducted, unclean SiC was adopted as the standard material for SiC matrices.

Efforts to improve the quality, strength and handleability of the SiC matrix were successful. One technique is that of sintering the matrix and electrode at the same time. A matrix was cast onto an unsintered electrode and preheated at 225°C for 40 minutes, then sintered at 350°C for 25 minutes. The result is a strong matrix that is tightly bonded to the electrode. The question of whether matrix or electrode performance would be adversely affected by such a sintering technique was also investigated. A cell ran well for over 2000 hours. The combined sintering technique would, therefore, appear to be a viable technique for enhancing the physical strength of the matrix as well as for reducing the handling and oven time required for electrode and matrix operations.

Another technique for strengthening the matrix is to increase the amount of plastic in the inking vehicle used by the bar casting technique. In order to increase the amount of plastic in the matrix without producing a slurry too viscous to mix or cast, a lower molecular weight of the

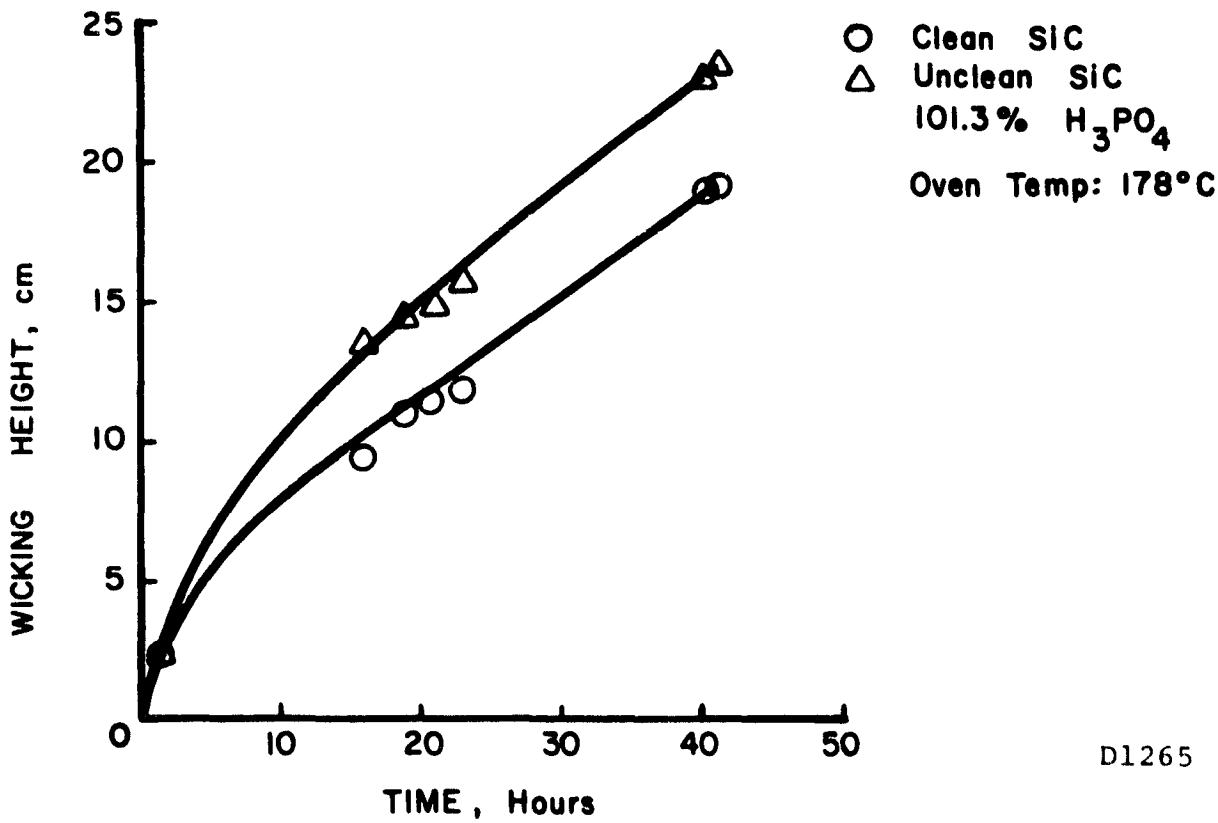

FIGURE 1.2. WICKING OF CLEAN AND UNCLEAN SiC MATRICES

same material presently in use was tried. The concentration of this plastic in the inking vehicle was 2.5% compared with 0.5% for the higher molecular weight grade. The result was a matrix strong enough to be cut to shape with a steel rule die without crumbling or flaking off. The matrix is safe and easy to handle up to the sintering process, during which time most, if not all, of the plastic burns off. After sintering, the matrix appears to be at least as strong as a matrix made with the standard inking vehicle, the porosity is greater (64 to 68%) and the bubble pressure is good (125 to 140 kPa).

Tests were also performed to determine the effects of sintering time, temperature and PTFE content in a silicon carbide matrix on the wicking characteristics, bubble pressure and integrity of the matrix. These experiments indicated that the wicking characteristics are more dependent on the sintering temperature than on the time of sintering or the percent of PTFE in the matrix. In general, the higher the sintering temperature, the less wickable the matrix becomes. It was found that the quality (uniformity, freedom from cracks and pinholes, etc.) of the matrix produced more significant changes in the bubble pressure than sintering conditions or PTFE content. To illustrate these interdependences, a matrix containing 2% TFE was cut in two pieces, with one half being sintered for 25 minutes at 275°C and the other half for 15 minutes at 350°C. The matrix sintered at the lower temperature wicked at a much faster rate than the matrix sintered at 350°C. Bubble pressures for these samples were identical at 22 psi although additional test data shown in Table 1.1 indicated slightly different bubble pressures for these sintering conditions. Variability in the quality of the matrix explains these bubble pressure measurements.

The sintering conditions must be selected by considering

TABLE 1.1

BUBBLE PRESSURE DATA FOR THE MATRICES AT DIFFERENT SINTERING CONDITIONS

MATRIX	BUBBLE PRESSURE
Sintered 25 min. at 275°C (4% TFE)	152 kPa (22 psi)
Sintered 10 min. at 330°C (4% TFE)	131 kPa (19 psi)
Sintered 25 min. at 330°C (4% TFE)	172 kPa (25 psi)
Sintered 25 min. at 275°C (2% TFE)	152 kPa (22 psi)
Sintered 15 min. at 350°C (2% TFE)	152 kPa (22 psi)

trade-offs between wicking ability (which is greater at lower sintering temperatures) and the need for strength and high bubble pressure. Originally the matrices were sintered to maximize their wicking ability, but over a period of time it became apparent from testing several stacks that the wicking was still adequate at higher sintering temperatures.

1.2 Bipolar Plate Technology

Cost effectiveness is an important criteria for all fuel cell components. The materials and processes used to manufacture bipolar plates were investigated with this in mind. Initially the program was concerned with graphite filled phenolic resin composites, but later in the program a heat-treatment process was introduced. Several parameters which affect cost, molding and processing were evaluated in addition to the heat-treatment.

New resins and mixes that improved the cost effectiveness of the bipolar plate were successfully molded and heat-treated. Molding trials with Varcum 24-655 resin (Reichhold Chemicals, Inc.) were successful and production rates were comparable to those of the previous bipolar plates made with Colloid 8440 resin from Colloid Chemical, Inc. The Varcum 24-655 resin is a one-stage phenolic resin and has a recommended shelf life of 60 days at 16°C, while Colloid 8440 is a two-stage resin. Compounds formulated with two-stage resins have a greater molding latitude, better dimensional stability, and better long-term storage capabilities than those formulated with single-stage resins. Varcum 24-655 resin compounds were, however, superior to Colloid 8440 resin compounds in corrosion resistance. Corrosion studies with H_3PO_4 showed that another resin (two-stage Varcum 29-703) had comparable, if not better, corrosion resistance to that of Varcum 24-655. Molding with Varcum 29-703 resin compounds indicated no special

problems in fabricating bipolar plates. Resin prices for less than truckload quantities were significantly less than for Colloid 8440:

Varcum 24-655: $1.50/kg

Varcum 29-703: $1.52/kg

Colloid 8440: $1.74/kg

The previous standard bipolar plates were 33 wt% Colloid 8440/67 wt% graphite. The graphite was composed of 27 wt% 850 and 73 wt% A-99 from Asbury Graphite Mills, Inc. Molding trials and physical property measurements showed no advantage in the usage of 850 graphite. This 850 graphite was therefore not used in the fabrication of plates with Varcum 29-703 resin. The graphite prices were:

Asbury Micro 850: $4.85/kg

Asbury A-99: $0.86/kg

The 1200 and 350 cm^2 bipolar plates were successfully molded with Varcum 29-703 resin and A-99 graphite. The molding characteristics of the compound were satisfactory compared with previous production materials and other experimental compounds. No significant difference was observed between Varcum 24-655 and Varcum 29-703 resins during preforming or molding. The preforming process is a low pressure compaction of powder into a flat cake which is subsequently pressed at high pressure. Preforms of both Varcum resins, however, were noticeably different from Colloid resin preforms: Varcum resin preforms were denser but not as strong as the Colloid resin preforms. Additions of Asbury 850 graphite (a flake graphite used with the Colloid molding compound) to Varcum molding compounds did not improve the strength. Varcum molding compounds were found acceptable for bipolar plate production, but require more careful preforming and handling procedures compared with Colloid 8440 molding compound.

Molding

Graphite/resin materials are preformed prior to the 400 ton, five minute compression molding at approximately 150°C. The procedure used in preforming was:

1. weighing the graphite/resin powder,
2. loading the material into the preform mold,
3. leveling the powder,
4. preform (pressing) at room temperature.

The distribution of the graphite/resin powder in the preform is a critical factor in achieving uniform dimensions. Figure 1.3 shows a typical weight distribution of material used for two types of 31 cm x 43 cm plates. These loadings were found by trial and error and are the result of several factors (e.g., bipolar plate design, flowability of the material, mold characteristics, etc.).

As an alternative to the full size rectangular preform, molding trials were also conducted using three 12.7 cm diameter disks as preforms to mold 350 cm^2 bipolar plates. Uniform thickness was not achieved. A change in mold design (e.g., breathing flats which would direct flow and allow gases to escape) might improve the molding of the disk preforms. Because of the cost of changing the current mold base or dies and the uncertainty that a significant improvement would result, no further work was performed with disk preforms.

Heat Treatment

After the plates are preformed and molded, they must be heated to cure them further. Post-curing of bipolar plates to promote cross-linking of the resin was investigated. Bipolar plates were heat-treated in air at various rates to 210°C. During the post-cure, gases are evolved and blistering

35	33	28	33	34
32	35	35	35	33
28	33	34	33	28
33	30	27	30	33

DIGAS PLATE

NOTE: WEIGHT VARIABILITY ± 2

32	32	30	31	31
30	33	33	33	30
29	33	33	33	28
30	30	30	28	29

C-C PLATE

NOTE: WEIGHT VARIABILITY ± 1

(NUMBERS IN GRAMS OF MIXTURE)

FIGURE 1.3 GRAPHITE-RESIN DISTRIBUTION IN THE PREFORM MOLD

of the plates occurs if the temperature increases too rapidly.

Experiments were conducted on 13 cm x 13 cm x 0.4 cm sections of bipolar plates. The plates were inspected before and after post-cure for observable blisters. Table 1.2 demonstrates the effect of three different post-cure cycles on the bipolar plates.

Low resin bipolar plates (13 cm x 38 cm) were fabricated with 75% A-99 Graphite/25% Colloid 8440. To achieve desirable dimensional tolerances, the weight of the plates was increased by 12.5%. Satisfactory plates were produced by this process.

Although some graphite/resin plates have lasted over 20,000 hours, there are several characteristics which are undesirable: a) high electrical resistance, b) acid absorption, c) corrosion, d) poisoning of electrodes. In order to eliminate these detrimental characteristics, the materials were heat-treated to 900°C.

Samples of graphite/resin composites were heated according to the schedule in Table 1.2 up to 900°C in a nitrogen atmosphere over a six day period. A programmable temperature controller varied the heating rate for this period. During this heat-treatment, sections of 13 cm x 38 cm x 0.40 cm bipolar plates did not blister, but thicker 10 cm x 10 cm x 0.55 cm plates blistered severely. The heating cycle and the length of the heating cycle will depend on the thickness of the parts. Bipolar plates will also warp during carbonization unless restrained. Weights (exerting pressure, 4.5 Pa) placed on plates reduced the amount of warping. Shims were used to distribute the load over the plates uniformly.

Table 1.3 and Figures 1.4 and 1.5 show the percentage change in linear dimensions as a function of the resin content. According to the figures, no significant differences between Colloid and Varcum exist. The confidence band was

TABLE 1.2 BIPOLAR PLATE POST-CURE AND HEAT-TREATMENT CYCLES

POST-CURE

HOURS 20°C TO 210°C	NUMBER OF BLISTERS	AVERAGE DIAMETER OF BLISTERS cm	RATE, °C/hr. TEMPERATURE RANGE, °C						
			20-160	160-170	170-180	180-190	190-200	200-210	210-220
11.7	0	-	60	5	5	5	5	5	5
4.8	3	0.2	60	20	20	20	20	20	20
1.8	12	0.2*	120	120	120	60	60	60	-

NOTE: Plate Composition - 67% Graphite/33% Colloid 8440

Plate Size - 13 cm x 13 cm x 0.4 cm

*Blisters with surface cracking.

HEAT-TREATMENT

Temperature Range, °C	20-130	130-202	202-260	260-350	350-490	490-602	602-721	721-802	802-930	930-947
Cycle, °C/hr.	23	6	23	6	4	3	6	13	95	17

TABLE 1.3

HEAT-TREATED BIPOLAR PLATE SHRINKAGE

RESIN		PLATE ANALYSIS		
TYPE	V/O*	SIZE, cm	NO. OF SAMPLES	SHRINKAGE, %
Colloid 8440	46	30 x 43	60	4.0 ± 0.4
Varcum 24-655	45	30 x 43	1	3.9
	45	13 x 13	1	4.0
	37	30 x 43	1	2.7
Varcum 29-703	45	30 x 43	1	3.8
	45	13 x 13	1	4.2

*Graphite density = 2.2 g/cm^3; Resin density = 1.3 g/cm^3.

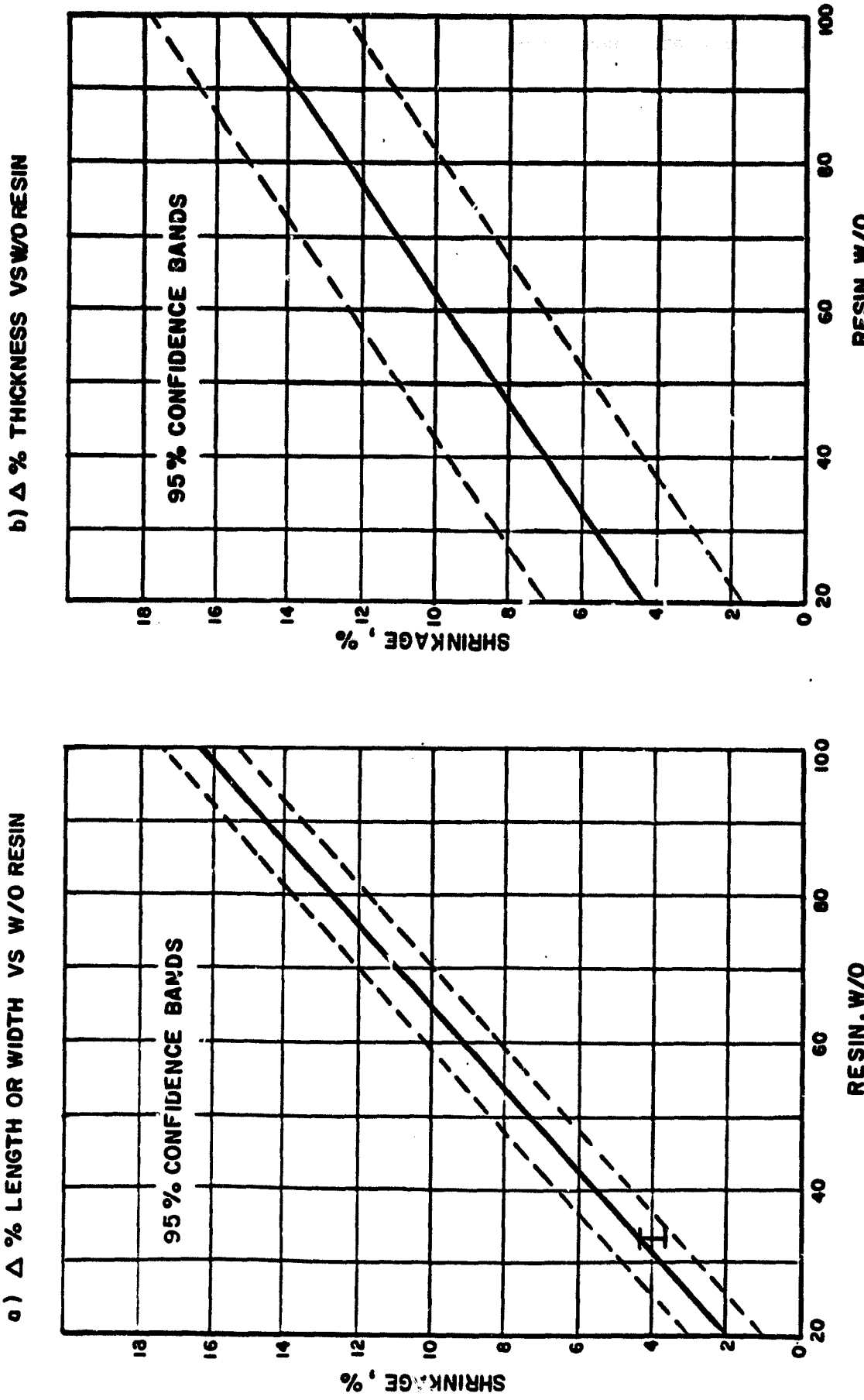

FIGURE 1.4 SHRINKAGE IN GRAPHITE/COLLOID 8440 RESIN FLAT SPECIMENS AFTER HEAT-TREATMENT

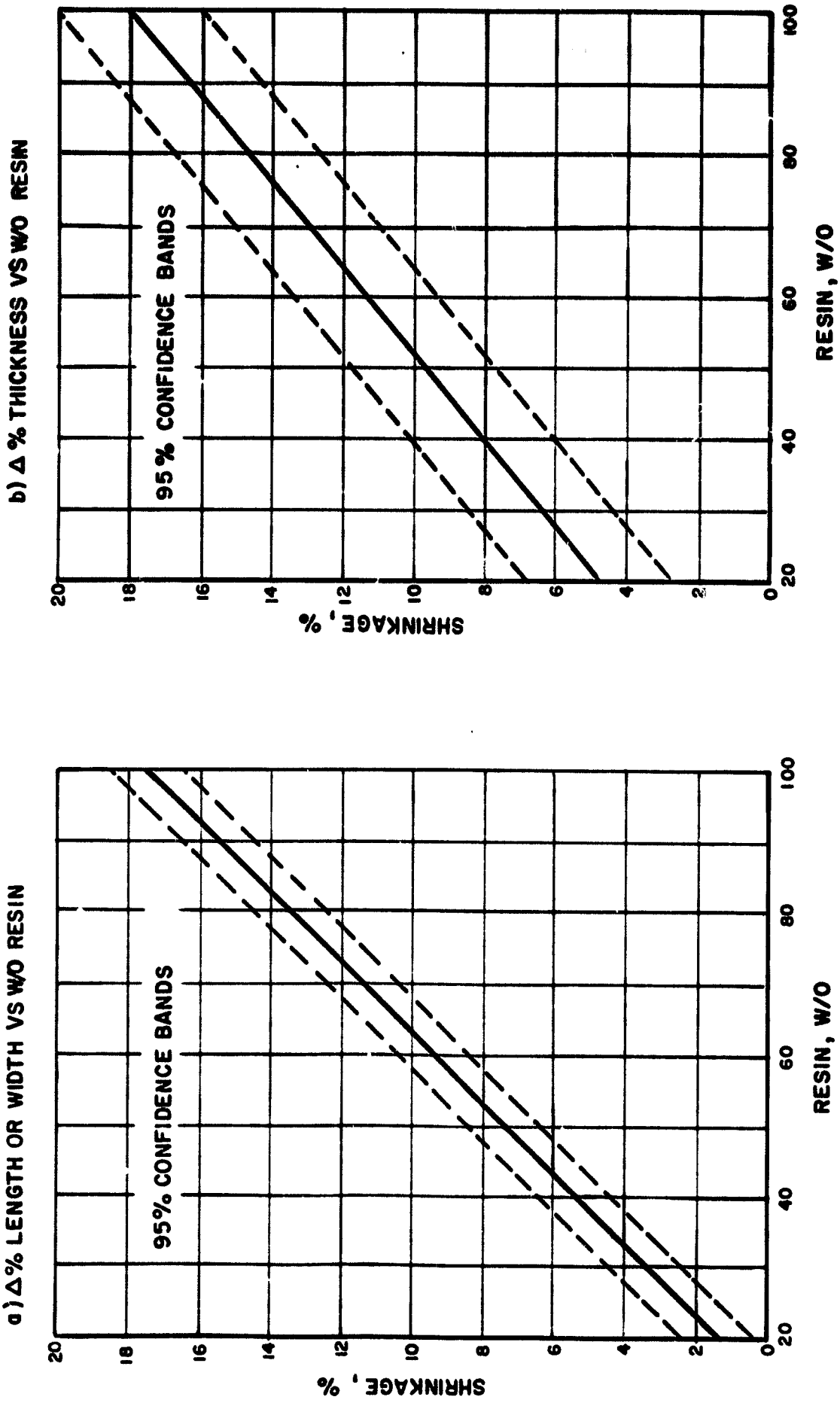

FIGURE 1.5 SHRINKAGE IN GRAPHITE/VARCUM 24-655 RESIN FLAT SPECIMENS AFTER HEAT-TREATMENT

D0698

further narrowed (as shown by I in Figure 1.4) after additional process control. This information will be of value in designing fuel cells with heat-treated parts.

A retort was designed, built and used to heat-treat sixteen 1200 and 350 cm^2 bipolar plates (Varcum 29-703 and Varcum 24-655 resins). The plate compositions varied between 32 and 25 wt% resin. Shrinkage was uniform during the heat-treatment: 2.5% $\pm$ 0.5% for 25 wt% resin and 4.0% $\pm$ 0.5% for 32 wt% resin.

Permeability to hydrogen is an important parameter since the plate is used to separate the hydrogen and oxygen. Although more testing is required to quantify the hydrogen permeability, initial testing indicated reductions in hydrogen permeability after heat-treatment of the 32 wt% resin plate.

Two fuel cell stacks were built with the heat-treated 32 wt% Varcum 24-655/68 wt% A-99 bipolar plates: a three cell, 350 cm^2 stack and a five cell, 1200 cm^2 stack (refer to Task 4 for performance information). Both of these stacks operated very well.

1.3 Backing Paper Technology

This subtask mainly focused on the questions of wettability before and after compression by bipolar plates. Flooding was sometimes observed in backing paper areas compressed by the bipolar plate ribs. In some disassembled stacks, it is evident that the rib pattern of the plates is impressed in the backings, and streaks of acid sometimes fill these impressions. Of particular concern was the possibility that the compressed areas were not only prone to wetting, but that they might actually wick acid, transporting it from a wet area to an area which might otherwise remain dry. In the case of the cathode, the impressed rib pattern runs in straight

lines across the backing from the area directly opposite the acid channel in the bipolar plate.

A test was conducted with pieces of wet-proofed backing to determine whether the compressed areas of the backing wick acid. These pieces were deliberately compressed between bipolar plates at 690 kPa (100 psi), more compression than occurs in an actual stack. Strips of the backing were suspended with one end submerged in a beaker of 102% phosphoric acid. The impressed lines in the backing were oriented vertically to the plane of the acid. The whole apparatus was enclosed within a bell jar and placed in an oven at 177°C (350°F). Periodically during the course of a 100 hour test, the samples were removed from the oven, visually inspected, lightly blotted to remove excess surface acid, and weighed. Three samples of an uncompressed backing were similarly tested. Although the samples were submerged equally in the two tests, all of the compressed samples picked up more acid than the uncompressed samples. To eliminate the possibility of acid wicking (inside the sample) a razor cut was made in each sample 1/4 inch (0.64 cm) above the highest point of submersion. A piece of pH paper was then placed into the slot and pulled back and forth several times. There was no change in the color of the pH paper with any of the samples, indicating that the acid had not wicked above the submersion line either up the surface or interior of the material. All of the acid pick-up occurred in the submerged portion.

In an effort to determine how much of a problem this flooding might be, two finished electrodes (a 0.3 mg Pt/cm^2 anode and a 0.5 mg Pt/cm^2 cathode) were deliberately compressed between two bipolar plates. The electrodes were cut in half and then arranged between the bipolar plates as they would be in a cell. The units were then placed in a small press and one set of half electrodes was compressed at 483 kPa (70 psi)

while the other set was compressed at 690 kPa (100 psi). Normal compression in a stack is 60 psi. Small samples cut from the electrode halves were then float filled. Figure 1.6 shows the acid pick-up of the compressed samples compared with the average of uncompressed Samples A and B. Samples A and B had a Pt loading similar to that of the cathode used for the compressed samples. The data indicate that the cathodes absorbed more acid than the anodes, which is to be expected because the higher loaded cathode has a thicker catalyst layer. The cathodes, compressed at 483 kPa and 690 kPa, picked up 40% and 60% more acid, respectively, than did the uncompressed sample in the same period. It was apparent from these tests that highly compressed backings became wet and probably would limit gas diffusion to the electrodes. Fuel cell tests were used to confirm this observation. A 25 cm^2 cell was built with electrodes compressed at 690 kPa. Cell performance was mediocre and began to deteriorate fairly soon. After two weeks, the cell was disassembled. The cathode backing showed moderate flooding in the compressed rib area but the anode backing gave no signs of being flooded. It is likely that the highly compressed backing paper got wet, reduced the porosity that lets gas into the electrode. There is a trade-off between compression crushing the paper and compression reducing the contact resistance between the paper and the bipolar plate. Shimming of each cell allows this compromise to be made.

1.4 Sealing Techniques

The seals in the fuel cell serve three basic purposes: they a) prevent mixing of reactants at plate edges, b) prevent acid overflow from the addition channel into the reactant gas channel, and c) protect the current collector from acid.

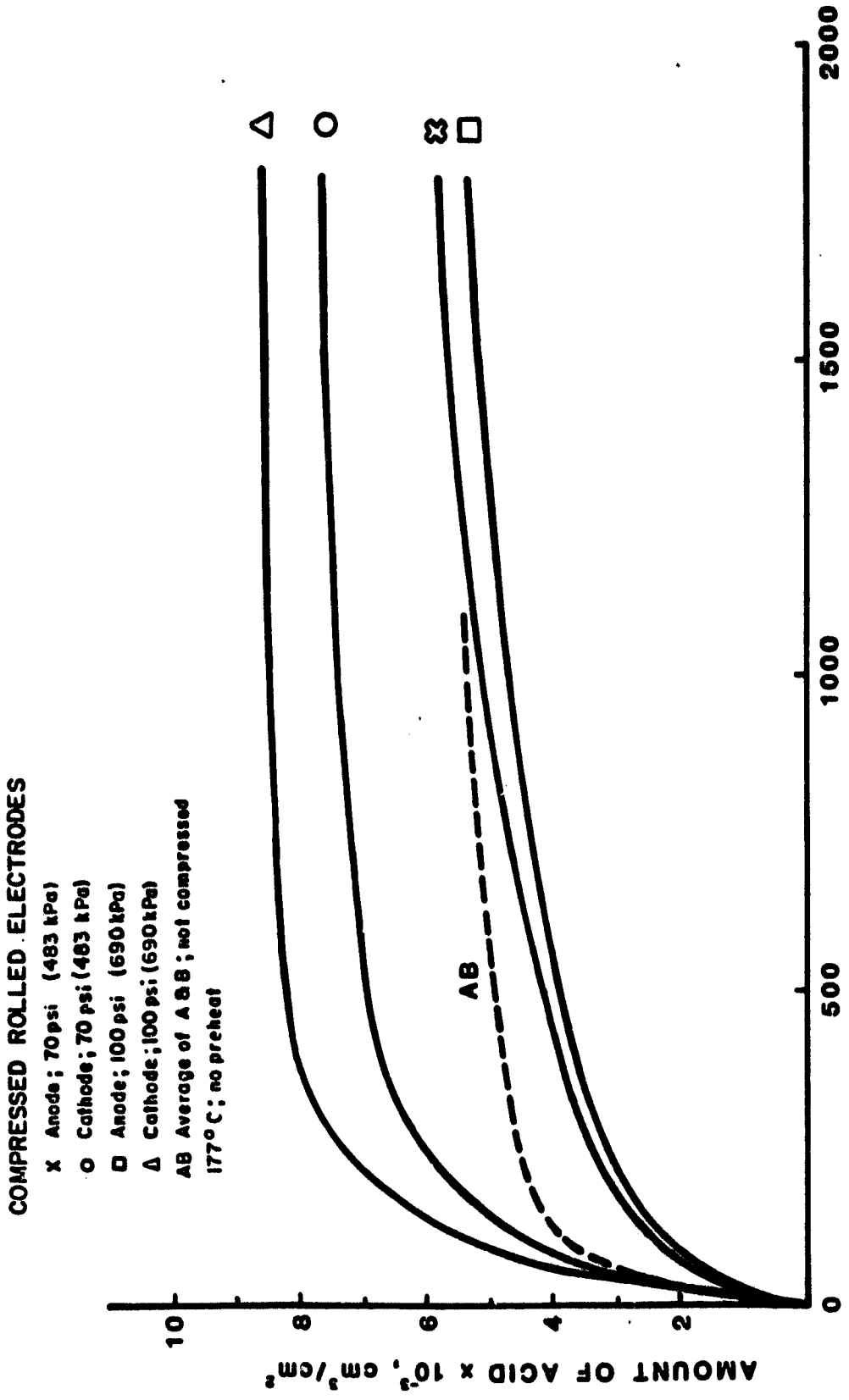

FIGURE 1.6 COMPARISON OF ACID PICK-UP IN COMPRESSED ROLLED ELECTRODES WITH ELAPSING TIME

D1611

The first two seals were initially provided by Kynol fiber mats which were wet with acid. These were replaced with Teflon sheets glued down with Viton. The non-degradable Teflon seals performed as well as the wet seals and should provide a long life.

Providing a protective seal around the copper current collector with strips of Viton was only partially effective when the current collector had tabs extending out beyond the edge. Extension beyond the edge made the collector ride up and over the Viton seal. This created the poor seal as shown in Figure 1.7. When the current collector was changed to a central post, the collector was cut to fit inside the seal. In addition, two new strips were added to surround the copper sheet completely. This has eliminated corrosion due to acid creeping in from the edges.

1.5 Definition and Control of Electrolyte Volume Changes

Acid volume is expected to change during operation of the fuel cell at various current densities and temperatures, and during assembly startup, shutdown and load changes. An assessment of the magnitude of the problem and development of a component to accommodate the changes were completed during this program. The problem was divided into the following areas:

a. Measurement of the acid volume in the components at a known condition;

b. Measurement of the rate at which acid penetrates the electrode;

c. Estimation of the expected volume changes at various conditions;

d. Devising a start-up procedure to minimize the volume changes;

e. Fabrication of an Acid Inventory Control Member to handle these volume changes.

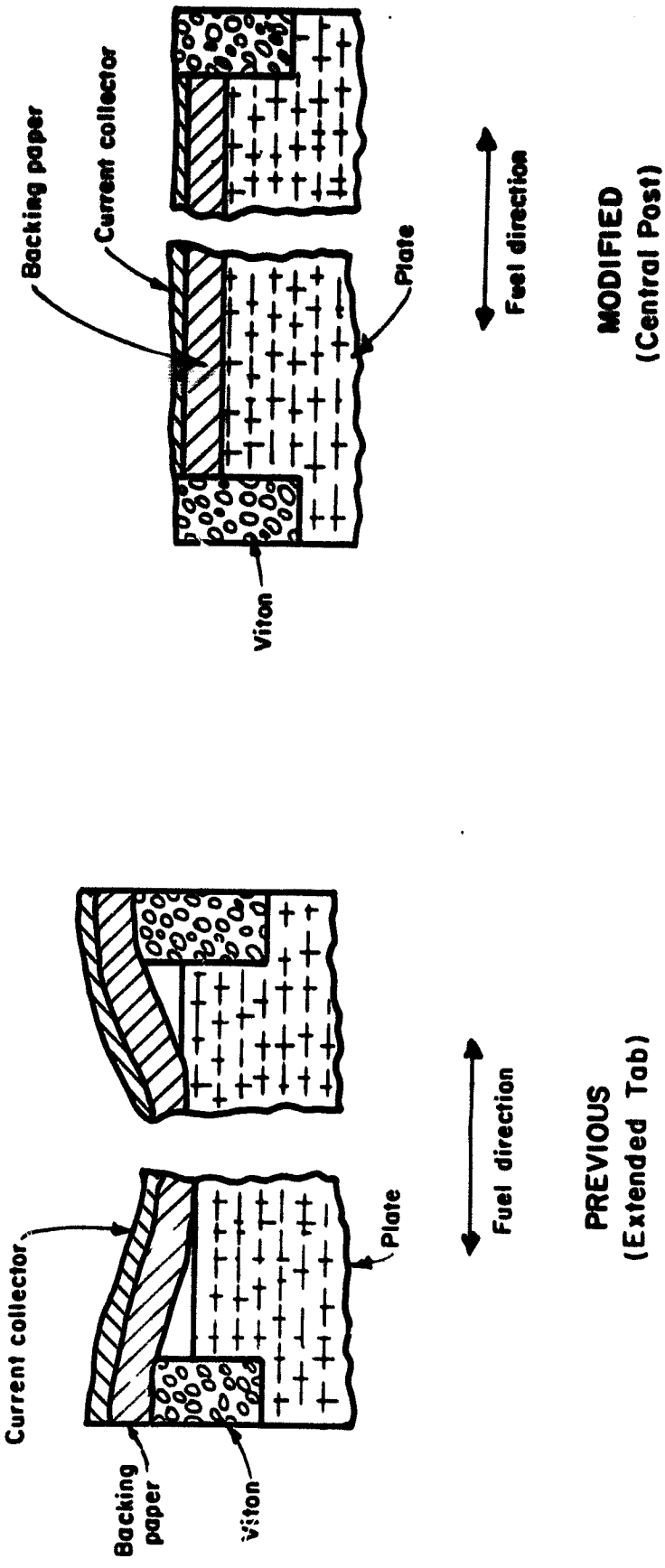

D0593a

FIGURE 1.7 CURRENT COLLECTOR DESIGN - PREVIOUS AND MODIFIED

Measurement of Acid Pick-Up

Tests were conducted to determine the maximum amount of acid that can be absorbed by various cell components as well as the amounts they are likely to pick up under cell assembly and test conditions. Table 1.4 lists a number of electrode components and the amount of acid they absorbed after 20 hours of being float-filled at 177°C. The float filling technique is performed by simply floating the component on the surface of acid contained in a dish.

Another technique for determining the acid absorption capacity of electrodes is to wick them from a matrix, as is done during cell assembly. In this method, a phenolic fiber matrix was soaked in hot acid and then placed between two electrodes. The assembly was compressed and placed in an oven at 177°C. The amount and rate of acid absorption was determined by periodically weighing the electrodes.

The different kinds of acid pick-up tests conducted included float filling, vacuum (float) filling, and wicking from a matrix. Some samples were checked periodically in order to establish rates of acid pick-up and other samples were weighed only at the end of the tests to measure the final pick-up. All of the data were corrected to allow for any concentration changes in the acid occurring during the test.

In a series of float filled electrodes, small samples (5.1 cm x 5.1 cm) were cut from a 13 cm x 38 cm rolled electrode. They were tested in duplicate under the conditions listed in Figure 1.8. Since the acid absorption results from two duplicate samples did not deviate from the average by more than 0.25×10^{-3} cm^3 of acid/cm^2 of sample, only the averages are shown.

TABLE 1.4

ACID PICK-UP OF ELECTRODES AND BACKINGS

SAMPLE			THICKNESS, cm	ACID PICK-UP, cm^3 of ACID/cm^2 of SAMPLE
1.	Electrode on Stackpole	0.7 mg Pt/cm^2	0.053	5.48×10^{-3}
1A.	Electrode	0.7 mg Pt/cm^2	0.023	5.48×10^{-3}
2.	Electrode on Kureha	0.3 mg Pt/cm^2	0.048	3.35×10^{-3}
2A.	Electrode	0.3 mg Pt/cm^2	0.013	4.12×10^{-3}
3.	Stackpole backing	35% FEP pick-up	0.041	0.69×10^{-3}
4.	Kureha backing	45% FEP pick-up	0.048	3.07×10^{-3}
5.	Stackpole backing	26% FEP pick-up	0.048	2.92×10^{-3}
6.	Kureha backing	27% FEP pick-up	0.046	2.92×10^{-3}
7.	Stackpole backing	No FEP	0.046	32.7×10^{-3}
8.	Kureha	No FEP	0.046	26.0×10^{-3}
9.	Kynol Matrix		0.047	40.4×10^{-3}
10.	SiC 125 (4% TFE)[a.]		0.015 SiC	13.1×10^{-3}

a. Sintered 25 min. @ 275°C on an electrode (0.54 mg Pt/cm^2).

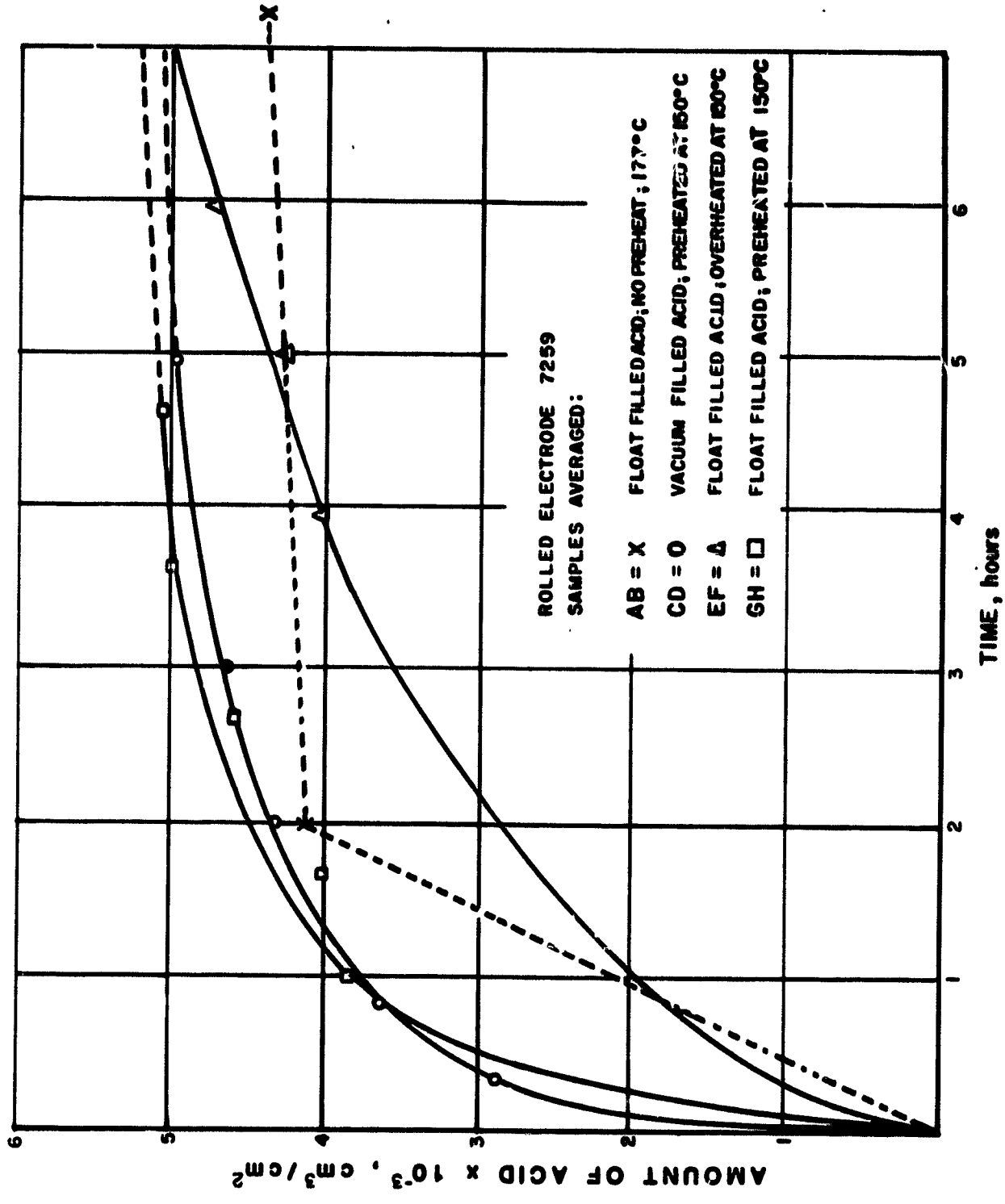

FIGURE 1.8 ACID PICK-UP OF ELECTRODE SAMPLES AS A FUNCTION OF TIME

Because only two data points (plus the origin) were taken for Sample AB, dotted lines are drawn rather than trying to assume the shape of a curve. In this test, as in all of the float filling tests, the electrode samples were placed with catalyst side down in a beaker of acid and then placed in an oven at the temperature listed on the figure. Sometimes the acid was preheated for one hour prior to the test.

Whenever it was time to weigh a sample, the electrodes were removed from the oven one at a time, gently blotted on Aldex paper to remove excess surface acid and then quickly weighed on a digital scale.

Sample CD in Figure 1.8, illustrates acid pick-up of electrodes float filled in a vacuum oven. It had been hoped that applying a vacuum would speed up the electrode filling process, but these results indicate that vacuum filling of electrodes is probably not worth the effort: it seems to speed up the early stages of electrode filling but, after the first hour or so, the rate of fill tapers off to that of other float filled electrodes.

Additional tests were done on small (5.1 cm x 5.1 cm) samples and other tests were performed on full size 13 cm x 38 cm (5 in. x 15 in.) and 31 cm x 43 cm (12 in. x 17 in.) electrodes. In this type of test, an acid-soaked Kynol matrix was placed between two electrodes, forming a sandwich. Weights were placed on top of the sandwich and the whole unit was placed in the oven. Figure 1.9 shows one such test where samples were all cut from the same electrode. The graph shows that in both cases the electrode on the bottom of the sandwich picked up more acid than the electrode on top. This trend holds in most of the tests of this type. Table 1.5 lists the conditions and results of other tests performed. Electrode filling is apparently slower when

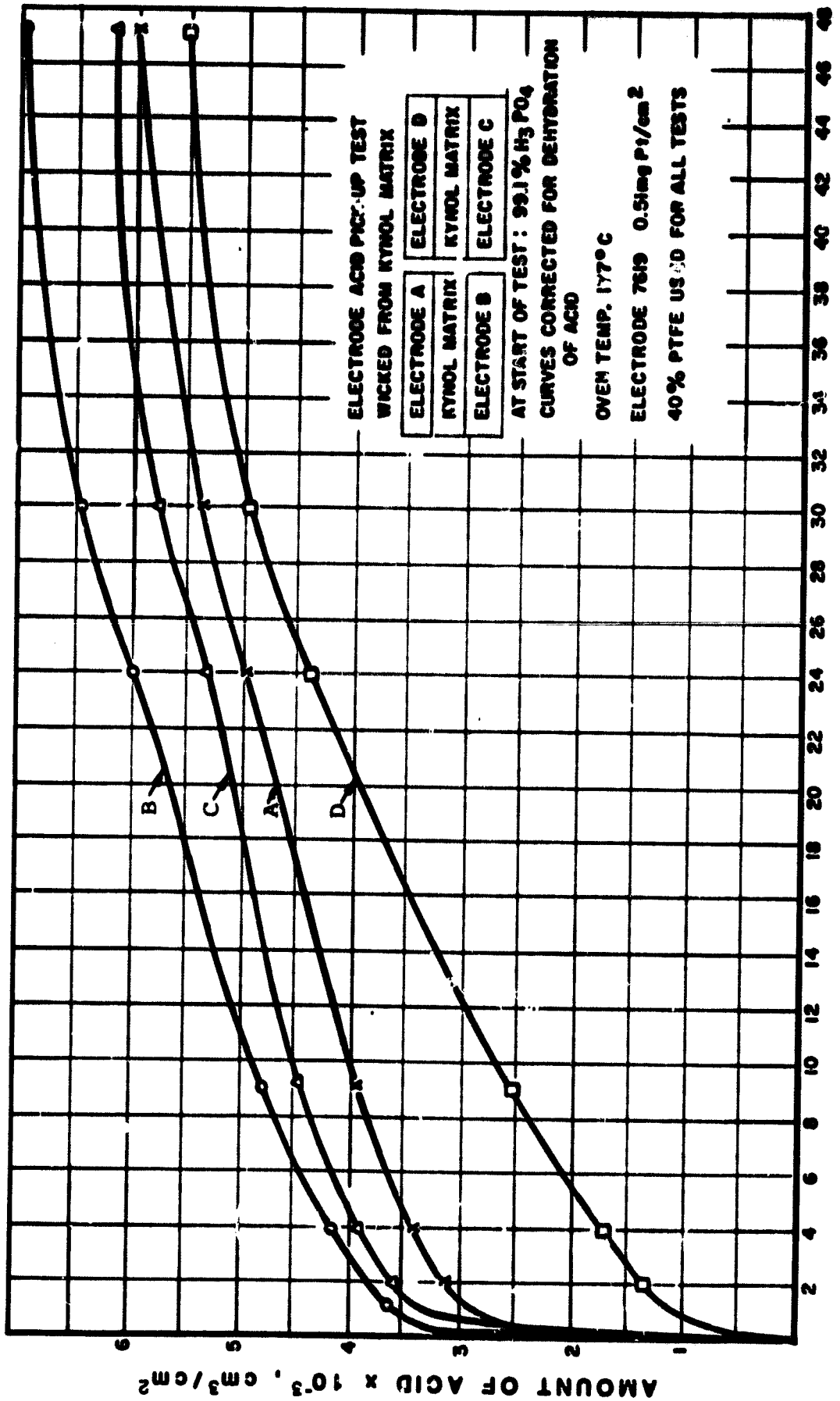

FIGURE 1.9 ELECTRODE ACID PICK-UP FROM WET MATRIX AS A FUNCTION OF TIME

TABLE 1.5

ACID PICK-UP OF ELECTRODES WICKED FROM MATRICES

(All Data Corrected for Concentration of Acid)

SAMPLE	SIZE, cm	MATRIX	TIME, days	TEMP, °C	PICK-UP cm^3 of acid/cm^2 of sample x 10^{-3}
• 0.67 mg Pt/cm^2 rolled electrodes 40% PTFE					
1A Top	13 x 38	Kynol	7	150	4.4
1B Bottom	13 x 38	Kynol	7	150	4.2
• 0.9 mg Pt/cm^2 rolled electrodes 40% PTFE					
5960 Top	13 x 38	Kynol	5	150	6.1
6030 Bottom	13 x 38	Kynol	5	150	6.5
• 0.6 mg Pt/cm^2 rolled electrodes 45% PTFE					
6974 Top	13 x 38	Kynol	5	150	4.2
6969 Bottom	13 x 38	Kynol	5	150	3.6
• 0.5 mg Pt/cm^2 rolled electrodes 40% PTFE					
X017 Top	30 x 43	Kynol	5	150	4.6
X015 Top	30 x 43	Kynol	5	150	3.3
• 0.9 mg Pt/cm^2 rolled electrodes 40% PTFE					
X022	30 x 43	Kynol	5	150	6.3
X025	30 x 43	Kynol	5	150	5.1

wicking from a matrix than when float filling, but the ultimate pick-up appears to be similar.

These tests indicate that a 13 cm x 38 cm (5 in. x 15 in.) uncompressed electrode with a typical loading of 0.5 mg Pt/cm^2 could be expected to hold approximately 2.0 cm^3 of acid and a similarly loaded 31 cm x 43 cm (12 in. x 17 in.) electrode would hold approximately 5.3 cm^3.

Knowing the amount of acid in the various components provided the basis for estimating the expected volume changes during start-up and operation. These changes might determine the speed of start-up, shutdown, and transient operation such that acid does not expand into the electrode or backing paper wetproofed porosity. Expansion into these areas would result in diffusion limitations.

Estimation of Volume Changes

The initial estimation of electrolyte volume changes during cell assembly and operation was obtained for two different dry room (where the stack is assembled) humidities and two different current loads.

As shown in Table 1.6, the volume changes depend on the environmental moisture content when the cell is prepared and operated. Before starting the cell, electrolyte wicking and stack heating in a dry atmosphere will produce less volume change. For a stack assembled and filled with electrolyte under P_{H_2O} = 1.2 mm Hg (4% RH at 30°C), an electrolyte volume contraction of 1.1 cm^3 would be experienced (Step 4 to 5) when heated to 121°C under the same humidity conditions. If it were to be heated under P_{H_2O} = 24 mm Hg (80% RH at 30°C), a volume expansion of 0.9 cm^3 would be expected (Step 4 to 5) according to the calculations. Starting the stack at 121°C (Step 6) would produce a volume expansion of 1.2 cm^3 at a current density of 54 mA/cm^2 and 2.1 cm^3 at a current density of 162 mA/cm^2, and then further heating would gradually contract

TABLE 1.6

ACID VOLUME CHANGES FOR 350 cm^2 CELL

(Calculated From Equilibrium Conditions)

STEP		DRY ROOM P_{H_2O} = 1.2 mmHg			
(1) Acid Filling in Electrodes at 77°C		C = 101.5% V = 2.1 cm^3			
(2) Cooling of Electrodes to 30°C		C = 93% V = 2.4 cm^3			
(3) Acid Filling in Matrices at 30°C		C = 100% V = 15.6 cm^3			
(4) Assembling of Cells and Compressing at 30°C		C = 98.29% V = 14.3 cm^3			
(5) Heating the Compressed Stack to 121°C		P_{H_2O} = 1.2 mmHg		P_{H_2O} = 24 mmHg	
		C = 105.8% V = 13.2 cm^3		C = 97% V = 15.2 cm^3	
(6) Starting the Stack at 121°C	I	54 mA/cm^2	162 mA/cm^2	54 mA/cm^2	162 mA/cm^2
	C%	93	90	93	90
	V (cm^3)	14.4	15.3	16.4	17.3
(7) Heating the Stack to 177°C	C%	99.75	97.8	99.75	97.8
	V (cm^3)	13.2	13.6	15.0	15.5

P_{H_2O} = 1.2 mmHg (4% RH @ 30°C)

C = acid concentration

V = acid volume

the electrolyte volume to 13.2 cm^3. To minimize the volume expansion during start-up, the stack should be kept as close to the steady operating temperature as possible. Comparing steps 4 and 6, the minimum AICM capacity per cell in a 350 cm^2 stack should be 1.0 cm^3 for cells heated under P_{H_2O} = 1.2 mm Hg and 3.0 cm^3 for cells heated under P_{H_2O} = 24 mm Hg (at a starting current load of 162 mA/cm^2 at 121°C). When the stack is assembled in a dry room of controlled moisture content, P_{H_2O} = 2.4 mm Hg (8% RH), the minimum AICM requirement appears to be 2.6 cm^3.

A gradual path was devised for stack wicking and starting to prevent excess acid volume change resulting in acid drippage and weeping from the cells. Figures 1.10 and 1.11 show the steps for computing a desirable cell condition from wicking to final operation. In the calculations, final stack operating conditions were assumed to be 177°C and 100 mA/cm^2.

From the information of flow rates, humidities of air and fuel, and current load, the partial water vapor pressures on the cathode and anode are estimated from overall mass balance equations. Acid density and concentration are then calculated using the estimated water vapor pressure on the cell. Based on the saturated cell condition at final stack operating conditions, a wicking condition can be determined from the following equation:

$$\frac{\text{Vol. of acid in cell at wicking}}{\text{Vol. of acid in cell during operation}} = \frac{\rho_{wick} W_{wick}}{\rho_{oper} W_{oper}} = 1.0 = \frac{V}{V_s}$$

Where,

ρ_{wick} and ρ_{oper} = densities at wicking and operating stages, respectively.

W_{wick} and W_{oper} = concentrations

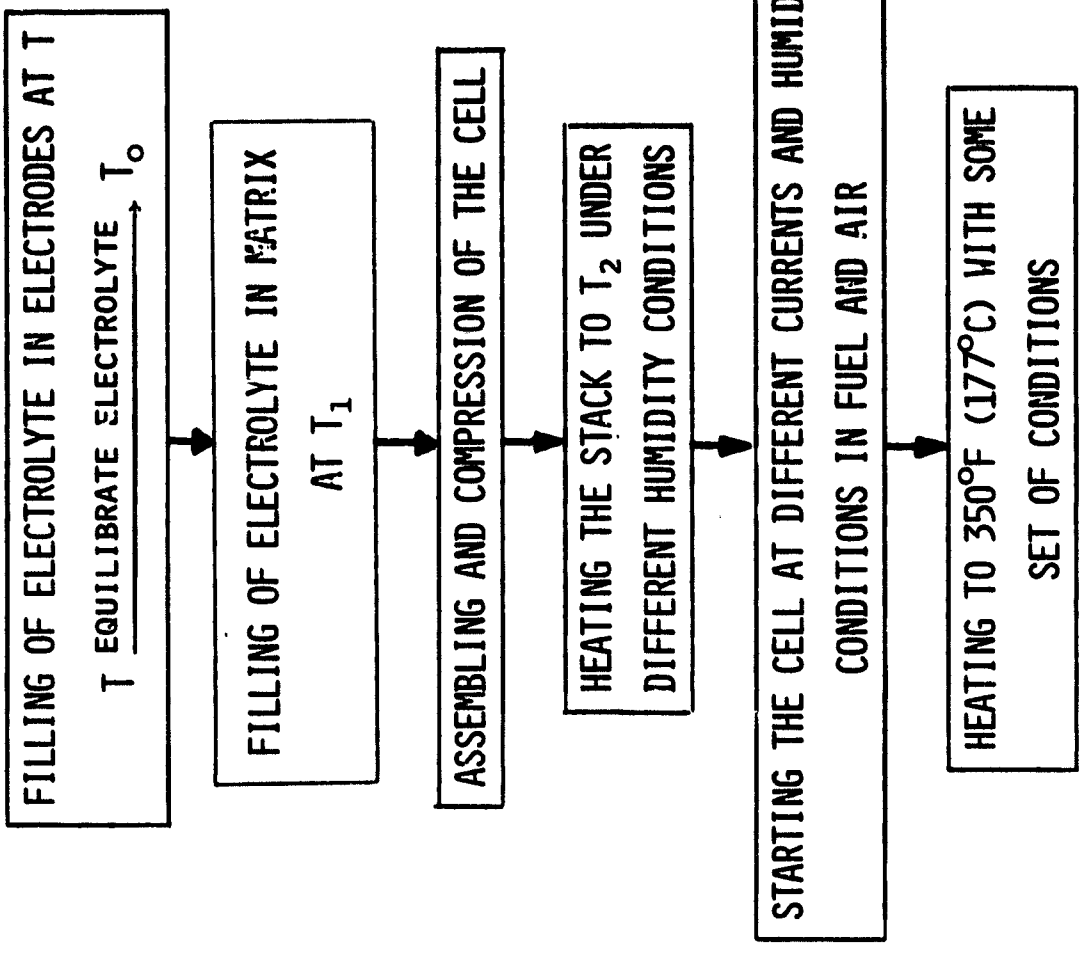

FIGURE 1.10 STEPS FOR A FUEL CELL STACK PREPARATION

ENERGY RESEARCH CORPORATION

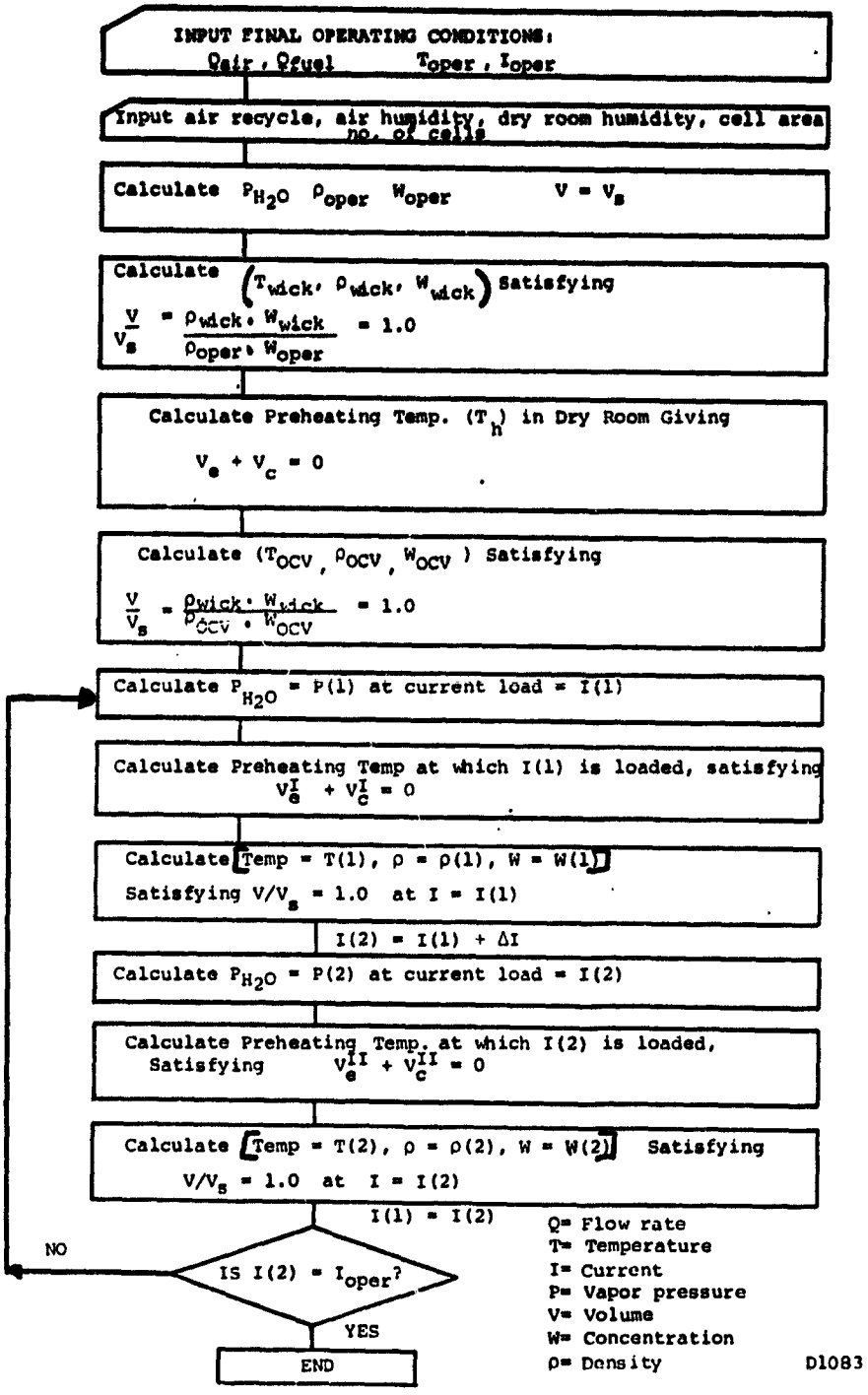

FIGURE 1.11

FLOW CHART FOR CALCULATING STACK WICKING AND STARTING CONDITIONS

The general rationale and procedure described in Figures 1.10 and 1.11 can be represented graphically. The following explanation of Figure 1.12 and description of several calculations made for the fuel cell system have resulted in a recommended procedure. After wicking, $V/V_s = 1$, the stack is preheated in the dry room prior to OCV testing. Figure 1.12 illustrates the point (T_h) to which the stack should be preheated in the dry room. As shown, the volume of acid in the cell will initially expand if the stack is placed under higher humidity and then gradually shrink as the stack temperature goes up. The behavior of volume change with temperature will depend on the rate of moisture absorption, i.e., curve r_1 represents the case of an infinitely fast absorption rate. When the rate is very slow, the volume expansion curve will decrease and approach the dry room contraction curve. The preheating temperature T_h is based on the extreme condition of the moisture absorption rate, to insure safety when the stack is standing for a prolonged period outside the dry room. At point T_h, the calculated volume contraction (V_c) and the equilibrium expansion (V_e) become identical for the conditions inside and outside the dry room, respectively. The stack is then moved out of the dry room with continued heating until the acid volume returns to the $V/V_s = 1$ point. The stack is again preheated to reduce the acid volume in the cell before loading current on the stack. This procedure is repeated until the initially assumed operating conditions are achieved.

In Figure 1.13 a three dimensional path was drawn for an air stoich* of 3.0, dry room humidity of 2.5 mm Hg, and a testing lab humidity of 12 mm Hg. Under the given conditions, the optimal wicking temperature becomes 75°C and the acid concentration is 97.6%. After wicking, the stack is preheated to 99.5°C (path a-b), before taking it out of the dry room to the 12 mm Hg humidity condition and heating it to 120°C (path b-c) before OCV testing. After OCV measurements, the stack is kept at 123°C (path c-d) before the 20

*Through the cathode channels.

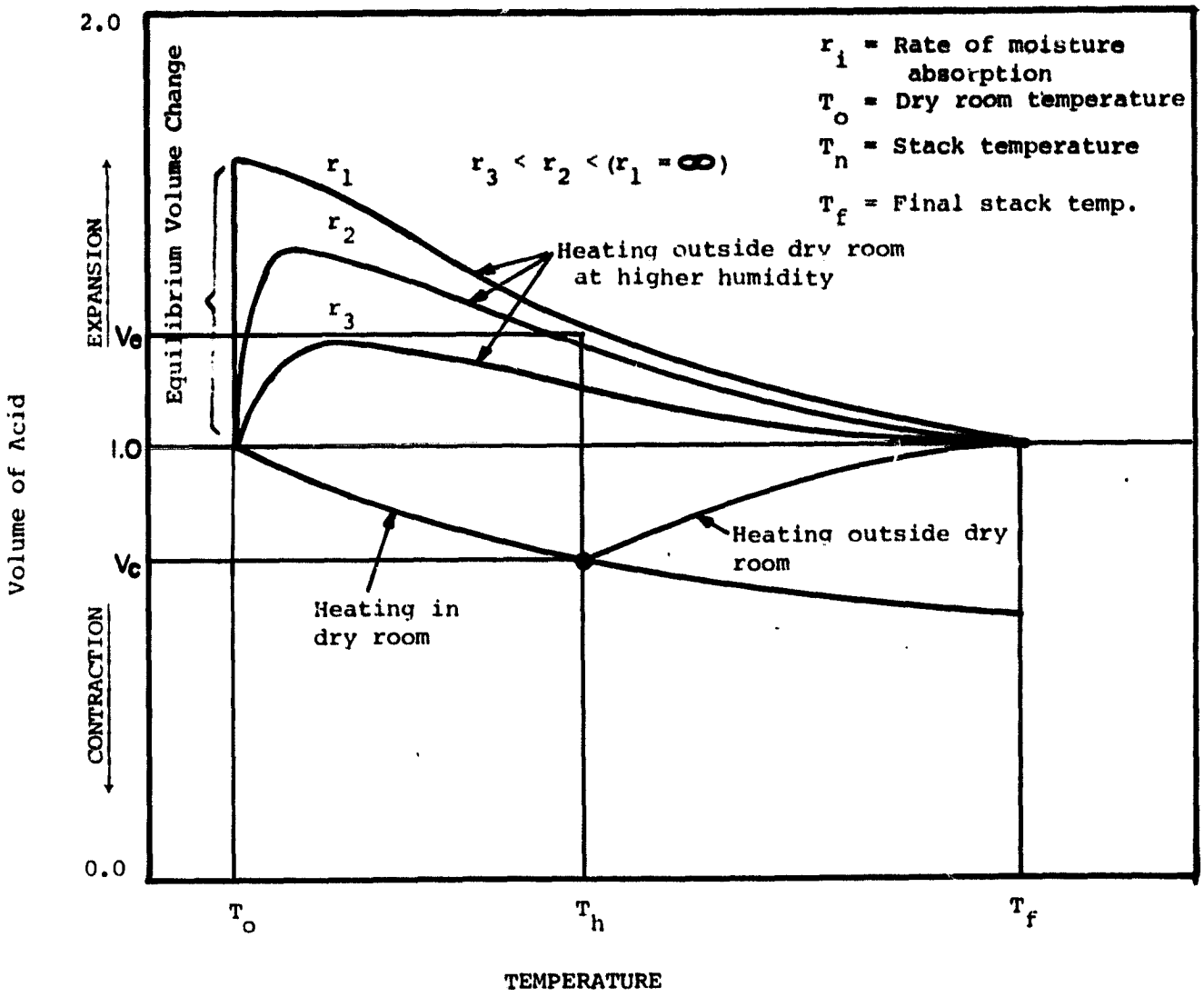

FIGURE 1.12 ACID VOLUME BEHAVIOR DURING HEATING

D1153R

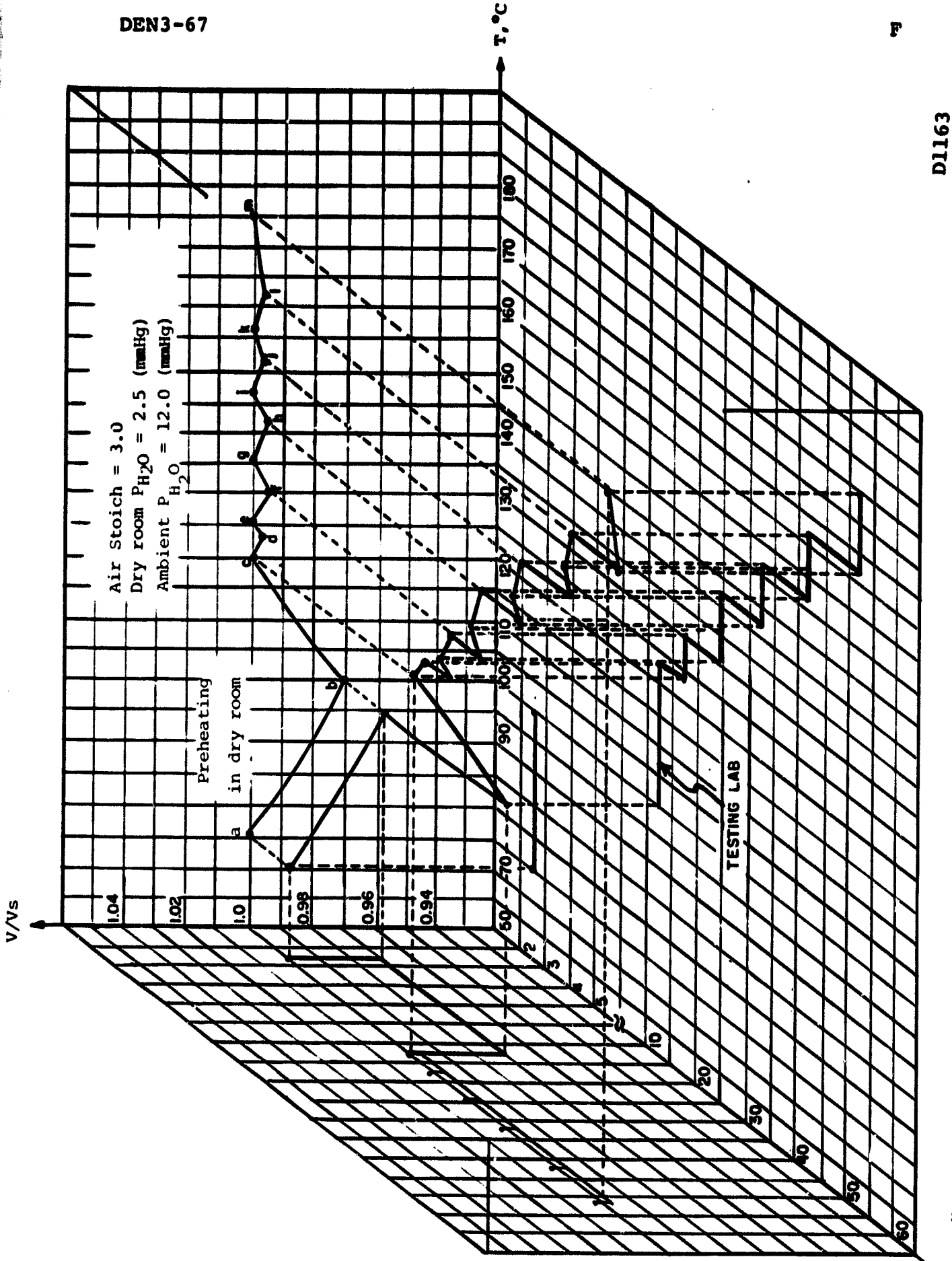

FIGURE 1.13 PATH TO BE FOLLOWED FROM WICKING TO OPERATING CONDITION

mA/cm^2 current loading. After the stack is put on load, the temperature is raised to 126°C (path d-e). When the starting current loads are 40, 60, 80 and 100 mA/cm^2, the preheating temperatures become 130, 142, 152 and 162°C, as shown in the figure.

Table 1.7 summarizes a comparison of stack conditions from wicking to loading for two and four air stoichs, and for zero and 40% recycling of air. According to the table, the optimal wicking temperature varies from 59 to 77°C, while the preheating temperature in the dry room varies from 91 to 108°C, and the temperature for OCV testing varies from 114 to 130°C. Based on the information given in the table, a set of stack parameters was chosen to allow tolerance of the varying environment within reasonably small volume changes. Table 1.8 shows the recommended parameters to be applied from stack wicking to starting. Maximum volume expansion encountered for the given set of parameters was estimated to be 2.5%.

Acid Inventory Control Member (AICM)

The development of a technique to wetproof a backing paper (AICM) selectively using an FEP solution was completed. Additional work is needed, however, to define the minimum amount of wetproof area necessary to prevent gas diffusion limitations at the design operating current density. The presently developed AICM was satisfactorily tested in a 3-cell 350 cm^2 size stack at 100 mA/cm^2 (see Task 1.6).

Several techniques which could be used to produce selectively wetproof backings were identified. These techniques result in backings that are completely wetproofed on one side (the gas side) and are spotted with wetproofed areas on the other (catalyst) side. The backing then becomes an AICM which can be used to store or supply electrolyte as the conditions of the cell dictate.

TABLE 1.7

COMPARISON OF STACK CONDITIONS* FROM WICKING TO STARTING

AIR STOICH	ZERO RECYCLE										40% RECYCLE									
	WICK			PREHEAT		OCV TEST			START		WICK			PREHEAT		OCV TEST			START	
	P_{H_2O}	T	W	P_{H_2O}	T	P_{H_2O}	T	W	I	T	P_{H_2O}	T	W	P_{H_2O}	T	P_{H_2O}	T	W	I	T
2	1.5	59	96.8	1.5	91	12	114	98.3	60	135	1.5	57	96.5	1.5	88	12	112	98	60	134
				1.5	97	16	124	98.6	60	132				1.5	94	16	120	98.3	60	134
	2.5	71	97.2	2.5	96	12	115	98.4	60	135	2.5	69	96.8	2.5	92	12	111	98	60	134
				2.5	101	16	125	98.7	60	133				2.5	98	16	120	98.3	60	131
4	1.5	65	97.5	1.5	98	12	123	99.2	60	143	1.5	63	97.2	1.5	95	12	119	98.8	60	135
				1.5	104	16	130	99.6	60	143				1.5	101	16	128	99	60	135
	2.5	77	97.8	2.5	102	12	122	99	60	142	2.5	75	97.6	2.5	100	12	120	98.9	60	142
				2.5	108	16	130	99.6	60	142				2.5	105	16	130	99.2	60	135

Units: P_{H_2O} (mm Hg); T(°C); W(%); I(mA/cm^2)

*Based on final operating conditions: 100 mA/cm^2 and 175°C.

TABLE 1.8

RECOMMENDED SET OF STARTING PARAMETERS

WICKING	PREHEATING IN DRY ROOM	OCV TESTING	LOADING
T = 70 W = 97 P_{H_2O} = 2.5	T = 110 P_{H_2O} = 2.5	T = 120 W = 99 P_{H_2O} = 12	T = 150 I = 60 P_{H_2O} = 12

Units: T (°C): W(%) of acid: I(mA/cm^2).

Sample AICMs containing 36% FEP were prepared by this technique and the quantities of acid picked up in float filling tests have averaged 15 x 10^{-3} cm^3 of acid/cm^2 backing. When translated to the scale of a 350 cm^2 stack, the acid storage capability of these AICMs is approximately 5.8 cm^3 per anode backing. The minimum storage necessary to accommodate electrolyte volume changes due to start-up conditions was estimated to be 1.0 cm^3 to 3.0 cm^3 per cell.

Since the AICMs are expected to absorb changes in acid volume, prefilling of anodes in some cells was an attempt to accelerate what might happen in operating cells. The extent to which filling the backings with acid interferes with the flow of hydrogen to the anodes will affect anode performance.

Table 1.9 relates cell performance to the cross-sectional area of the anode backing wetproofed and to the amount of acid picked up during prefilling. The percentage of FEP in the backings is higher than might be expected because the FEP used for selective wetproofing was of a much higher concentration than is commonly used in the standard wetproofing operation. This was necessary due to the greater tendency of dilute FEP emulsions to spread out. The approximate percentage of the area next to the electrode covered by the FEP (listed in Column C) indicates that, in these wetproofed areas, there is a much greater concentration of FEP than normal. The effect of this on the uniformity of current flow through the backings has not yet been determined. Column D lists the amount of acid that was picked up by the anode during prefill. All of the anode loadings were approximately 0.3 mg Pt/cm^2. In comparison, a typical electrode of that loading would pick up 0.11 cm^3 of acid, presumably all in the catalyst layer. Column E shows the amount of acid that would be stored in an equivalent anode scaled up to a 1200 cm^2 size.

TABLE 1.9

COMPARISON OF NON PREFILLED AND PREFILLED 25 cm^2 AICM CELLS

CELL	PEAK PERFORMANCE, mV @ 200 mA/cm^2 IR-FREE A	ANODE* BACKING, Wt% FEP B	FEP COVERED AREA APPROX., % C	ACID PICKED-UP IN PRE-FILL, cm^3 D	ACID IN EQUIV. 1200 cm^2 ANODE, cm^3 E	PEAK O_2 GAIN, mV @ 200 mA/cm^2 F
100	648	27	25	None	0	42
101	607	36	28	0.283	13.4	78
102	607	24	46	None	0	82
103	600	25	40	0.338	16.0	75
105	643	35	40	None	0	68
106	632	35	40	0.434	20.5	76

*Selectively wetproofed.

The average IR-free peak performance of prefilled cells is only 610 mV, while the average of cells not prefilled is 630 mV, all at 200 mA/cm^2. Analysis of cell polarization curves indicated that, to a large extent, cell performance was indicative of backing flooding. The oxygen gains remained low, while the drop in performance was steep as the load increased.

In addition to the selective wetproofing of anode backings for an AICM, several backings were uniformly wetproofed but with low FEP contents. As indicated by the data in Table 1.10 the low FEP backing cells performed 17-22 mV higher at peak performance. As the testing time increased these cells gradually flooded.

1.6 Component Evaluation and Screening

Forty 350 cm^2 three-cell stacks were built to evaluate various components including SiC and MAT-1 matrices, Stackpole and Kureha backing papers, Varcum and Colloid resin plates, heat-treated and nonheat-treated plates, and selectively wetproofed AICM's. Typical data are summarized in Table 1.11. The most significant differences are apparent between nonheat-treated plates and heat-treated plates. A large increase in performance was obtained using heat-treated plates; this can be attributed to improved electrical conductivity of the plate material, reduced contact resistances, and removing an electrode poison. Some of the variations in the performance of stacks used to compare different components may be a result of variable degrees of poisoning. It is most likely that this poisoning arises from the corrosion of plate material described in Task 2. Since the poisoning was not clearly defined until late in the program when funding was limited, the tests were not repeated. Assuming, however, equal poisoning of all cells, the data indicate a successful scale-up of the SiC matrix, rolled electrodes, backing

TABLE 1.10

25 cm^2 TEST CELLS WITH AICM ANODE BACKINGS

	LOW FEP BACKINGS			SELECTIVELY WETPROOFED BACKINGS				
Cell No.	1278	1316	1384*	1341	1374	1378	100	103*
Anode Loading (mg Pt/cm^2)	0.3	0.3	0.3	0.3	0.3	0.3	0.3	0.3
Cathode Loading (mg Pt/cm^2)	0.5	0.5	0.5	0.5	0.5	0.5	0.5	0.5
% FEP, Anode Backing	20	28	20	9.0	13.0	11.6	27	25
% FEP, Cathode Backing	40	37	39	36	34	39	39	39
Peak Performance, Air, IR-FREE								
@ 100 mA/cm^2 (mV)	723	715	675	530	665	705	---	---
@ 200 mA/cm^2 (mV)	670	665	610	---	600	650	648	600

*Pre-filled Anode.

TABLE 1.11

TYPICAL STACK PERFORMANCE OF DEVELOPMENTAL COMPONENTS[1]

COMPONENT	NONHEAT-TREATED PLATES													HEAT-TREATED PLATES		
	KUREHA BACKING	STACKPOLE BACKING	SHEETMOLD ELECTRODES		ROLLED ELECTRODES	SiC MATRIX		MAT-1 MATRIX		VAPCUM RESIN		COLLOID RESIN		VARCUM RESIN	VARCUM RESIN	AICH
Stack No.	389	395	391	413	385	600	601	602	428	616	618	608	427	619	431	620
Size, cm^2	5 x 15	5 x 15	5 x 15	12 x 17	5 x 15	5 x 15	5 x 15	5 x 15	12 x 17	5 x 15	5 x 15	5 x 15	12 x 17	5 x 15	12 x 17	5 x 15
No. of Cells	3	3	3	5	3	3	3	3	5	3	3	3	5	3	5	3
Plate Resin:	Colloid	Colloid	Colloid	Colloid	Colloid	Colloid	Colloid	Colloid	Colloid	Varcum	Varcum	Colloid	Colloid	Varcum	Varcum	Colloid
% Resin	33%	33%	33%	33%	33%	33%	33%	33%	33%	33%	33%	33%	33%	32%	32%	33%
% A99	49%	49%	49%	49%	49%	49%	49%	49%	49%	67%	67%	49%	49%	68%	68%	49%
% 650	18%	18%	18%	18%	18%	18%	18%	18%	18%			18%	18%			18%
Matrix	Kynol	Kynol	SiC	SiC	SiC	SiC	SiC	MAT-1	MAT-1	Kynol	MAT-1	MAT-1	MAT-1	MAT-1	MAT-1	MAT-1
Anode Loading, mg Pt/cm^2	.3	.3	.3	.3	.3	.3	.3	.3	.3	.3	.3	.2	.3	.3	.3	.3
Cathode Loading, mg Pt/cm^2	.5	.5	.5	.5	.6	.5	.5	.5	.5	.5	.5	.4	.5	.5	.5	.5
Total Test Hrs.	1392	2427	3856	355	1400	8418	6369	10,171	7566	3389	2710	7228	2159	6075	7188	6740
Avg. Peak Terminal Volt 100 mA/cm^2	.55	.59	.62	.61	.60	.61	.61	.61	.58	.59	.60	.61	.59	.69	.68	.68
OCV	.83	.86	.76	.79	.76	.79	.77	.79	.81	.85	.78	.81	.83	.85	.90	.87
Avg. Terminal Volt @ 1400 Hrs. 100 mA/cm^2	.51	.50	.61	.55	.57	.59	.56	.59	.56	.58	.58	.59	.55	.69	.67	.67
OCV	.81	.81	.80	.75	.72	.79	.76	.78	.80	.84	.77	.79	.79	.84	.88	.86

1. Complete stack listing is in Appendix A.

papers, and bipolar plates. The selectively wetproofed AICM was also successfully tested in a 350 cm^2 stack and should be easily scaled up to 1200 cm^2 cells.

During the program an ERC matrix (MAT-1) became available that had a superior bubble pressure and was easily manufactured in 1200 cm^2 sizes. Tests suggested the cell performance with MAT-1 was equal to that with the SiC matrix cells. Results of the 10,000 hour endurance tests described in Task 3 further demonstrated the superior nature of the MAT-1 matrix.

Based on material cost, handling, manufacturability and long-term performance, the following components were found to be effective:

1. Rolled electrodes, 0.25 mg Pt/cm^2 anodes, 0.5 mg Pt/cm^2 cathodes;
2. Carbon paper backings (Stackpole carbon);
3. Heat-treated phenolic resin bipolar plates with 33% or greater Varcum resin 29-703 and 67% or less Asbury A99 graphite;
4. MAT-1 matrix;
5. Teflon seals.

TASK 2. MATERIALS EVALUATION

The effort in this task focused on diagnostic analysis of materials used for fuel cell stacks so that guidance could be provided in their development. The areas of investigation were:

- Component corrosion resistance
- Physical property measurements
- Bipolar and cooling plate erosion.

2.1 Component Corrosion Resistance

Exposure of the fuel cell components to concentrated phosphoric acid results in both chemical and electrochemical corrosion. A number of resins and resin/graphite composites (heat-treated and nonheat-treated) were investigated under various test conditions:

- Apparent chemical corrosion - immersion in acid followed by weight and thickness changes;
- True chemical corrosion - apparent corrosion corrected for acid absorption (see Figure 2.1);
- Slow sweep voltammetric corrosion - under different gas atmospheres and various corrosion times;
- Continuous corrosion at constant potential.

During these studies several limitations for each type of measurement were discovered. Initially samples of material were immersed in hot acid, superficially washed, dried, and weighed. It quickly became apparent that some materials required extensive extraction to remove acid while others required only a simple rinse. This variability resulted at times in no apparent corrosion when corrosion had occurred. Acid absorption also caused variable swelling and subsequent

F

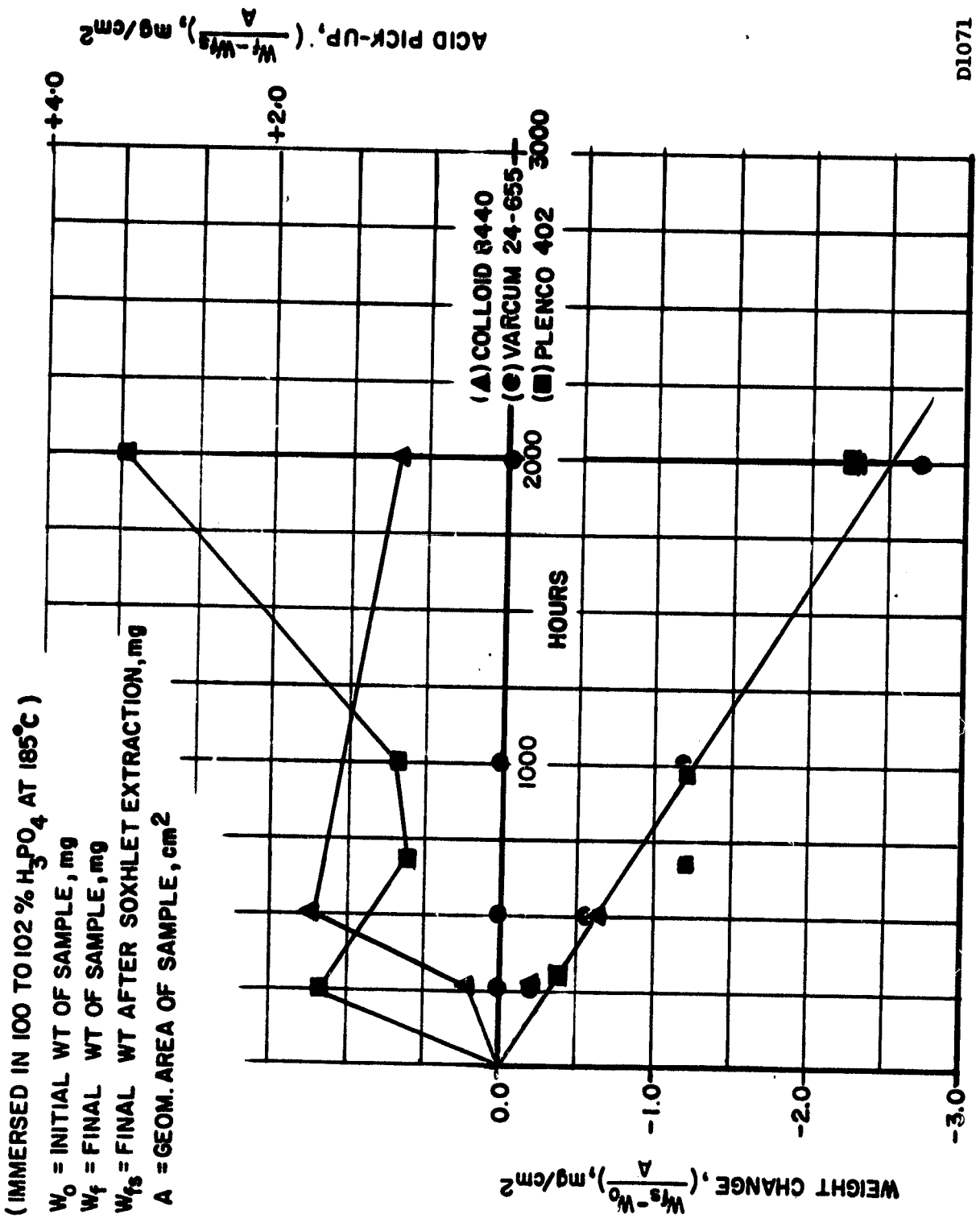

FIGURE 2.1 TRUE CORROSION AND ACID ABSORPTION CHARACTERISTICS OF PURE RESINS

shrinkage on acid removal. Careful attention to these possibilities was required to achieve meaningful chemical corrosion data.

Voltammetric sweep corrosion curves were confused by a very slow surface equilibration reaction that results in a significant hysteresis between the anodic and cathodic sweeps. This is not unexpected since the equilibrium surface oxide concentration might very well change slowly during reduction and also as new surface sites are created when oxidized. In addition, the corrosion current decreases significantly for long time periods (10-100 hours). The magnitude of the long-term corrosion current can only be obtained, however, by a constant potential versus time plot, while the voltammetric sweep curve provides the approximate effect of potential at any point in time.

Apparent Chemical Corrosion

The investigation of the chemical corrosion of component materials in 100 to 102% H_3PO_4 at 185°C was completed. Using the weight and thickness change data for 4000 to 5000 hours, the phosphoric acid tolerance of these materials has been evaluated. Rates of weight and thickness change are reported for thermoset resins, thermoplastic resins and thermoset based composites in Tables 2.1, 2.2 and 2.3, respectively. The following important observations can be made from these results.

- All thermoset resins studied (except Plenco 653) have comparable apparent corrosion rates between 1 and 2 $\mu g/hr/cm^2$ (Table 2.1).
- Varcum resins in general have low corrosion rates and, in this group, Varcum 29-703 showed maximum acid tolerance.
- Plenco 653, a cresol modified phenolic resin of the single-stage type, disintegrated in the acid

TABLE 2.1 ACID TOLERANCE OF 100% THERMOSET RESINS

(Immersed in 100 to 102% H_3PO_4 at 185°C for Approximately 4000 Hours)

SAMPLE TYPE	APPARENT CORROSION RATE, $\mu g/hr/cm^2$	RATE OF THICKNESS CHANGE, cm/hr x 10^6		REMARKS	EXPECTED THICKNESS CHANGE, mils/year
		EXPERIMENTALLY OBSERVED*	PREDICTED CHANGE FROM WEIGHT LOSS DATA		
Varcum 24-655 (one step phenolformaldehyde)	-1.22	-0.79	-1.00	9 samples	-3.5
Varcum 29-703 (two stage phenolic)	-0.99	-0.65	-0.79	3 samples	-2.7
Varcum 29-319 (two stage phenolic)	-1.10	-0.43	-0.88	2 samples	-3.0
Plenco 956 (two stage phenolic)	-1.15	-0.86	-0.97	3 samples	-3.4
Plenco 402 (two stage phenolic)	-1.31	-0.49	-1.08	3 samples	-3.7
H-Resin, H-A43 (polyphenylene resin)	-1.96	-2.10	-1.74	3 samples	-6.0
98 w/o Xylok, 2 w/o Hexa (thermoset resin)	-1.28	-1.02	-1.12	2 samples	-3.9
Colloid 8440 (two step phenolformaldehyde)	-1.11	-1.31	-0.98	5 samples mat'l. initially absorbed acid. Calculations determined after initial absorption.	3.4
Plenco 653 (Cresol modified phenolic)	Disintegrated				

*Rate of thickness change = $\frac{\text{Final thickness - Initial thickness}}{\text{Time}}$

TABLE 2.2

ACID TOLERANCE OF THERMOPLASTIC RESINS

(Immersed in 100 to 102% H_3PO_4 Acid at 185°C)

SAMPLE TYPE	WEIGHT CHANGE RATE, $\mu g/hr/cm^2$	EXPERIMENTAL THICKNESS CHANGE RATE, $\mu m/hr$	PREDICTED THICKNESS CHANGE*	
			$\mu m/hr$	mils/year
Radel 5010-3	+0.030	-	$+0.024 \times 10^{-2}$	+0.08
Radel C (polyphenylsulfone)	+0.008	$+1.01 \times 10^{-2}$	$+0.062 \times 10^{-2}$	+0.02
Udel A	-0.004	Warped	-0.003×10^{-2}	-0.012
Udel B (polysulfone)	-0.003	-	-0.004×10^{-2}	-0.013
PMP A	-1.60	-1.5×10^{-2}	-1.88×10^{-2}	-6.5
PMP B (polymethylpentane)	-0.35	-	-0.42×10^{-2}	-1.5
Victrex 300 P-1	-0.025	-0.3×10^{-2}	-0.02×10^{-2}	-0.06
Victrex 600 P-1 (polyethersulfone)	-0.014	-0.03×10^{-2}	-0.01×10^{-2}	-0.03

* Based on the measured weight change and the measured initial density

TABLE 2.3

SUMMARY OF ACID TOLERANCE OF THE COMPOSITES

(Approximately 4000 Hrs. in 100 to 102% H_3PO_4 at 185°C)

SAMPLE TYPE	RESIN CONTENT	AVERAGE RATE OF WEIGHT CHANGE		RATIO OF $\frac{R_2}{R_1}$
		0 to 3000 hrs. R_1 $\mu g/cm^2/hr.$	>3000 hrs. R_2 $\mu g/cm^2/hr.$	
H-Resin/A-99 Graphite	32	-0.17	-0.56	3.2
	28	-0.15	-0.52	3.3
	22	-0.13	-0.62	4.7
Varcum 24-655/A-99 Graphite	32	-0.10		
	28	-0.23	-1.1	4.8
	22	-0.20	-1.7	8.7
		100 to 2500 hrs., $\mu g/cm^2/hr.$		
Colloid/A-99 Graphite	32	+1.4		
	28	+2.0		
	22	+1.7		

but other phenolics showed good acid tolerance characteristics. The above observations suggest that modification of the resins may significantly change their acid tolerance characteristics.

- The observed thickness change for most of the thermoplastics is less than would be predicted from the corrosion rate, suggesting a nonuniform etching of the sample surface (see Figure 2.2).

- Polysulfone resins are corroded more than 200 times less in phosphoric acid than thermoset resins. These samples are expected to have a thickness change of only 0.012 to 0.0135 mils/yr. (Table 2.2). Polyethersulfone is about six times more corroded than polysulfone and moreover, it is twice as expensive. Polyphenylsulfone, a costly thermoplastic, increases in weight and thickness in phosphoric acid, probably due to acid absorption.

- H-resin based composites have the lowest chemical corrosion rate of the composites (Table 2.3).

- Both H-resin and Varcum based composites have two different corrosion rates. The initial rate, probably associated with the skin corrosion, is dominant up to the first 3000 hours and seems to decrease with decreasing resin content. The corrosion rate past this point is perhaps representative of the bulk material, and appears to have a minimum corrosion rate with respect to resin content.

- Colloid composites increase in weight and thickness continuously due to acid exposure. Approximately 2 to 3% swelling in thickness is observed in about 4000 hours.

The acid absorption of thermoplastic materials has been measured and is summarized in Table 2.4. Both the colloid resins and the composites absorb significant amounts of acid. Although Varcum 24-655 does not absorb acid, its composites probably absorb a small amount of acid due to the presence of surface defects created during the manufacturing process. Absorbed phosphorous has been detected deep inside the acid-immersed colloid resins by EDA (energy dispersion spectroscopy

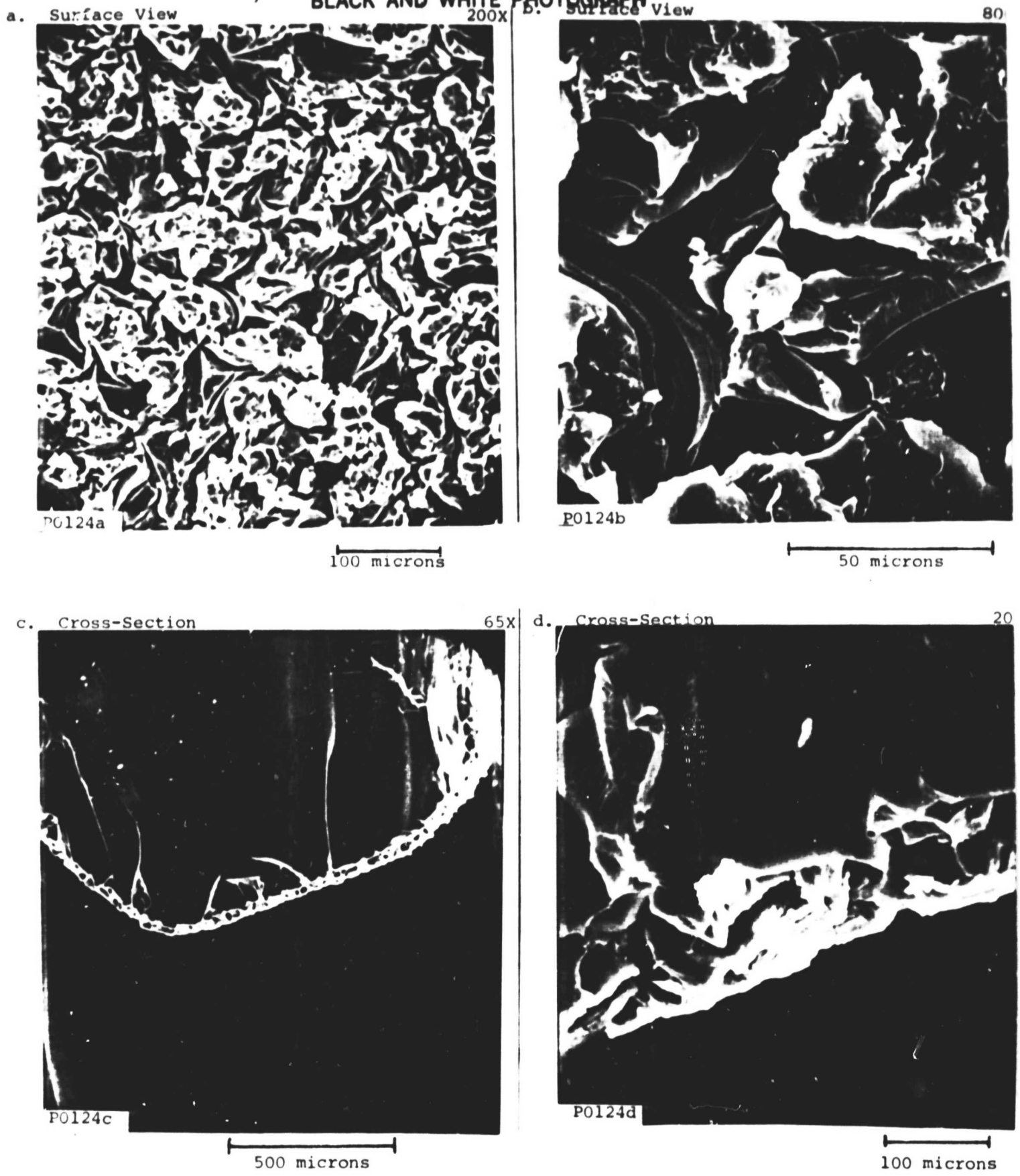

FIGURE 2.2 SEMS OF 100% VARCUM 24-655 RESIN AFTER 2250 HOURS OF 185°C H_3PO_4 EXPOSURE (Sample 349-1B)

TABLE 2.4

ACID ABSORPTION OF THERMOSET MATERIALS

MATERIAL COMPOSITION	RESIN TYPE	ABSORPTION OF PHOSPHORIC ACID
P U R E R E S I N	Varcum 24-655 (one step phenol-formaldehyde)	No
	Varcum 29-703 (two stage phenolic)	No
	Varcum 29-319 (two stage phenolic)	No
	Plenco 956 (two stage phenolic)	No
	Plenco 402 (two stage phenolic)	No
	H-Resin (polyphenylene resin)	No
	98 w/o Xylok & 2 w/o Hexa	Yes (Small quantity initially)
	Colloid 8440 (two step phenol-formaldehyde)	Yes (Initially for about 500 hrs.; significant amount)
Composites (Resin/A-99 Graphite)	Varcum 24-655	Yes (Small quantity initially)
	H-Resin	No
	Colloid 8440	Yes (Large quantity throughout the period of study)

analysis) using line scan, RBSI (Robinson Back Scatter Imaging), and dot maps. These photomicrographs (Figure 2.3) suggest that acid penetration takes place along cracks and surface defects and that this absorbed acid can be removed by a physical process such as water extraction. Acid penetrates to an approximate depth of 0.13 mm in about 3330 hrs.

True Chemical Corrosion

The true corrosion characteristics of some composites evaluated from the initial 2000 hour corrosion measurement data of the controlled experiments are discussed below.

Weight loss measurements of each sample type in the time interval of 150 to 2000 hours were observed to be quasi-linear with the time of acid immersion (Figure 2.4). The rate of weight loss for each of the composites, reported in Figure 2.5, was calculated from the slope of the $(W_{fs}-W_o)$ against time plot. The W_{fs} denotes the weight of the sample in g/cm^2 after aging in acid, and then the extraction of the acid with water and drying. W_o is the initial weight in g/cm^2 and t is the aging time in hours. Acid absorption of these samples at 2000 hours of aging, calculated from (W_f-W_{fs}), is also reported in Figure 2.5. W_f is the weight of the aged sample after a water rinse and drying. The following observations can be made:

- Of the four samples compared, the Varcum 24-655 based composite has the lowest corrosion rate (-0.125 $\mu g/cm^2$ hr).
- Raising the resin content in the range of 22 to 32% seems to improve the corrosion rates of only those samples with high corrosion rates.
- In general, samples with a higher acid absorption tend to have higher true corrosion rates.
- The acid absorption of each sample increases as the resin content decreases.

EDA, Line Scan & Dot Maps for phosphorus. Samples a, b, c - acid exposed for 3300 hours in 100 to 102% H_3PO_4 at 185°C and not boiled. Sample d - acid exposed for 3072 hours, then boiled in water for 8 hours.

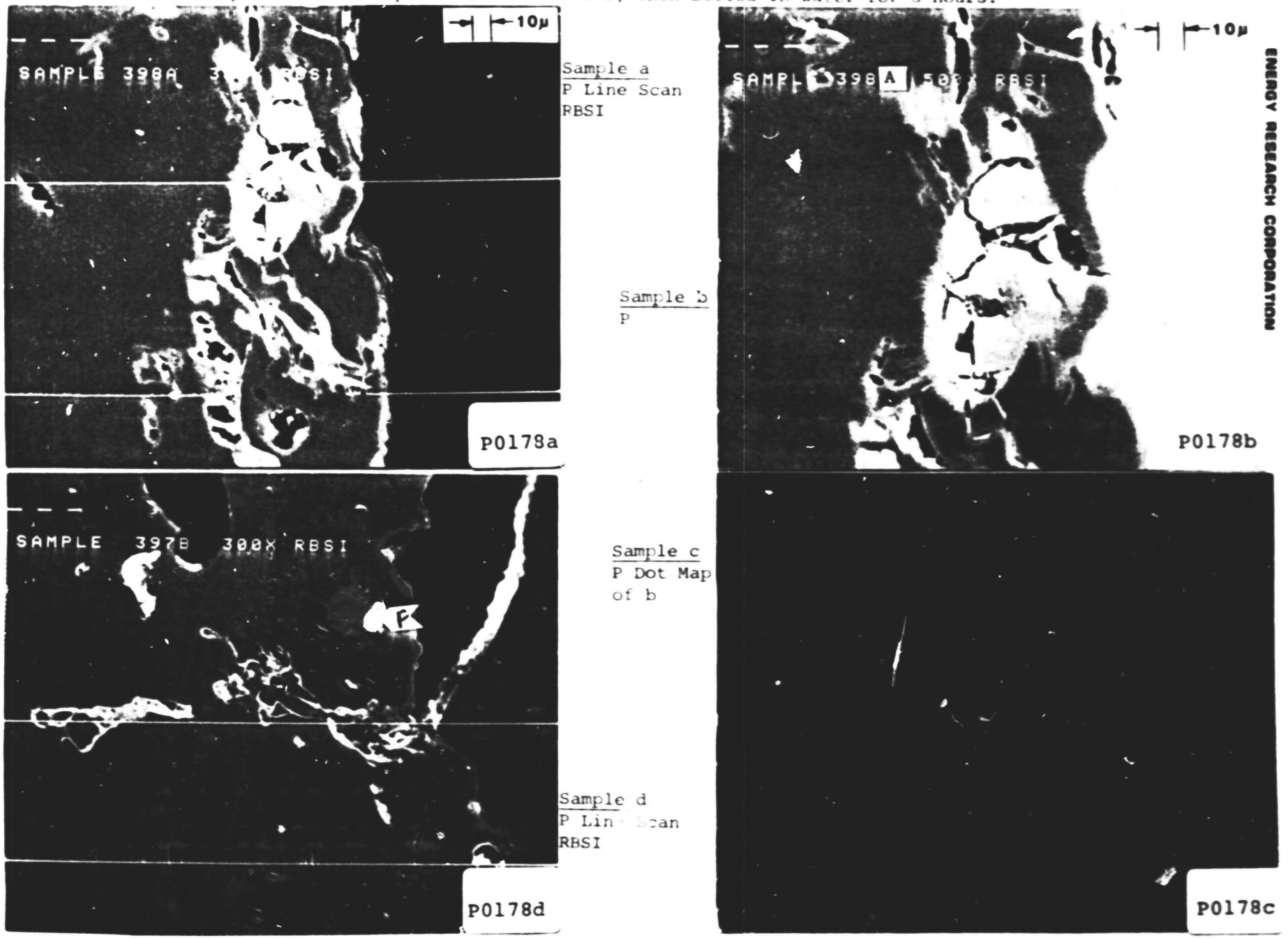

FIGURE 2.3 PHOSPHOROUS ADSORPTION BY COLLOID SAMPLES (100% COLLOID 8440)

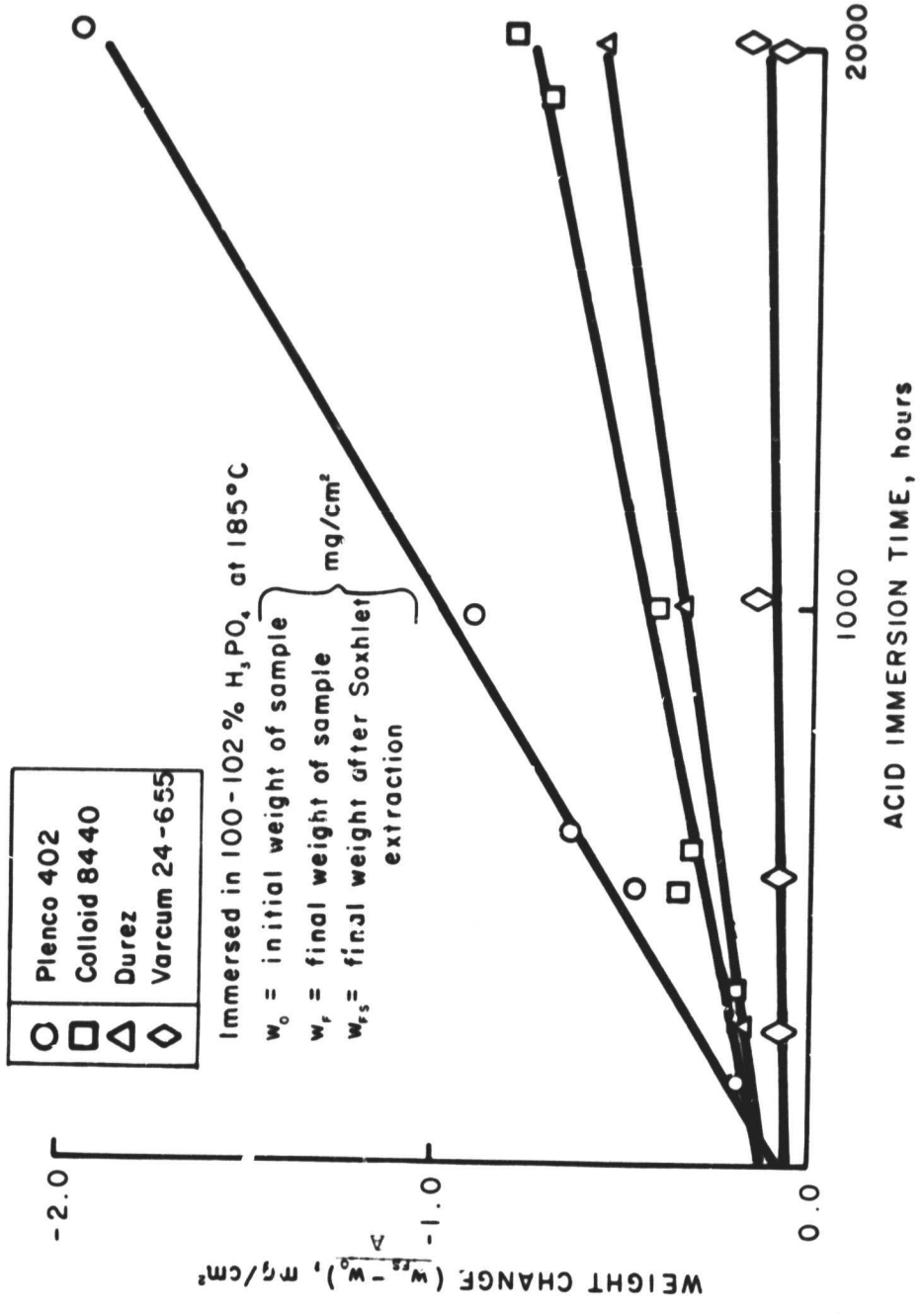

D1200

FIGURE 2.4 TRUE CORROSION CHARACTERISTICS OF 22% RESIN/78% A-99 GRAPHITE COMPOSITES

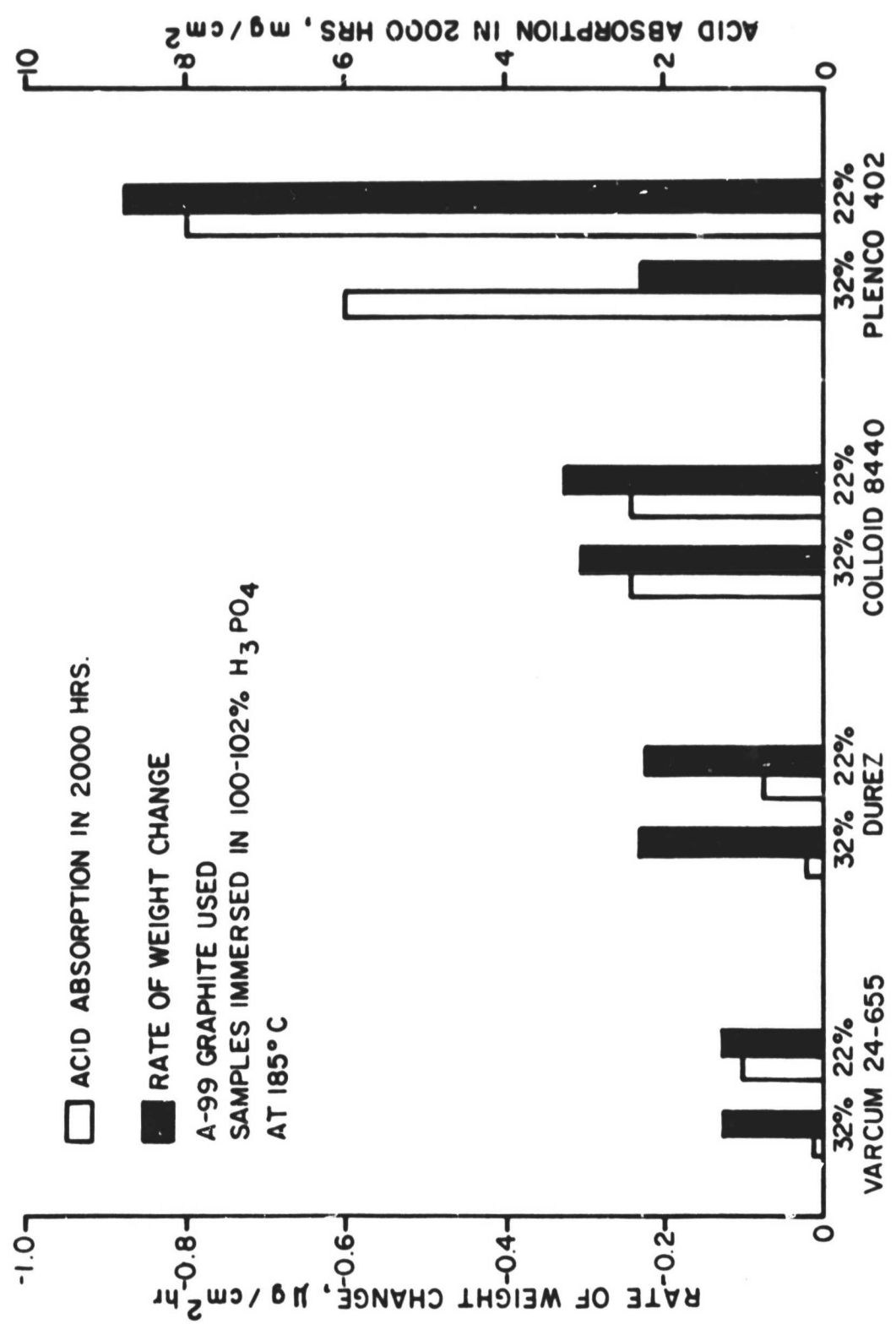

FIGURE 2.5 ACID ABSORPTION IN 2000 HOURS AND THE TRUE RATE OF WEIGHT CHANGE OF SEVERAL COMPOSITES

D1156

These findings are in accord with the SEM photographs of the corroded samples and also with our current notion of the nonpotentiostatic corrosion mechanism, i.e., that corrosion mostly advances via crack propagation and that acid absorption takes place along these cracks.

Measurements of the chemical corrosion and acid absorption were necessary for defining the corrosion characteristics expected for anode conditions. Electrochemical corrosion was not expected for potentials near reversible hydrogen but was expected to be very significant at cathode potentials greater than 0.8V vs RHE.

Slow Sweep Voltametric Corrosion Measurement

Investigation of the electrochemical corrosion required the design and construction of a cell. A cross-sectional view of this electrochemical cell is shown in Figure 2.6.

Teflon was used to make the body and its fittings, and a standard reversible hydrogen electrode was used as the reference. Test samples were mounted on Teflon supports with only one surface of the sample exposed to the electrolyte, and a same size Pt black counter electrode was used to ensure uniform current distribution. Electrical connections were accomplished via a 0.32 cm diameter stainless steel rod and a 0.06 cm diameter gold wire. The stainless steel rod, covered with heavy wall Teflon tubing, was kept above the electrolyte level and the gold wire was covered with heat shrinkable Teflon. The central plug provides a flexible option for choosing proper cell environment.

The electrochemical corrosion behavior of 32% Varcum 24-655 was studied in 100 to 102% H_3PO_4 at 191°C employing different environments. The following gases were bubbled through the electrochemical polarization cell for about four hours before

D0927

ITEM NO.	DESCRIPTION
1	BOTTLE
2	COVER
3	WORKING ELECTRODE TUBE
4	ELECTRODE HOLDER
5	REF ELECTRODE TUBE
6	PLUG
7	TOP PLUG
8	CENTER PLUG
9	PLUG
10	SET COLLAR
11	ELECTRODE ROD
12	TUBE
13	TUBE
14	THERMOMETER
15	SCREWS
16	SAMPLE ELECTRODE
17	NUTS
18	OUTER JAR
19	SET SCREWS
20	THERMO-COLLAR

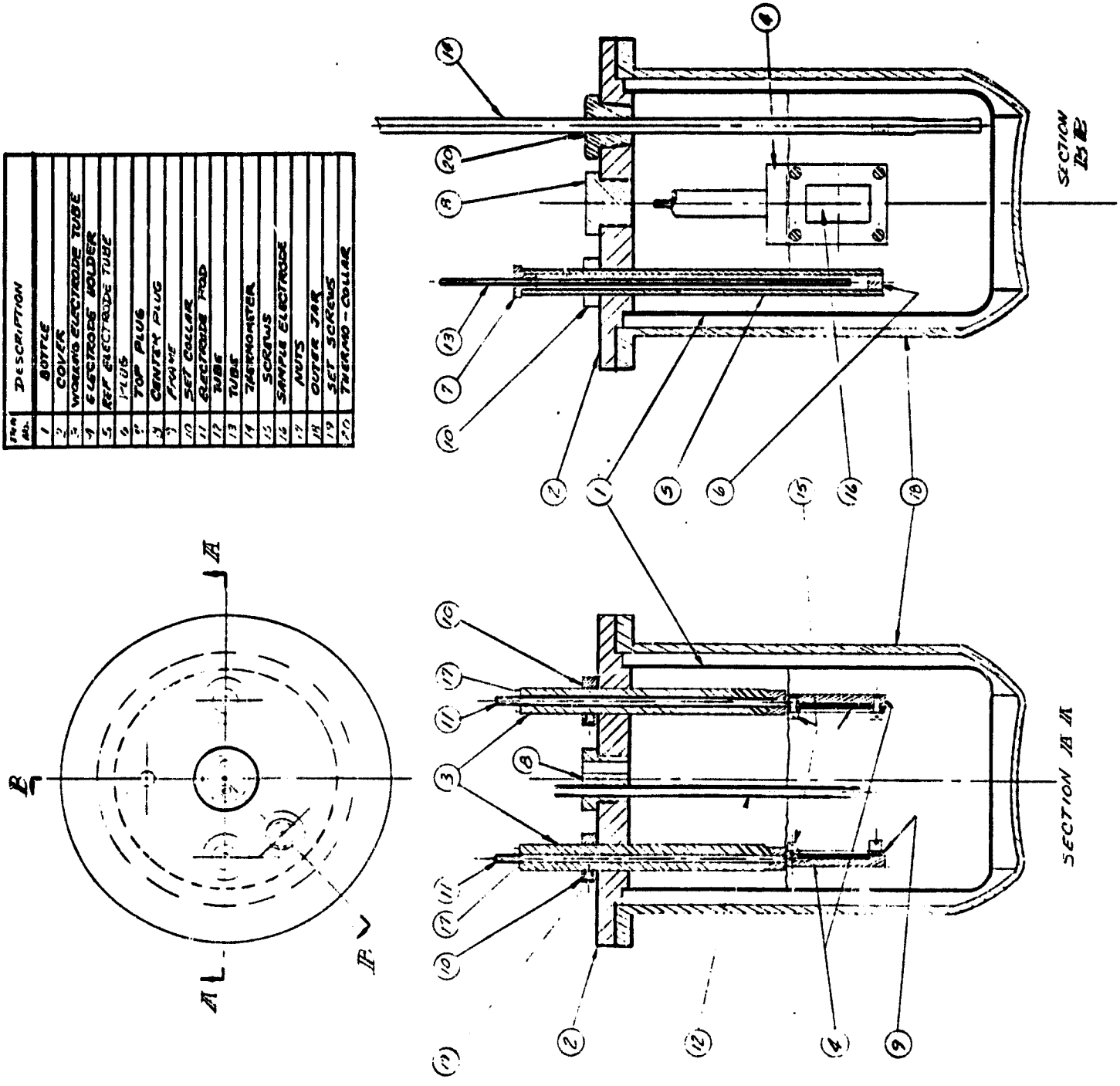

FIGURE 2.6 CROSS-SECTIONAL VIEWS OF THE CORROSION CELL

starting polarization of the sample:

- Oxygen (O_2)
- Nitrogen (N_2)
- Carbon Dioxide (CO_2)
- Air.

The corresponding polarization curves are shown in Figure 2.7. All curves appeared to be similar in nature in the potential range of 0.60 to 1.0V (RHE) while in the lower potential range of 0.45 to 0.575V (RHE) some scattered points were observed. This scattering may be partly due to the oxidation of impurities at lower potential. The kinetic parameters corresponding to the corrosion reactions are tabulated in Table 2.5. The large Tafel slopes for these nonheat-treated materials do not appear to be diffusion limited when compared with the heat-treated data presented in Figure 2.8. Assuming that diffusion is not important, the data suggest that the overall corrosion reaction is one with water since previously mentioned surface analyses had ruled out a reaction with phosphoric acid. The shape of the current-potential curve does suggest that different mechanisms or different reaction sites are important in the various potential ranges. Additional work would be required to elucidate the detailed mechanisms.

To investigate the possibility that the reaction pathway may shift as the reaction advances, polarization studies were performed on 32% Varcum 29-703 composite at three different stages of the corrosion reaction. Corresponding corrosion currents observed at different polarization potentials at 182°C are reported in Figure 2.9. Tafel slopes observed after 64 and 128 hours of corrosion are the same but significantly different from the slopes observed after eight hours of corrosion. Transfer coefficients, α, and activation energies calculated from exchange current density against 1/T plots are reported in Table 2.6

ORIGINAL PAGE IS
OF POOR QUALITY

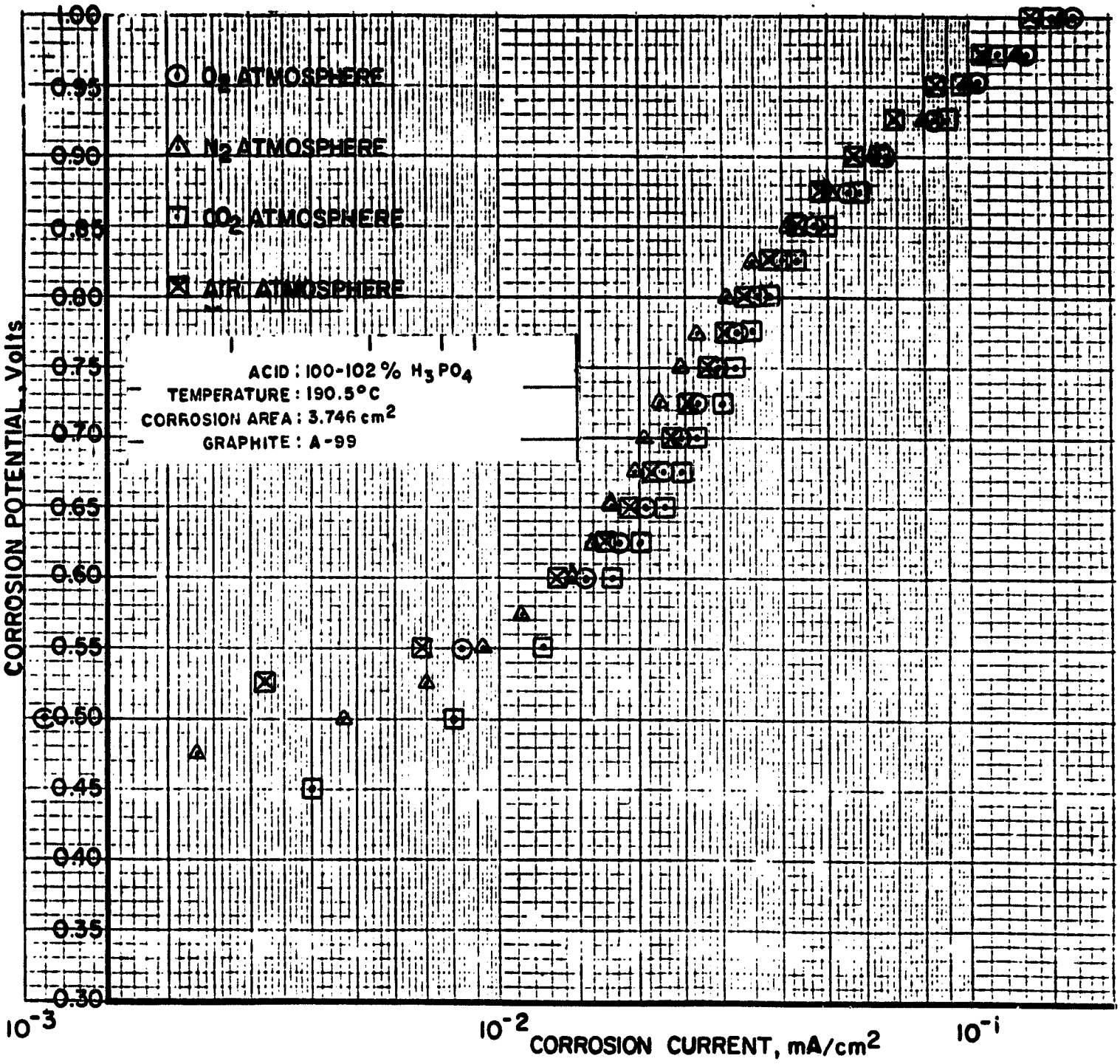

FIGURE 2.7 EFFECT OF ENVIRONMENT ON THE ELECTROCHEMICAL CORROSION OF A 32% VARCUM 24-655 SAMPLE

TABLE 2.5

KINETIC PARAMETERS OF VARCUM COMPOSITE CORROSION REACTION IN DIFFERENT ENVIRONMENTS

ENVIRONMENTAL GASES	POTENTIAL RANGE BETWEEN 0.8 AND 1.0V (RHE)		
	EXCHANGE CURRENT DENSITY, i_o, A/cm^2	TAFEL SLOPE $\frac{RT}{\alpha_2 F} \times 2.303$, mV/decade	TRANSFER COEFF. α_2
CO_2	1.5×10^{-7}	299	0.31
N_2	0.5×10^{-7}	253	0.37
O_2	0.7×10^{-7}	267	0.36
Air	1.1×10^{-7}	290	0.32

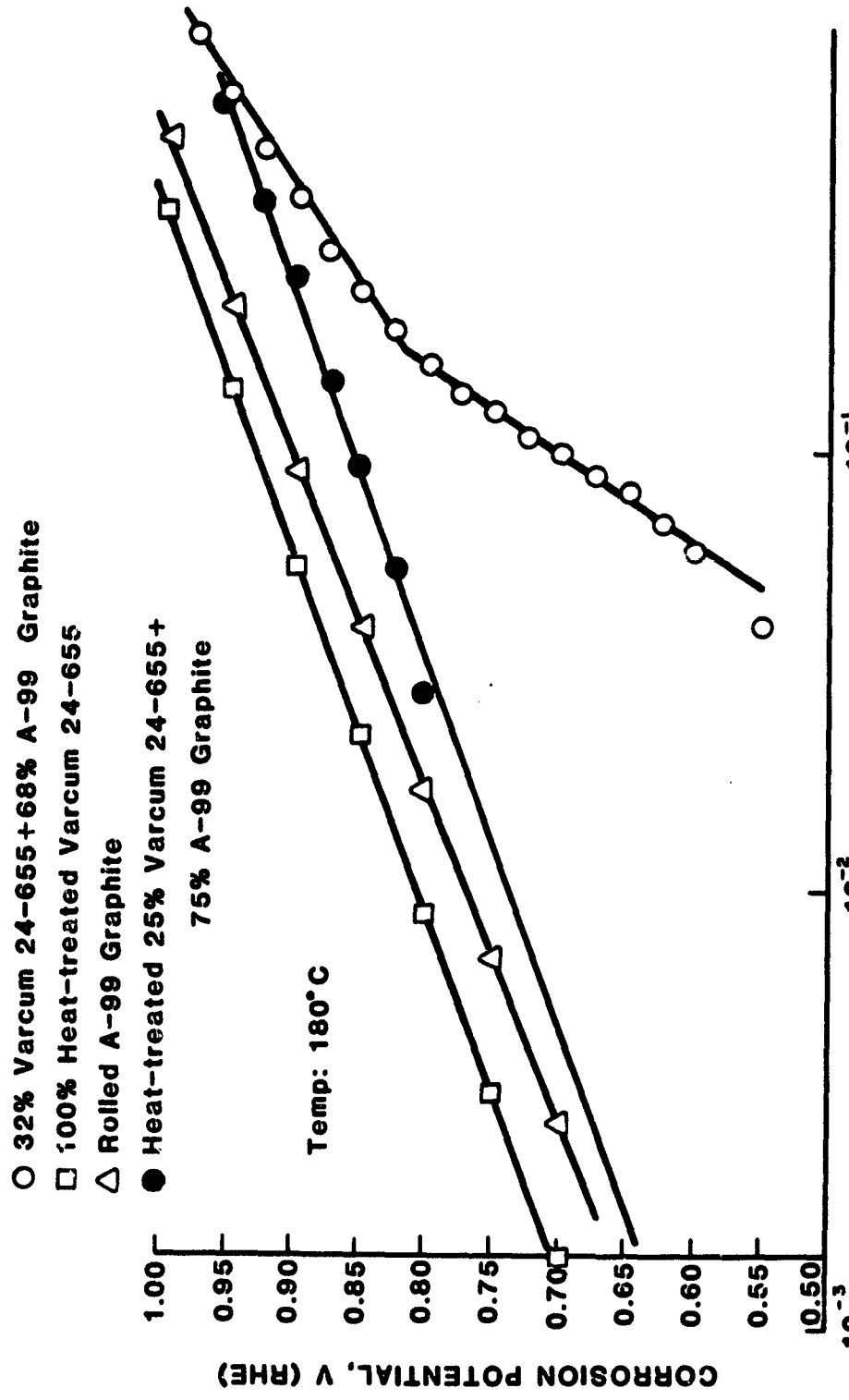

FIGURE 2.8 POLARIZATION CURVES OF VARIOUS BIPOLAR PLATE MATERIALS

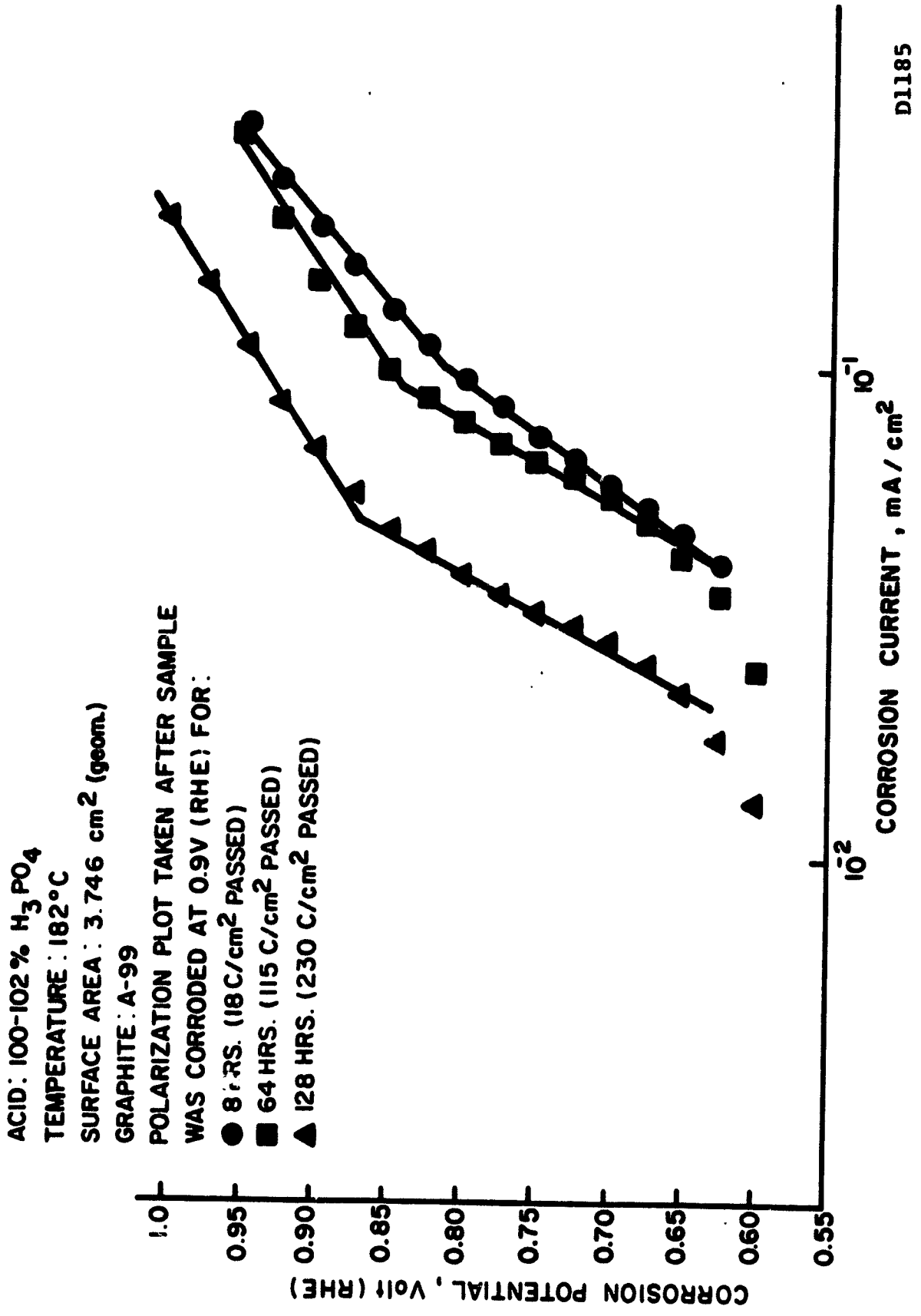

FIGURE 2.9 EFFECT OF CORROSION ON THE POLARIZATION PLOT OF A 328 VARCUM 29-703 COMPOSITE

TABLE 2.6

CHANGE OF REACTION PARAMETERS WITH CORROSION

CORROSION AT 0.9V (RHE) PRIOR TO POLARIZATION STUDY	0.625 to 0.825V (RHE)		0.825 to 1.0V (RHE)	
	AVERAGE TRANSFER COEFF. $\overleftarrow{\alpha}_1$	ACTIVATION ENERGY kcal/mol	AVERAGE TRANSFER COEFF. $\overleftarrow{\alpha}_2$	ACTIVATION ENERGY kcal/mol
8 Hours (18 C/cm^2 passed)*	0.20	13	0.35	12
64 Hours (115 C/cm^2 passed)	0.16	49	0.45	44
128 Hours (230 C/cm^2 passed)	0.17	41	0.47	39

*C = coulombs.

and Figure 2.10 for two different cases. Activation energies were similar for the samples corroded over 64 hours and 128 hours but significantly higher than the sample corroded for eight hours. This suggests the presence of a faster reaction during the initial period and is possible related to the corrosion of a surface skin.

Observations Relative to the Mechanism of Corrosion

All electrochemical results for nonheat-treated composite materials showed that transfer coefficients and exchange current densities were distinct in two different potential ranges. This seems to represent two reaction mechanisms in the potential range of 0.5 to 1.0V (RHE).

The observed current density, i, at any potential, V, is represented as the sum of currents, i_1 and i_2, contributed by the individual reactions.

$$i = i_1 + i_2$$

$$= i_{o_1} \exp [(V-E)\ \alpha_1 F/RT] + i_{o_2} \exp [(V-E)\ \alpha_2 F/RT]$$

Where,

i_o = exchange current density

E = theoretical open circuit potential

α = transfer coefficient

The predominance of one reaction over the other depends on the electrode potential, exchange current density, transfer coefficients and the operating temperature. Depending on the resin type, pretreatments and temperatures, the 'change-over' potential (at which the predominance of one mechanism over the other occurs) varied between 0.775 and 0.95V (RHE).

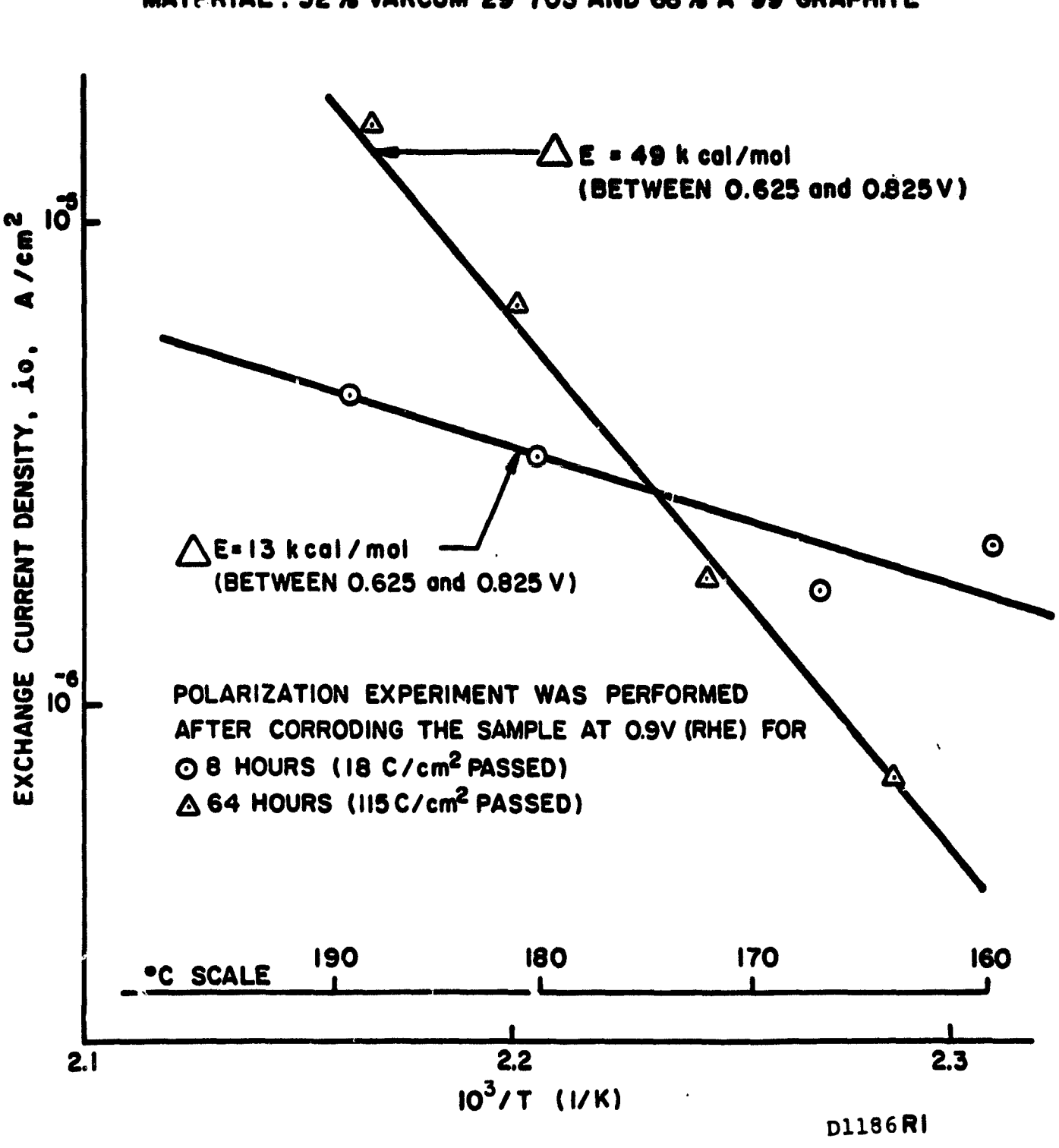

FIGURE 2.10 ENERGY OF ACTIVATION

This changeover potential, evaluated from the point of intersection of two straight lines on the polarization plot for 32% Varcum 29-703 (Figure 2.9), is plotted against operating temperatures for three different pretreatments (Figure 2.11). The changeover potential is observed to decrease as the temperature increases.

It is apparent from the polarization data of the nonheat-treated composite samples that the overall half cell carbon corrosion reaction represented as:

$$C(s) + 2\,H_2O(l) \rightarrow CO_2(g) + 4H^+ + 4e^-;\ E_{o,\ 25°C} = 0.21V\ (RHE)$$

shows two different reaction mechanisms or there are two different reaction sites. Reported in Table 2.7 are: Tafel slopes, b; transfer coefficients, α; exchange current densities, i_o; and activation energy ΔE, for two nonheat-treated materials. The theoretical open circuit corrosion potential (TOCP) E_T, used for the evaluation of the exchange current densities was calculated using:

$$E_T = E_o + \frac{RT}{4F} \ln \left[\frac{a^2_{H_2O\ (l)}}{a_{CO_2} \quad x \quad a^2_{H_2}\ (g)}\right]$$

and assuming that the electrolyte present on the surface of the sample is saturated with CO_2 (i.e. for calculation purposes a_{CO_2} is 1.)

The following important observations for the nonheat-treated composite samples can be made from the calculated electrochemical parameters, as reported in Table 2.7.

- Tafel slopes and transfer coefficients differ in the different potential regions.
- As expected, Tafel slopes increase with temperature. Activation energies for both reactions are between 10 and 13 kcal/mol.
- Nonsensitivity to the gas atmosphere supports the choice of the overall reaction as $C + 2H_2O$.

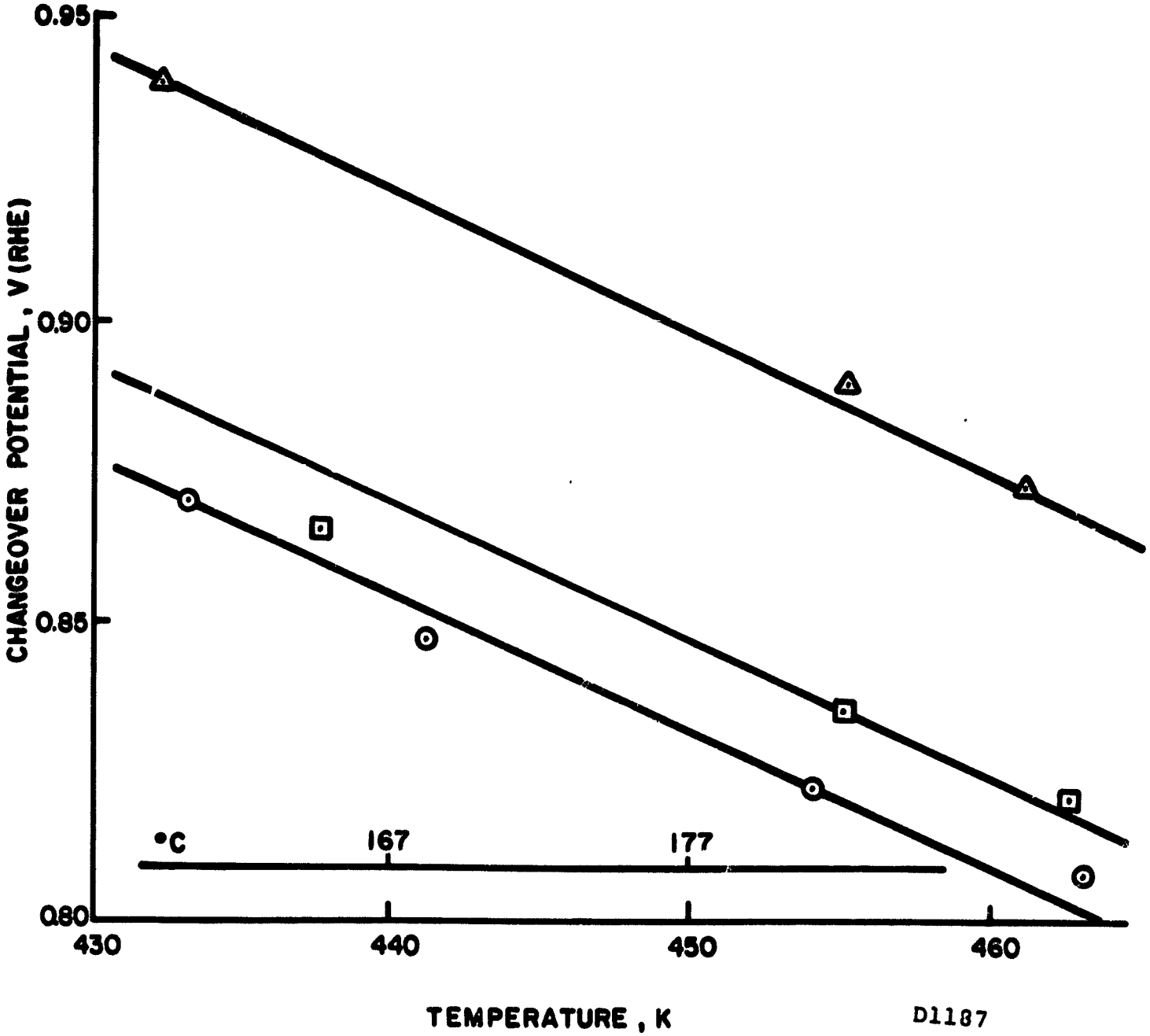

FIGURE 2.11
EFFECT OF TEMPERATURE ON THE CHANGEOVER POTENTIAL
OF 32% VARCUM 29-703

TABLE 2.7

KINETIC PARAMETERS OF THE ELECTROCHEMICAL CORROSION REACTION

SAMPLE	TEMP., °C	BETWEEN 0.60 AND 0.80V (RHE)				BETWEEN 0.825 AND 1.0V (RHE)			
		TAFEL SLOPE $b = \frac{RT}{\overleftarrow{\alpha}} \times 2.303$, V/decade	TRANSFER COEFFICIENT $\overleftarrow{\alpha}$	EXCHANGE CURRENT DENSITY i_o, (A/cm^2) x 10^6	ACTIVATION ENERGY ΔE, kcal/mol	TAFEL SLOPE $b = \frac{RT}{\overleftarrow{\alpha}} \times 2.303$, V/decade	TRANSFER COEFFICIENT $\overleftarrow{\alpha}$	EXCHANGE CURRENT DENSITY i_o, (A/cm^2) x 10^6	ACTIVATION ENERGY ΔE, kcal/mol
22% Plenco 402 + 78% A-99 Graphite	190.0	0.625	0.147	37.6	10.1	0.299	~ 310	1.98	11.25
	183.4	0.590	0.154	32.9		0.309	0.290	2.30	
	167.8	0.531	0.160	23.0		0.297	0.290	1.20	
22% Varcum 29703 + 78% A-99 Graphite	190.0	0.586	0.156	16.2	13.1	0.222	0.417	0.16	10.90
	183.3	0.600	0.152	15.2		0.231	0.400	-	
	173.9	0.575	0.154	10.9		0.280	0.320	0.18	
	166.7	0.540	0.161	6.6		0.231	0.378	0.11	

The kinetic parameters, especially α and ΔE, enable us to predict the corrosion rates corresponding to other operating temperatures and potentials for which the experimental results are not available. As an example, according to the calculations shown below, at a cathode potential of 0.75V, the expected 22% Varcum bipolar plate corrosion rate, i_2, at 190°C in 100% acid is expected to be about twice the corrosion rate, i_1, observed at 177°C and at 0.65V cathode potential.

$$\frac{i_2}{i_1} = \exp\left[\frac{-\Delta E}{R}\left(\frac{1}{T_2} - \frac{1}{T_1}\right)\right] \times \exp\left[\frac{\alpha F}{R}\left(\frac{V_2 - E_{T_2}}{T_2} - \frac{V_1 - E_{T_1}}{T_1}\right)\right]$$

$$= \exp\left[\frac{-13.1 \times 10^3}{1.987}\left(\frac{1}{463} - \frac{1}{450}\right)\right] \times \exp\left[\frac{0.154 \times 96493}{8.31}\right.$$

$$\left.\left(\frac{0.75 - -0.11}{463} - \frac{0.65 - -0.13}{450}\right)\right]$$

$$= 2.05$$

Heat treatment to 900°C has been used to improve both electrical and corrosion properties. The resin is converted to a glassy carbon at these temperatures, and therefore the resin/graphite composite becomes a glassy carbon/graphite composite. Slow sweep voltametric analyses were performed on several materials to distinguish the contribution of corrosion from the glassy carbon and the graphite. The polarization curves shown in Figure 2.8 demonstrate the decrease in corrosion current obtained by heat-treatment. Only one Tafel slope was evident over the potential range investigated which was quite different from the nonheat-treated plate. Both the glassy carbon and graphite exhibited less corrosion than the composite. This may indicate that stress corrosion may play an important role. More work is required in defining the effect of stress, heat-treatment temperature, and resin content.

Corrosion Measurements at a Constant Potential

Several composite samples were examined under constant potentiostatic corrosion conditions to evaluate the long-term relative corrosion characteristics. The effects of resin content on corrosion rate and structural integrity of the sample were also studied. These samples were potentiostatically corroded at 0.9V (RHE) in 100 to 102% H_3PO_4 at 190.5°C (± 0.5°C) for about 200 to 300 hours.

The corrosion rate decreased sharply for all 22% resin content samples after 140 to 200 hours of potentiostatic corrosion. It is speculated that beyond tne point where the rate starts falling sharply, the structural integrity of the sample deteriorates rapidly. After termination of the experiments, the 22% Colloid and Plenco samples were found to be completely disintegrated. The 22% Varcum sample was just holding together but the mechanical properties seemed to have deteriorated greatly and tiny blisters (probably caused by electrochemical gas generation beneath the resin 'skin') were also observed on the surface of the sample. There was no observable loss of physical strength in the cases of 32% Varcum 24-655 and 32% Varcum 29-703. Although SEM photographs of these samples did not reveal any sign of deterioration in the structural integrity, tiny blisters were visible on the surface. The rate of weight loss of various composites due to electrochemical corrosion is compared with the rate of weight loss due to self-corrosion in Figure 2.12.

Photomicrographs of electrochemically corroded and acid immersed samples are compared in Figure 2.13. The surface photomicrographs show that the electrochemical corrosion is much more severe than the chemical corrosion. The absence of cracks on the surface of the electrochemically corroded sample suggests that the corrosion may be different. SEM photographs

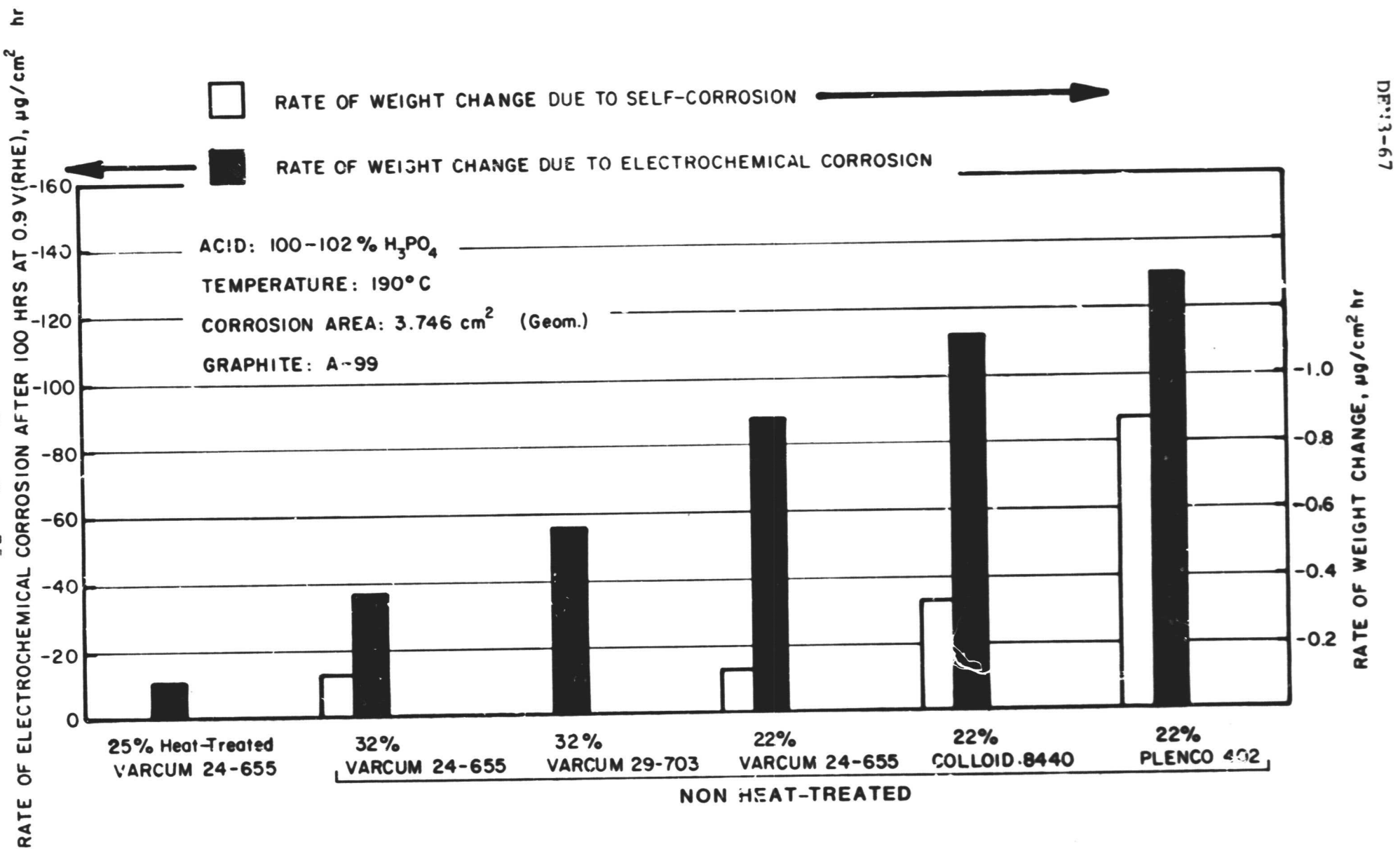

FIGURE 2.12 ELECTROCHEMICAL AND SELF-CORROSION OF DIFFERENT SAMPLES AT 0.9V (RHE) AND 190°C

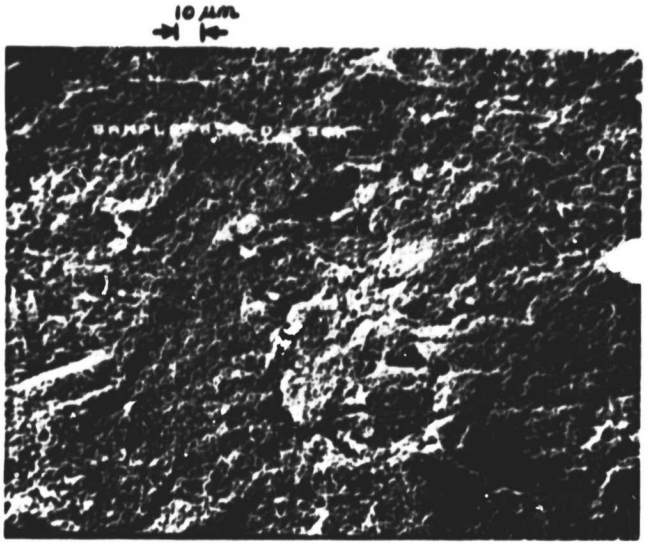

Unpolished surface (650X)

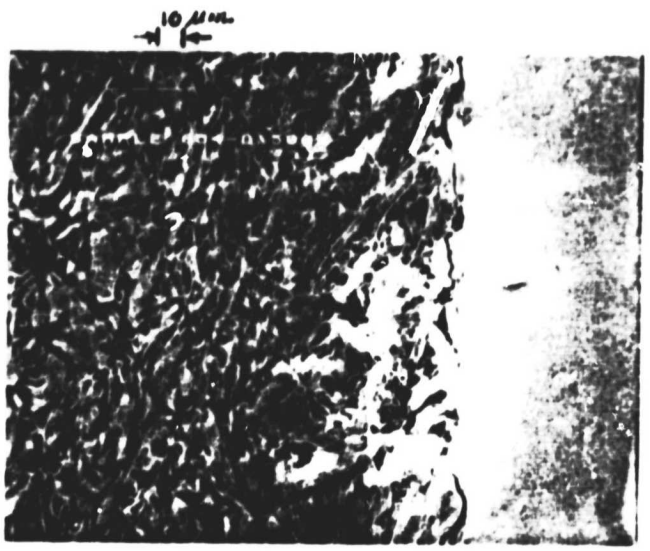

Polished Edge (500X)

PO235

32% VARCUM 24-655 IMMERSED IN 100-102% H_3PO_4 AT 185°C FOR 1000 HOURS

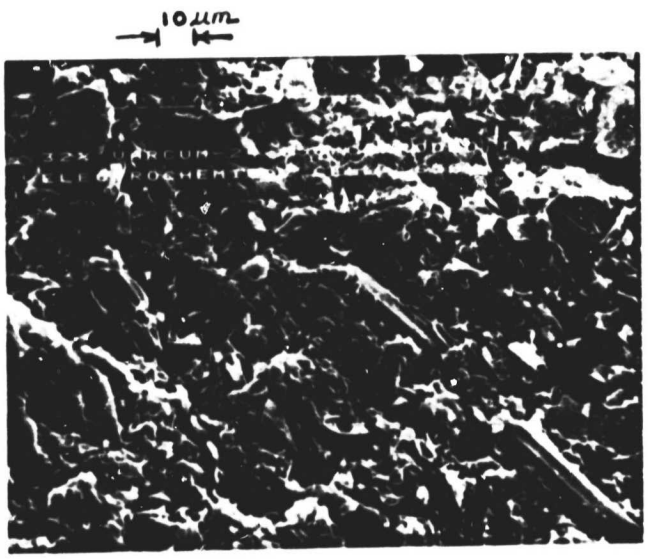

Unpolished surface (650X)

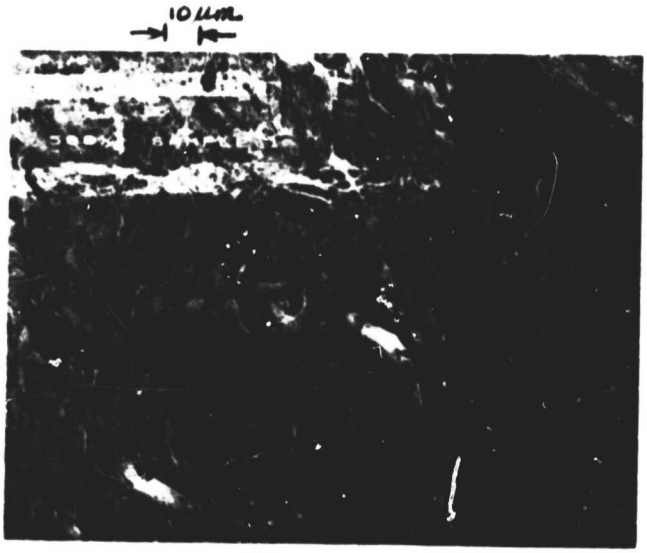

Polished Edge (500X)

PO236

32% VARCUM 24-655 CORRODED IN 100-102% H_3FO_4 AT 0.9V AND 190°C FOR 360 HOURS

FIGURE 2.13

COMPARISON OF ETCHED SURFACES OF ELECTROCHEMICALLY CORRODED AND ACID IMMERSED SAMPLES

of the edges illustrate that in both samples of 32% Varcum 24-655, corrosion is predominantly localized on the surface.

The high rate of corrosion under electrochemical polarization conditions is probably related to: enhanced corrosion of carbon atoms at the binding sites; electrochemical oxidation of the resin present at the bond sites; and/or attack on the binding resin by the peroxide radical which is one of the plausible intermediates in the reaction pathway of graphite $\rightarrow CO_2$.

It is obvious from Figure 2.12 that, among the other evaluated samples, the 25% heat-treated Varcum 24-655 has exhibited the lowest rate of weight loss due to the electrochemical corrosion.

2.2 Physical Property Measurements

Development of large fuel cell stacks and new components requires a baseline of engineering data. Much of this data were not available from the literature or previous contracts. A few of the most critical material properties as listed below were chosen for investigation. Backing paper properties were considered to be important in understanding the effects of stack compression. Flowability of resin/graphite mixtures was necessary to improve the molding cost and uniformity. Basic properties of the nonheat-treated compression molded composite materials was vital in identifying the direction for performance improvements which was confirmed by the heat-treated material measurements.

The following properties were investigated:

- Backing paper - thickness and compressibility;
- Phenolic Resin/graphite - flowability;
- Molded resin/graphite composites - compressibility, density, electrical properties, and thermal conductivity;

- Heat-treated composites - thermal conductivity and electrical properties.

Backing Paper

Backing paper thickness as shown in Figure 2.14 is affected by Teflon FEP content and compression. These relatively soft components allow considerable compression during cell assembly and operation. Scanning electronmicrographs of stackpole fibrous mats with and without Dupont FEP are shown in Figures 2.15 and 2.16. It is apparent that the structure remains open after applying the FEP. An open hydrophobic structure is required for adequate gas transport to the electrode.

Phenolic Resin/Graphite Mixes

Flow tests were used to evaluate and screen thermoset resin/graphite materials for bipolar plates. The molding parameters and density of bipolar plates were a function of how much the material flowed during compression molding.

Preformed disks of graphite/resin (5.7 cm diameter and 35 grams in weight) were compressed between flat steel plates to evaluate their flow characteristics. After pressing to a set pressure, the disk thickness and diameter were found to be dependent on the percentage of resin and the temperature of the steel plates. Based on the assumption that the flowability of the composites is inversely proportional to the thickness at the center of the pressed disk, a flow index was defined and calculated:

$$f = \frac{C_1}{T}$$

Where,

f = Flow Index

T = Final Thickness (inches)

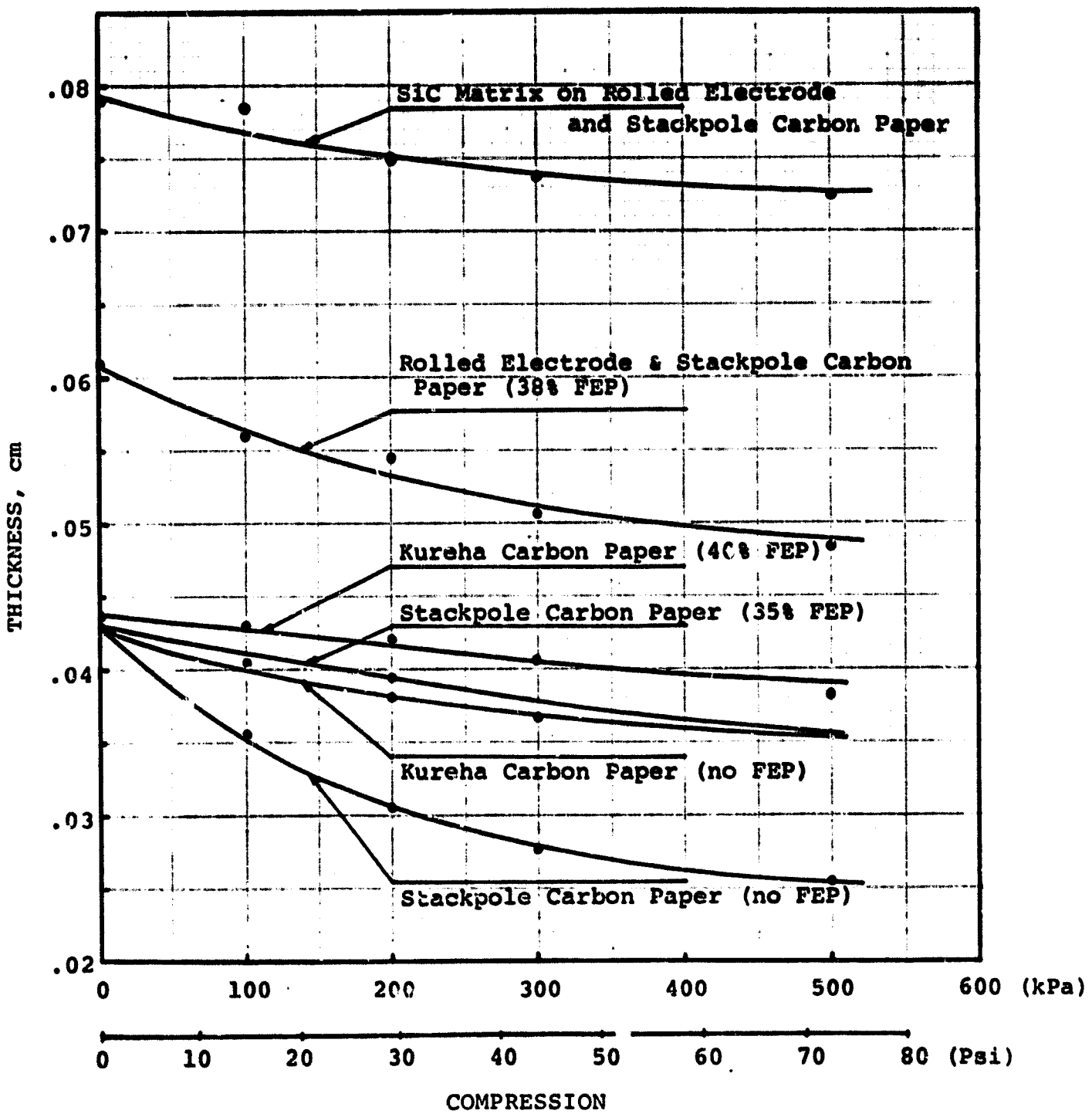

FIGURE 2.14 VARIATION OF CELL COMPONENT THICKNESS AT DIFFERENT PRESSURES

D0484

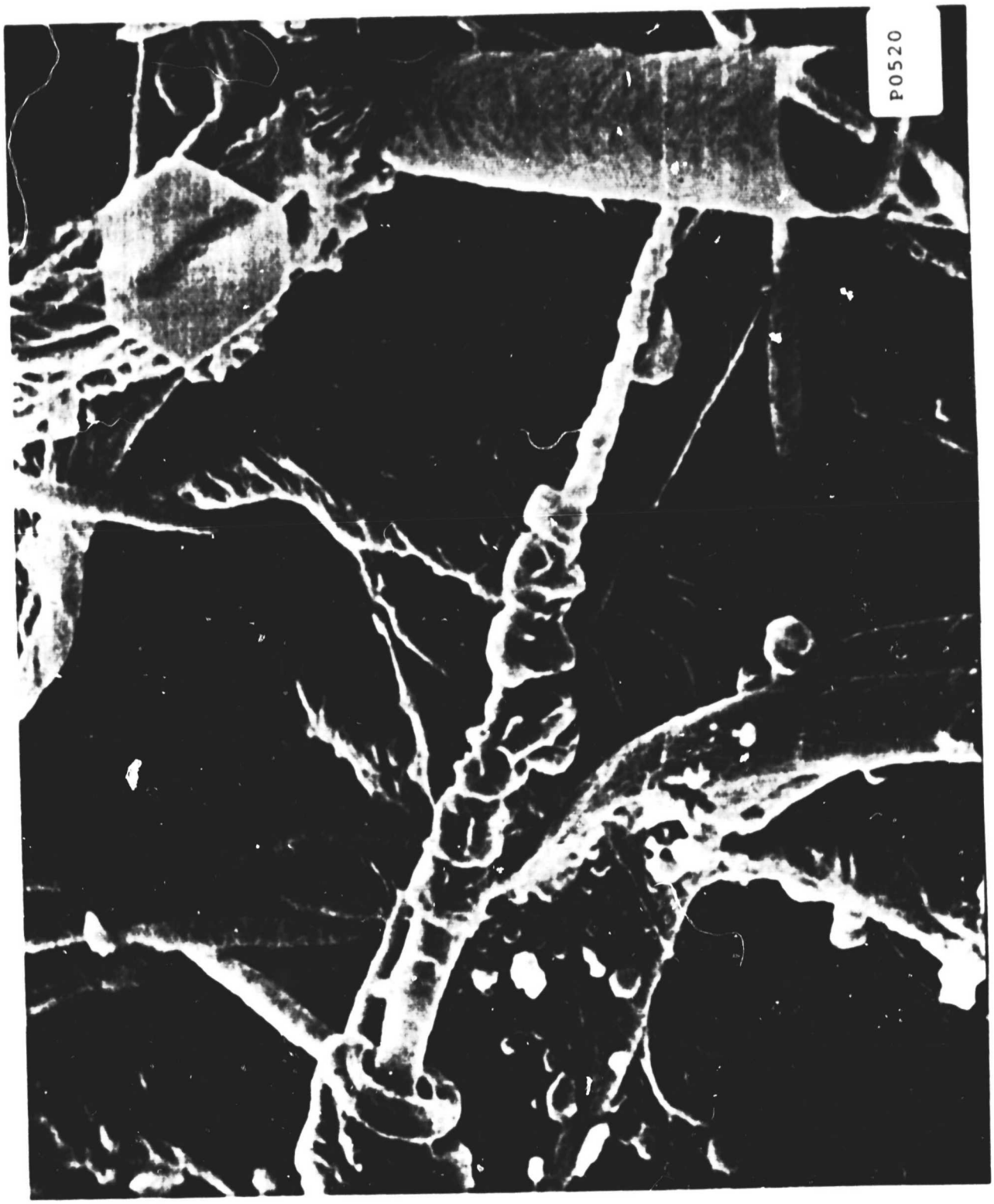

FIGURE 2.15 PACKING PAPER WITH FEP

ENERGY RESEARCH CORPORATION

ORIGINAL PAGE
BLACK AND WHITE PHOTOGRAPH

FIGURE 2.16 BACKING PAPER WITHOUT FEP

The factor C_1 was arbitrarily selected to be 0.05 so that values of f are close to unity. Figure 2.17 shows a plot of temperature against flow indices for a typical graphite/resin composite. The maximum flow for Varcum 24-655 occurs between 130°C and 145°C, and for Colloid 8440 between 140°C and 155°C. At temperatures below 130°C, the composite materials were thermoplastic, requiring cooling under pressure to achieve a uniform, dense material.

Changes in the amounts of resin also affect the flow which decreased with decreasing resin content as shown in Figure 2.18. The addition of flake graphite (Asbury 850) while maintaining a constant wt% resin slightly increases the flow. For example, by substituting the standard graphite with a flake graphite (Asbury 850), the flow index increased ~ 11%.

The above flow tests were made using flat steel plates as dies. The effect of ribbed plates on the flow was also investigated. A flow test using two ribbed plates did not yield a circular disk after pressing. The graphite/resin tends to flow in the direction of the ribs, which distorts the former circular pattern obtained between flat steel plates. The amount of flow was not observed to decrease due to the ribbed dies, but the direction of flow was changed. The effects of preheating the preforms and additives of organosilane ester on the flow of molding compounds were also evaluated.

Preheating graphite/resin preforms prior to compression molding produced no significant advantage in flow by the flow test and actual pressing of 400 cm^2 bipolar plates. Preheating the material did improve the moldability of thick parts (greater than 0.8 cm) in that blistering was avoided.

Additions of 1 and 3% Union Carbide A-189 organosilane ester were made to graphite/Colloid 8440 composites. Silane additives are reported to promote bonding between some resin

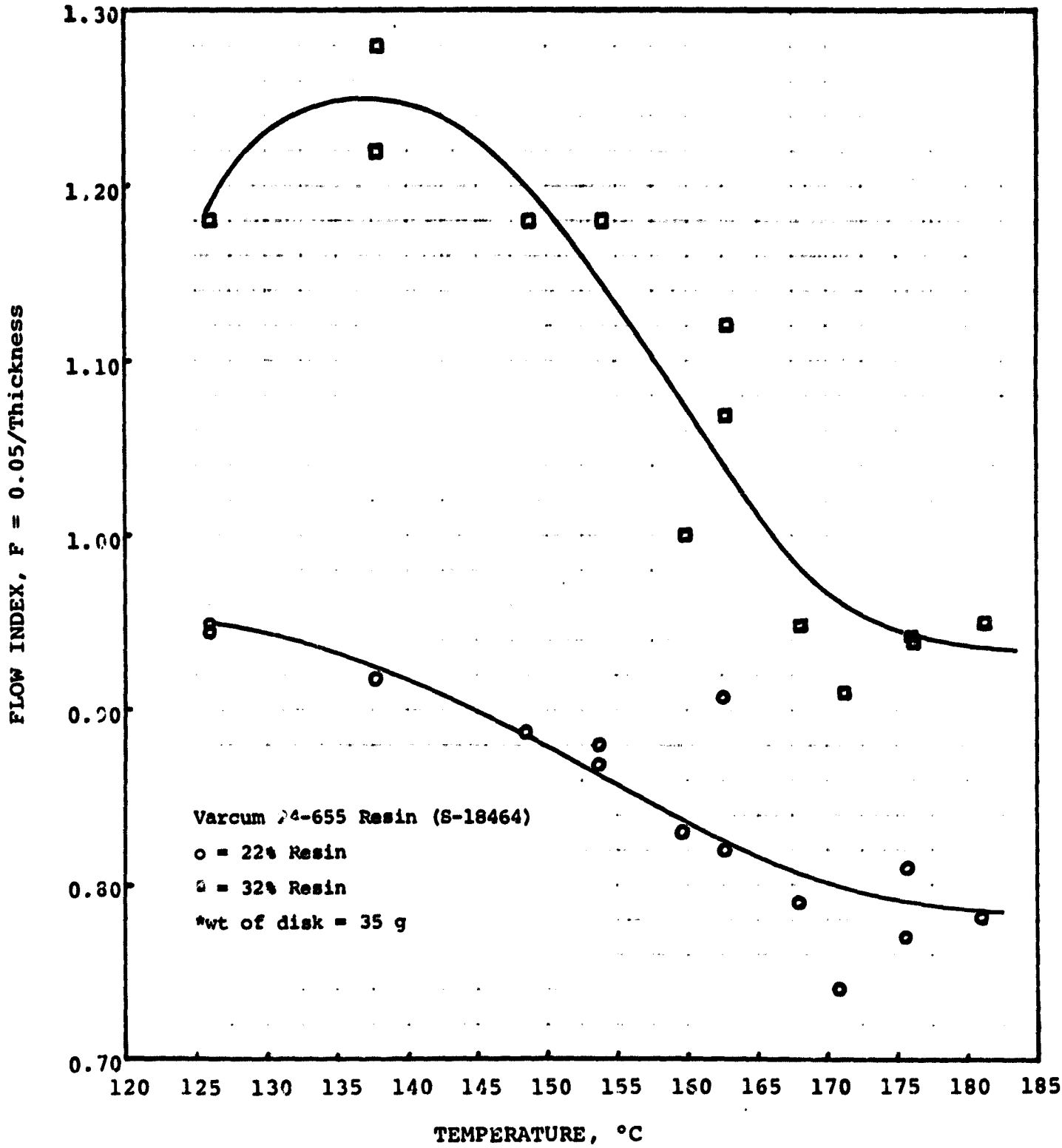

FIGURE 2.17 FLOW VARIATIONS OF A-99 GRAPHITE/VARCUM RESIN AGAINST TEMPERATURE

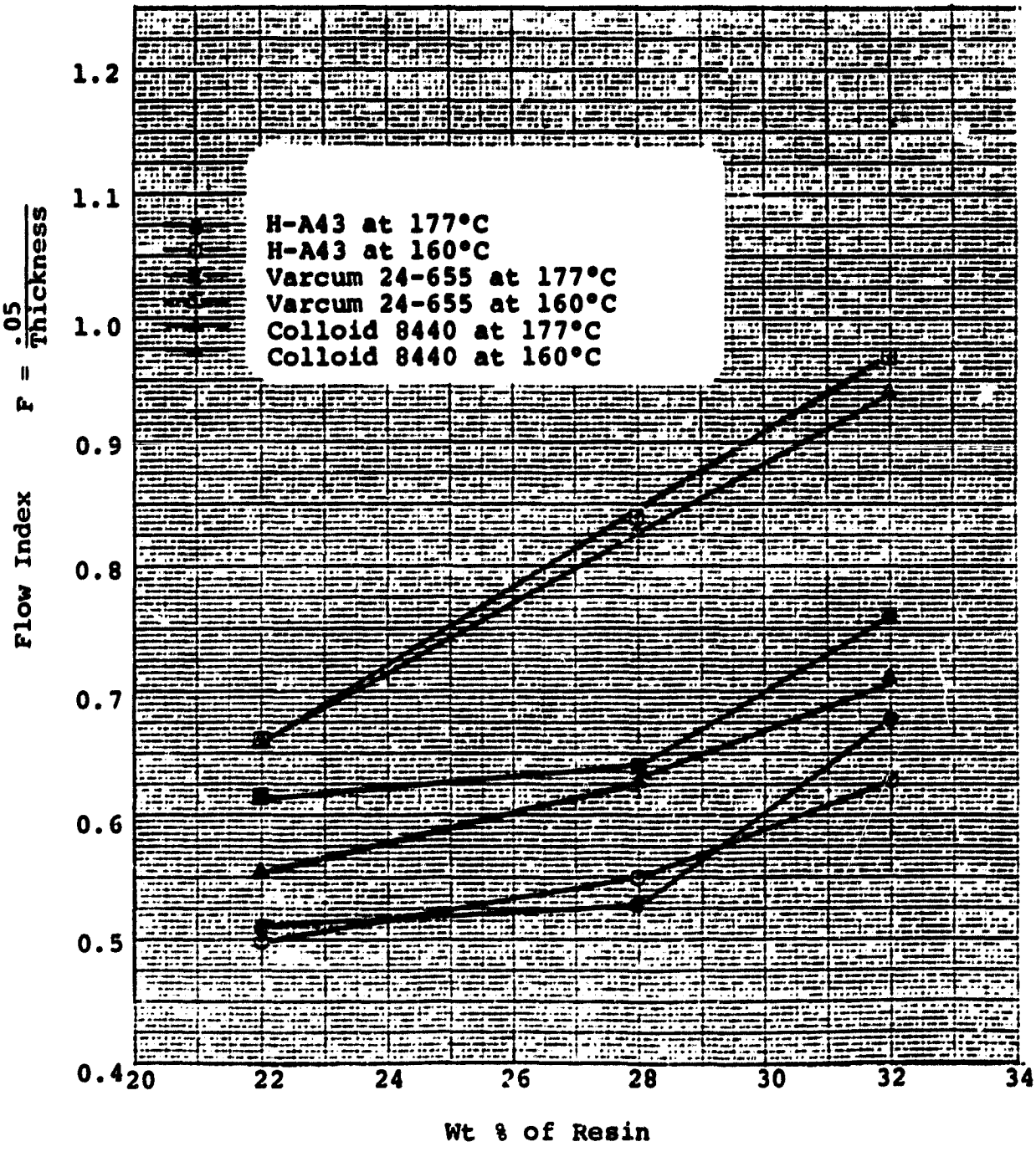

FIGURE 2.18 FLOW VARIATION OF A99 GRAPHITE/RESIN

and filler systems, resulting in a stronger material. The silane addition did not significantly improve the flow of the material, and the fumes from the addition were extremely odorous.

Molded Resin/Graphite Composites

Compression tests of the nonheat-treated bipolar plate material were conducted to characterize its behavior in large stacks. Several test samples (one inch square) were prepared from a few bipolar plates; Table 2.8 summarizes the test results. When a sample was compressed, two major inflections occurred. Visual observation suggested that the first inflection may correspond to the breaking of a surface skin on the cathode side ribs and the second inflection to the breaking of a surface skin on the anode side ribs. As shown in Table 2.8, the unused plate shows less variation of inflection load than for the used plates. This fact has been interpreted as an indication of deterioration of the plate. Figure 2.19 shows a typical compression curve for two different samples.

Densities of samples cut from pressed 10 cm x 10 cm plates and from flow test specimens were measured before and after post-cure. The densities decreased after post-cure and also decreased with increasing resin content as expected. The post-cure treatment consisted of the following steps:

1. 146°C for two hours
2. 182°C for two hours
3. 204°C overnight.

Heat-treated and Nonheat-treated Composites

The thermal and electrical properties of cell components are important to the performance of fuel cell stacks. Thermal

TABLE 2.8

BIPOLAR PLATE COMPRESSIBILITY*

PLATE	CELL HOURS	SAMPLE NO.	FIRST INFLECTION		SECOND INFLECTION	
			LOAD, kg	COMPRESSION, cm	LOAD, kg	COMPRESSION, cm
5638	0	A	940	.083	1160	.150
		C	940	.079	1130	.142
		D	860	.074	----	----
5717	5218	O	690	.064	----	----
		P	520	.066	770	.114
		Q	920	.081	1040	.132
		R	930	.076	910	.114
5694	4490	H	800	.071	610	.119
		I	1090	.084	1240	.129
		J	750	.069	700	.122
		K	780	.074	610	.119
5693	1533	1A	790	.071	1120	.142
		1D	725	.074	1020	.135

*Plates contain 33.5% Colloid Resin and 66.5% Graphite (Asbury A99 and 850).

C-2

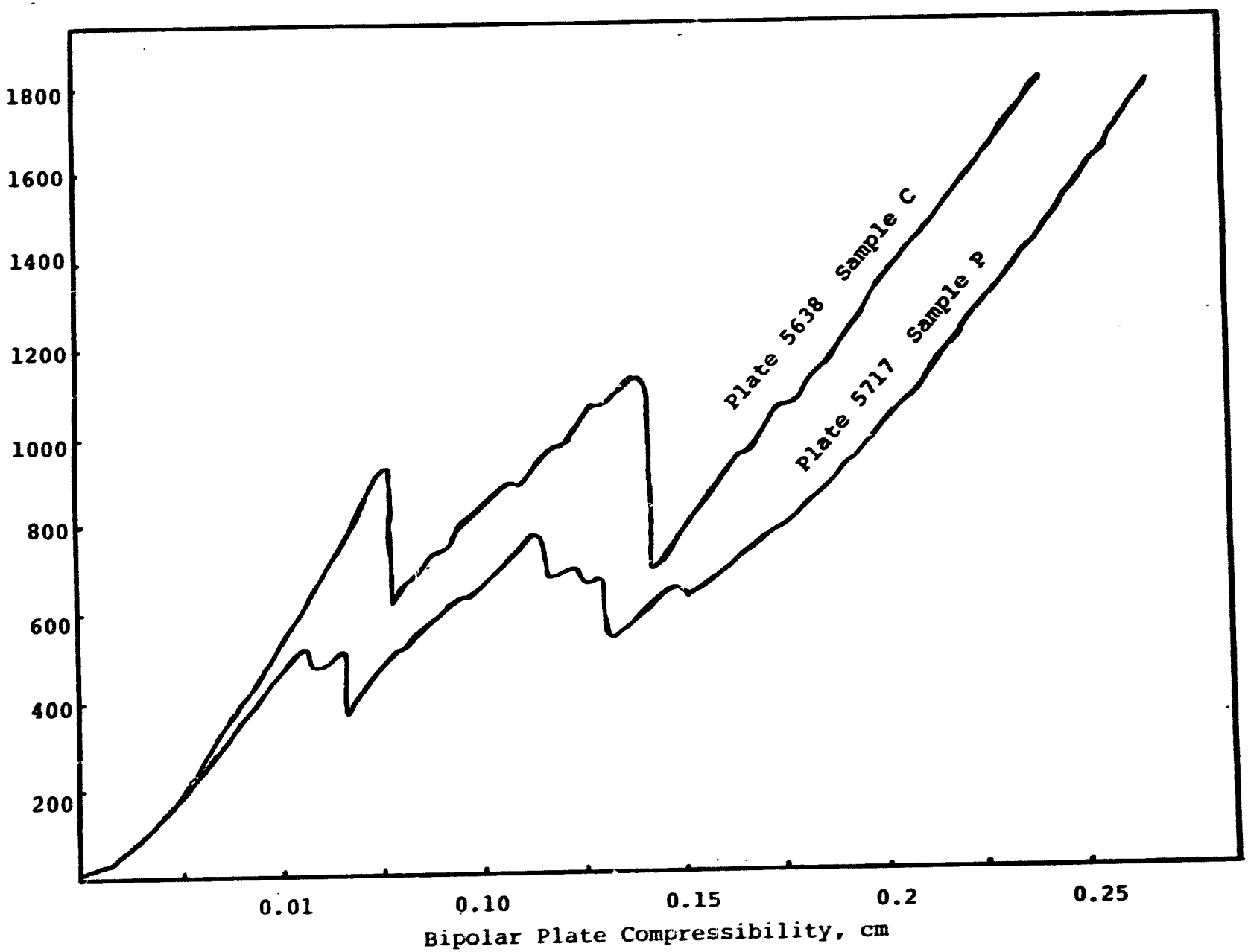

FIGURE 2.19 BIPOLAR PLATE COMPRESSIBILITY

conductivity of the heat-treated and nonheat-treated materials was evaluated in the "in-plane" direction which is the direction of heat removal. Heat-treatment of the plate increased the conductivity from 5.3 $Wm^{-1}K^{-1}$ to 7.7 $Wm^{-1}K^{-1}$. The 50% increase in plate thermal conductivity will significantly decrease its importance relative to the backing paper, matrix and electrodes. The contribution of these cell components requires additional study.

Electrical conductivity in the current flow direction is critical to optimizing cell performance. Although the details of the measurements are described below, Table 2.9 summarizes our best estimate of the various resistances that make up the observed stack resistance. It appears that the contact resistances and the matrix resistance are the main contributors.

Factors accounting for the difference between the total of the calculated values and stack measurements include: the current collectors in the stack, the pressure distribution, the percent porosity of the matrix, the acid distribution, the actual electrical conductivity of the acid, and errors in physical dimension measurements for samples used in resistivity measurements.

The values in Table 2.9 were determined by the following:

1. Resistance of bipolar plates;

2. Contact resistance of plate-backing paper interface;

3. The in-plane resistance of backing paper was determined from in-house electrical resistivity measurements on a backing paper (#10,006, 37.4% FEP) and from physical dimensions. The in-plane resistance of a backing, R_b, is defined below.

$$R_b = \frac{2\ \rho_3 \ell_3}{N_1\ t_1\ x}$$

TABLE 2.9

INTERNAL RESISTANCE OF FIVE-CELL, 1200 cm^2 STACKS

LOCATION IN STACK	ESTIMATED RESISTANCE, mΩ		COMMENTS
	RESIN PLATES	HEAT-TREATED PLATES	
Plate	0.78	.01	Values based on dimensions of C2C2 bipolar plates.
Contact plate-backing interface	0.47	.30	Values based on 37.4% FEP in backing paper, and 41 kPa (60 psia) on end plates.
In-plane backing paper	0.08	.08	Values based on 37.4% FEP in backing paper #10,006. In-house resistivity measurement was 19 mΩ cm.
MAT-1 Matrix	0.44	.44	Parameters included: 180°C, H_3PO_4 and acid resistivity of 1.7 Ω cm.*
TOTAL	1.77	.83	
Actual measurement on stacks, excluding current collectors	(Stack 428) 2.02	(Stack 431) 0.95	
Stack resistance accounted for:	88%	87%	

*Electrical resistivity value was extrapolated from data in MacDonald, D. and Boyack, J., "Density, Electrical Conductivity and Vapor Pressure of Concentrated Phosphoric Acid," Journ. of Chem. and Eng. Data, 14, No. 3, July 1969.

Where,

ρ_3 = the in-plane resistivity of the backing paper,

ℓ_3 = the mean path length,

t_1 = the backing paper thickness,

x = the unit length of the anode, cathode, or DIGAS rib of a plate,

N_1 = the number of repeat units in a specimen,

4. The resistance of the matrix R_m, is defined below.

$$R_m = \frac{t_3 \rho_4}{EA}$$

Where,

t_3 = the matrix thickness,

ρ_4 = the electrical resistivity of the electrolyte,

E = the percent porosity of the matrix,

A = the conducting or active area of the cells.

An extrapolation method was used to determine both the bulk and the contact electrical properties. Although this method has been described previously by Mengali and Seiler, Advanced Energy Conversion, 2, 59 (1962), a specific outline of the procedure is provided in the following sections. Several parameters will be discussed as outlined below:

Contact Resistivity - heat-treated and nonheat-treated plates

1. Ohmic behavior
2. Pressure effects
3. FEP treatment of backing paper
4. Temperature effects.

Bulk Resistivity - heat-treated and nonheat-treated plates

1. Ohmic behavior
2. Resin content and directional anisotropy
3. Temperature effects.

Contact Resistivity

The initial experiments were conducted for two types of phenolic resin/graphite composites: 33 wt% Colloid 8440/67 wt% A-99 and 850 graphite; and 32 wt% Varcum 24-655/68 wt% A-99 graphite. For each phenolic resin/graphite material, two 5.7 cm diameter by 1.9 cm thick disks were compression molded and machined round. The disks shall be referred to as "conductors" and the material placed between the disks as "inserts", e.g., wetproofed backing paper was a type of insert (Figure 2.20). The initial measurements conducted on the two 33 wt% Colloid 8440 disks were designed to determine the significance of pressure and current, and to refine the technique.

Figure 2.20 explains the principle used to measure the voltage drop, E_4, across the contacts. E_4 is defined as:

$$E_4 = Y_4 - Y_3$$

Where,

$$Y_4 = m_2 x_2 + b_2$$

$$Y_3 = m_1 x_1 + b_1$$

For conductors of the same composition,

$$m_1 = m_2 = \frac{\Delta Y}{\Delta x} = \rho_2 = \frac{I}{A}$$

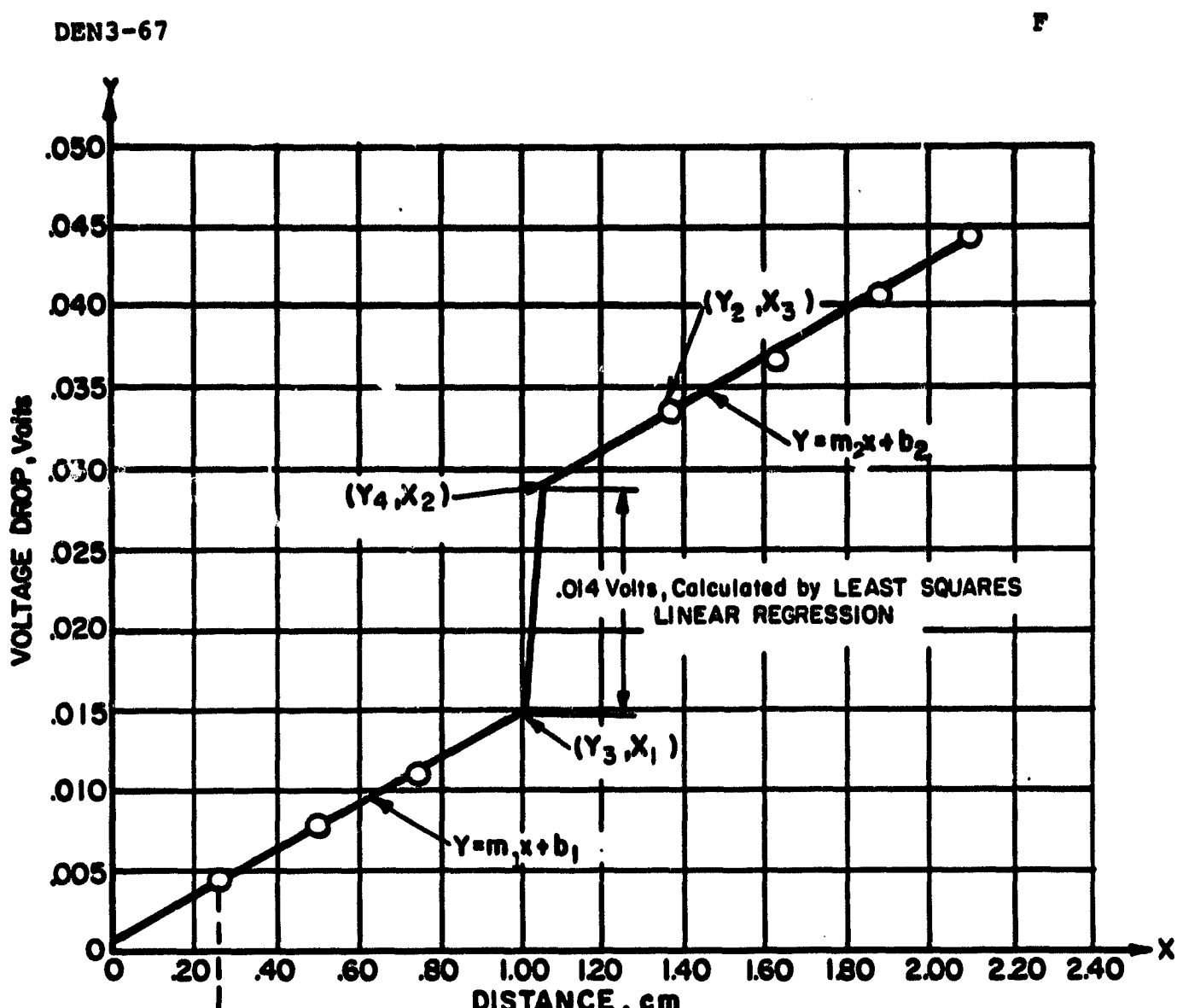

Ⓐ AND Ⓑ – 33 W/o COLLOID 8440/67 W/o GRAPHITE WITH A-99 AND 850 CONDUCTORS
Ⓒ BACKING, 37.4 % FEP (INSERT)

a, b, c, d, e, f, g, h ARE PROBES MEASURING VOLTAGE DROP ACROSS SAMPLES.

PARAMETERS : 1. PRESSURE = 276 kPa
2. SAMPLE CROSS SECTIONAL AREA = 11.40 cm^2
3. COLLOID 8440/GRAPHITE MATERIAL SANDED WITH 320 GRIT AL_2O_3
4. CURRENT DENSITY = 100 mA/cm^2
5. MACHINED ROUND SAMPLES

D1085A

FIGURE 2.20 MEASUREMENT OF RESISTIVITY

Where,

I = current,

A = Area (cross-sectional),

$\rho_1 = \frac{VA}{I\ell}$ = resistivity of the conductors,

ℓ = path length

$$E_4 = \frac{\rho_1 I}{A} (x_2 - x_1) + b_2 - b_1$$

From Figure 2.20

$$b_1 = 0$$

$$b_2 = Y_2 - m_1 x_3$$

(Y_2 and x_3 are experimental values).

Therefore,

$$E_4 = \frac{\rho_1 I}{A} (x_2 - x_1 - x_3) + Y_2$$

The apparent contact resistivity, ρ_2 , may be defined as:

$$\rho_2 = \frac{E_4 A}{I} = \rho_1 (x_2 - x_1 - x_3) + \frac{A}{I} Y_2$$

For experiments with an insert between the conductors, ρ_2 is for two contacts and the insert. The separation of backing paper resistance from electrical contact resistance requires further work. Based on the symmetry of the above equation, the resistivity of a single contact including half the resistance of an insert, ρ_c, equals

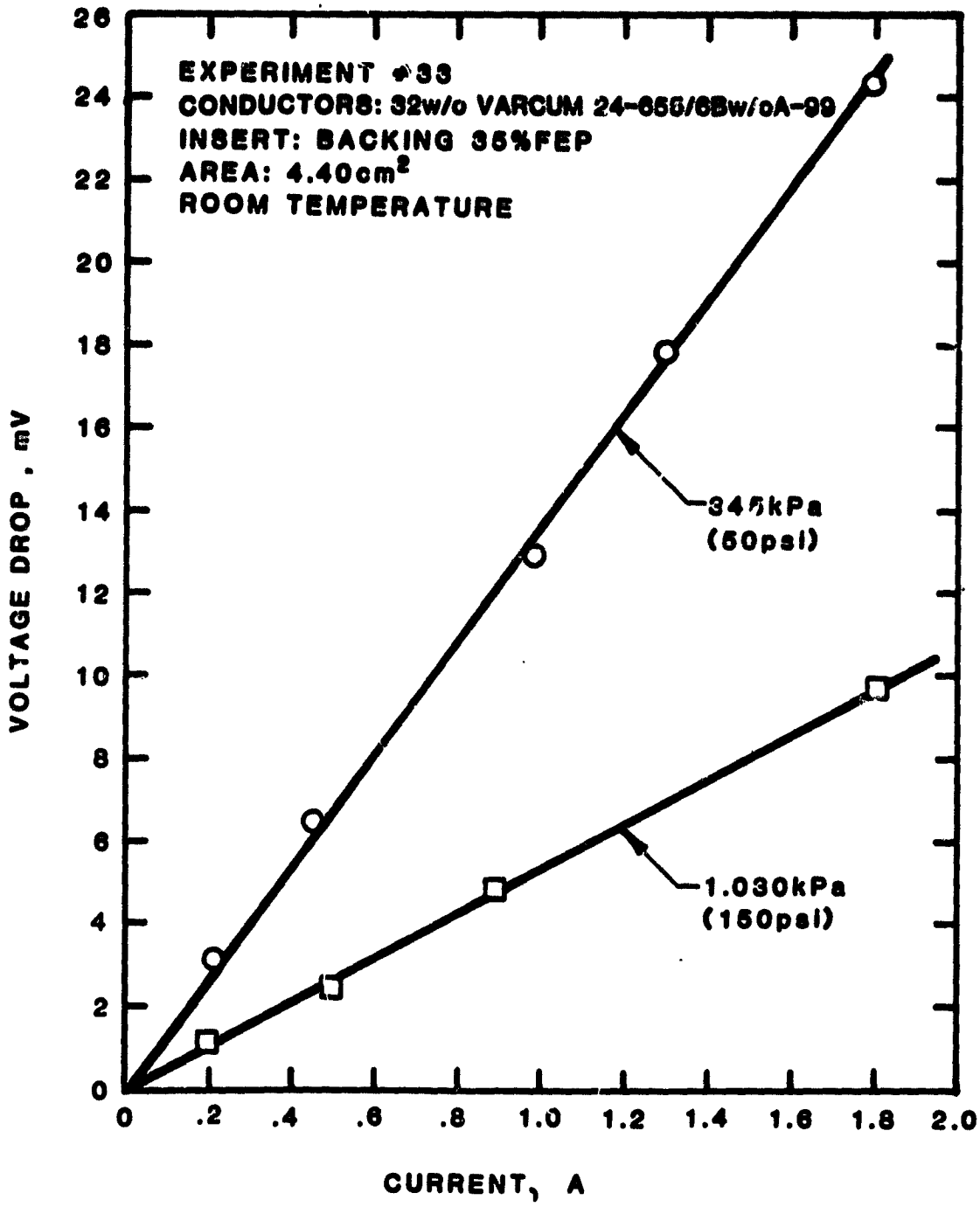

D1601

FIGURE 2.21 OHMS LAW OBEYED FOR CONTACT WITH HEAT-TREATED MATERIAL

$$\rho_c = \frac{\rho_2}{2} = \frac{E_t A}{2I}$$

Therefore in scaling to one cell, the resistance of one backing was not taken into account or, for a 23-cell stack, for example, the contact resistance calculation would include only 23 backings instead of the actual 46 backings in the stack. Since the backing will contribute very little to the total resistance, this omission should not affect the result.

The conductor resistivity, ρ_1, used for calculating ρ_2 was evaluated from a series of initial voltage drop measurements across the conductor. Least square estimates of slopes m_1 and m_2 were converted to resistivity and averaged. Using these algorithms, a computer program was developed for data processing and calculating the contact resistances from the experimental results. Contact resistances of 32 wt% Varcum 24-655/68 wt% A-99 graphite disks with no insert, a backing paper insert, a wetproofed backing paper insert and a gold plated copper foil insert were thus measured at different applied pressures. In each experiment, Ohm's Law (V = IR) was obeyed. A typical V against I plot when no insert was used is shown in Figure 2.21. The effect of applied pressure on the contact resistance was similar for different inserts. A typical ρ_2 against $\frac{1}{P}$ plot is shown in Figure 2.22. The experimental results always agreed with the following simple relationship:

$$\rho_2 = \frac{C_1}{P} + C_2$$

Where, C_1 and C_2 are the least square estimates of the parameters.

In a fuel cell stack, pressure is applied on flat (non ribbed) end plates and the stack pressure reported on the basis of the surface area of an end plate. The pressure between the ribbed bipolar plate and backing paper depends on their contacting area, A_1, and the applied force, F.

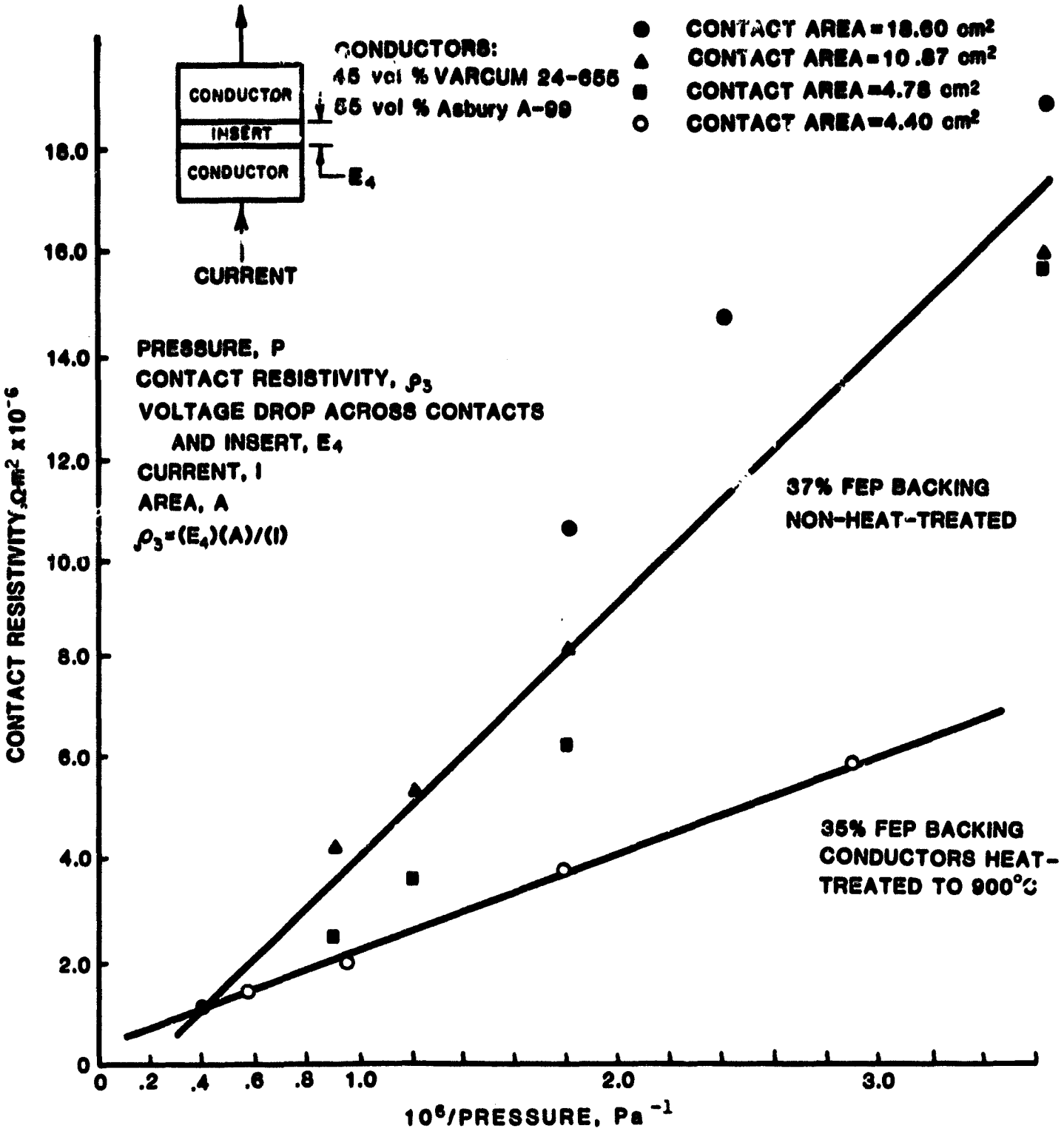

NOTE: Each data point represents the average of 3 to 5 voltage measurements at different current setting. Conductor surfaces sanded with 320 grit Al_2O_3

FIGURE 2.22 ELECTRICAL CONTACT RESISTIVITY WITH STACKPOLE BACKING INSERTS/HEAT-TREATED PLATES

$$P = \frac{F}{A_1}$$

An equation to compute the contact resistance, R_c, in a cell between the bipolar plate and backing, and the resistance of half a backing paper can be developed by combining the above equations.

$$R_c = \frac{\rho_c}{2A} = \left(\frac{C_1 A_1}{F} + C_2\right) \frac{1}{2A}$$

The following conclusions were made concerning these electrical contact resistivity measurements:

1. Electrical contact resistance of graphite materials in fuel cell stacks obeys Ohm's Law, V = IR

2. The accuracy of the measurements was sufficient to discern differences between the various types of contacts that occur in fuel cell stacks.

3. The electrical contact resistance for current bipolar plate materials is slightly lower between plate - backing paper - plate, than between just two plates. This agrees with our measurement on 1200 cm^2 DIGAS coolers. The compressibility of the backing paper and irregular surface of the plates probably account for this fact.

4. The scaling of contact resistance from subscale electrical contact resistivity measurements appears feasible.

5. With constant pressure on the end plates, a reduction of contacting ribbed surface area will not affect the overall contact resistance as significantly as previously thought, because the increased pressure at the rib - backing paper interface reduces the contact resistivity.

The effect of temperature on bipolar plate/backing paper contact resistance shown in Figure 2.23, was as expected for an activated process.

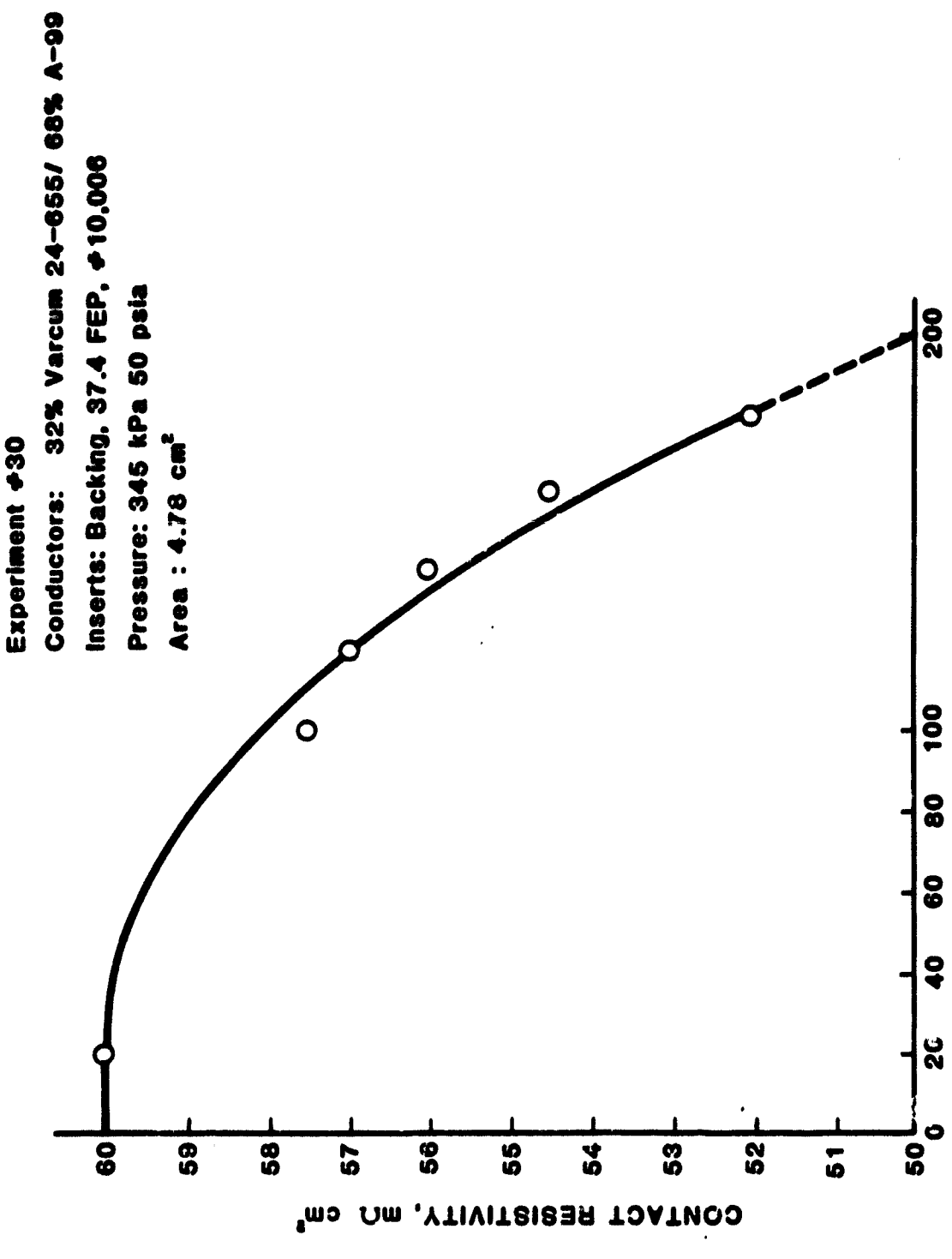

D1602

FIGURE 2.23 TEMPERATURE EFFECT ON CONTACT RESISTIVITY, NONHEAT-TREATED MATERIAL

Bulk Resistivity

The same extrapolation technique required for the contact resistance was utilized to measure the bulk resistivity of the conductor materials. A check was made for the ohmic behavior. As expected the phenolic resin/graphite materials were ohmic whether heat-treated as shown in Figure 2.24 or nonheat-treated. This behavior provided the basis for using the technique with materials of various resin contents. Initial experiments indicated that the resistance changed when measured parallel and perpendicular to the direction of pressing during sample preparation and extensive measurements were made to confirm this observation.

The results demonstrate the anisotropic nature of the materials (Figure 2.25 and Table 2.10). The phenolic resin/graphite composites were compression molded. Cylindrical samples were machined from the molded parts for three orientations: an axis parallel to the pressing direction, an axis perpendicular to the pressing direction and a 45 degree angle. Electrical contacts were connected to the ends of the cylinders and the electrical resistivity measured. The parallel to pressing samples had electrical resistivity three to four times greater than samples perpendicular to pressing. The current in a fuel cell stack flows parallel to pressing. From the results in the parallel to pressing direction, the values of electrical resistivity for Varcum 24-655 material appear to be 10 to 20% lower than the Colloid 8440 materials. Electrical resistivity values for Varcum 24-655 or Colloid 8440 materials with Asbury A-99 graphite were approximately 10 to 30% lower than with a mixture of 27 wt% Asbury 850 and 73 wt% Asbury 100% A-99 graphite. Asbury A-99 graphite is an artificial graphite with 5 to 44 μm particles and Asbury 850 graphite is a natural graphite with 0.5 to 0.6 μm particles.

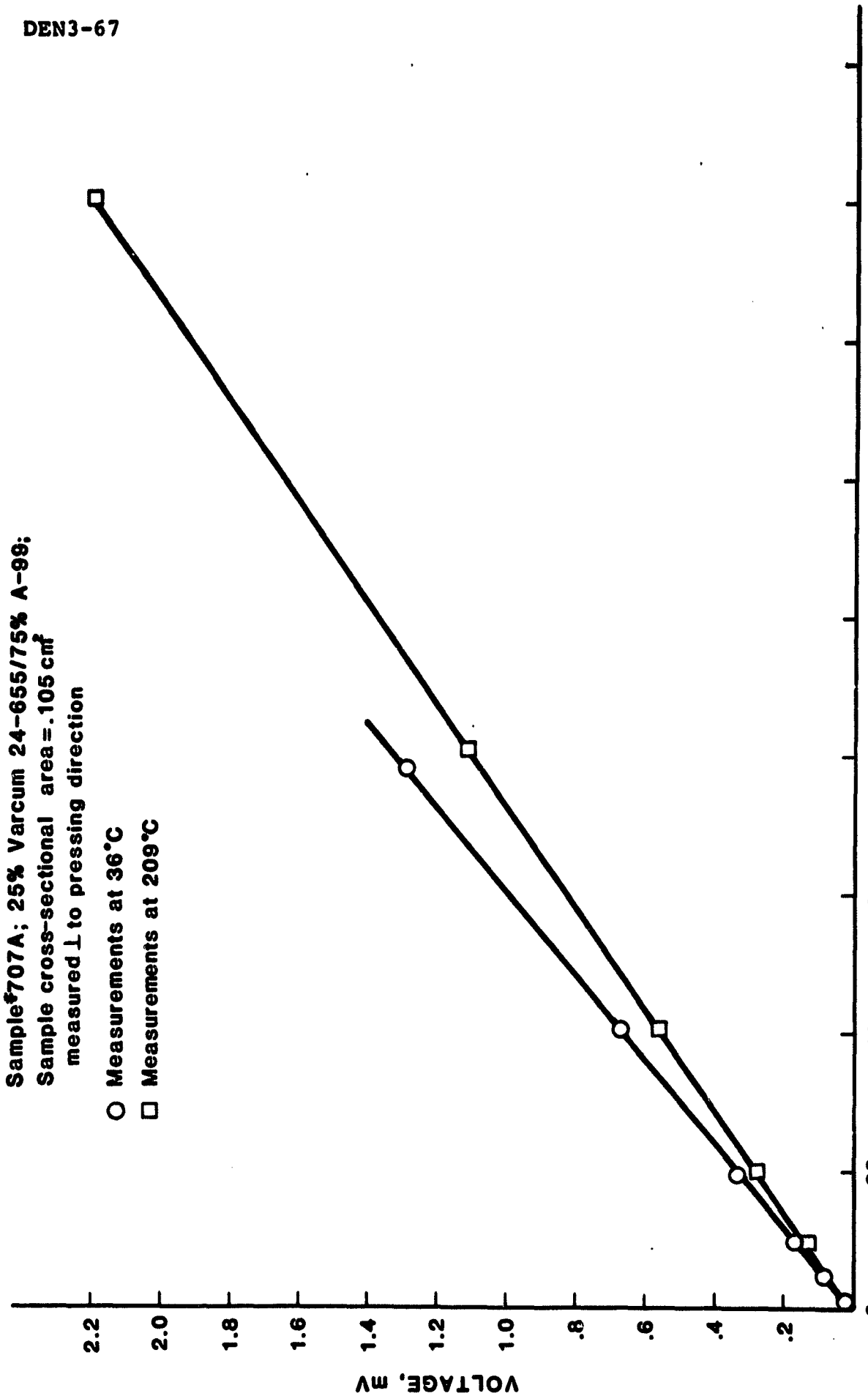

FIGURE 2.24 OHMS LAW FOR 900°C HEAT-TREATMENT MATERIAL

D1603

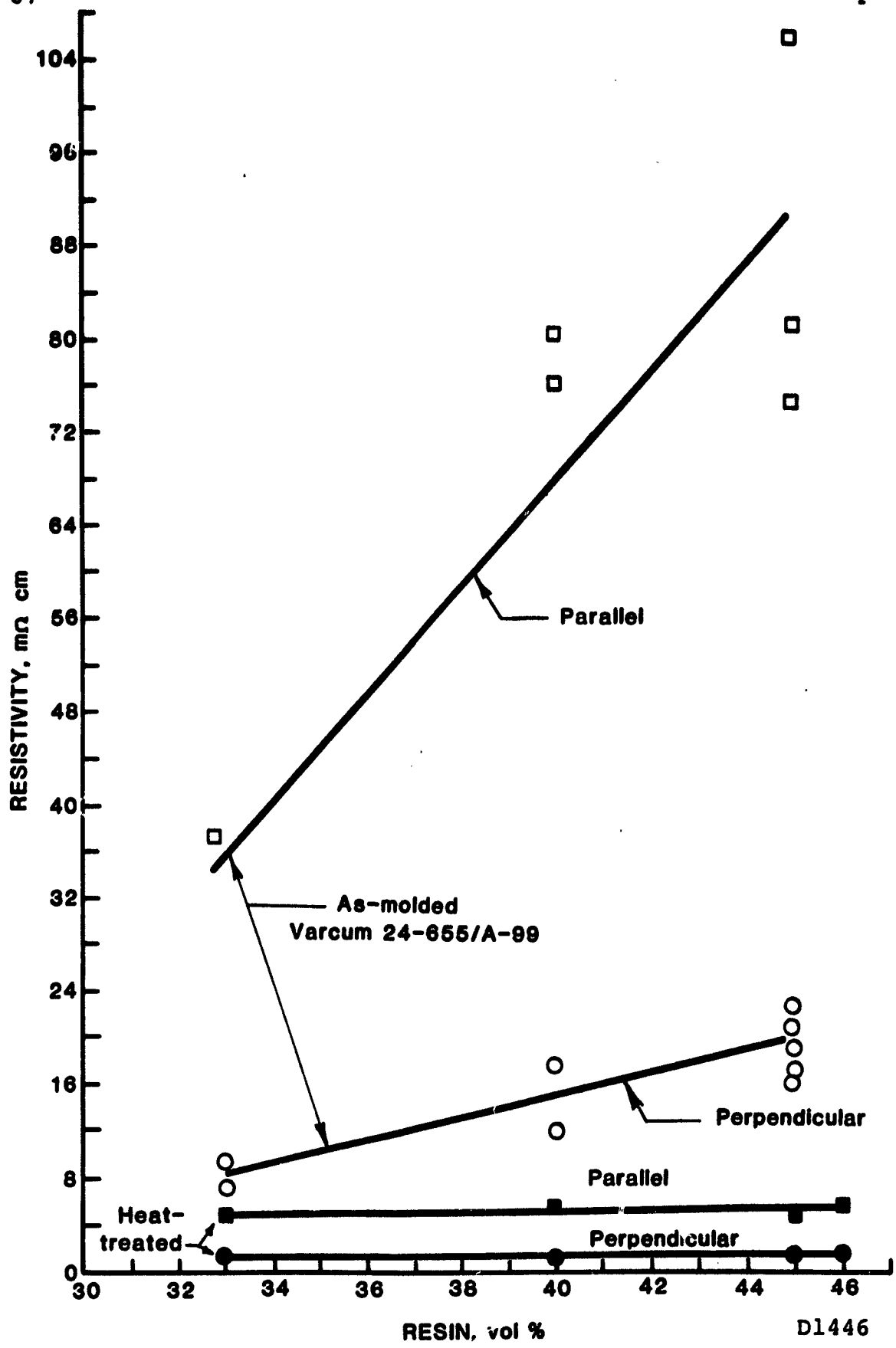

FIGURE 2.25 ELECTRICAL RESISTIVITY OF GRAPHITE/PHENOLIC RESIN

TABLE 2.10

ANISOTROPY OF FOUR-POINT ELECTRICAL RESISTIVITY MEASUREMENTS

RESIN	MOLDING COMPOUND	GRAPHITE	AS MOLDED				HEAT-TREATED, ~ 900°C			
			RESISTIVITY, mΩ cm			RATIO	RESISTIVITY, mΩ cm			RATIO
	v/o GRAPHITE / v/o RESIN*	v/o A-99 / v/o 850	PARALLEL ∥	∠45°	PERPENDICULAR ⊥	∥:⊥	PARALLEL ∥	∠45°	PERPENDICULAR ⊥	∥:⊥
Varcum 24-655	55/45	100/0	82	53	21	3.9	5.0	3.5	1.6	3.1
	60/40	100/0	76	--	18	4.3	5.7	---	1.5	3.8
	67/33	100/0	38	--	9.3	4.0	---	---	---	---
	55/45	73/27	--	--	30	---	---	---	1.4	---
	60/40	73/27	75	--	15	5.1	5.4	---	1.3	4.2
	67/33	73/27	48	--	11	4.4	4.6	---	1.3	3.5
Colloid 8440	54/46	73/27	120	--	32	3.9	5.6	---	1.5	3.7
	67/33	73/27	51	33	12	4.3	5.2	3.2	1.2	4.3
	67/33	100/0	--	32	11	---	---	4.1	1.4	---

*CONVERSION: wt% - 22 28 32 33
vol% - 33 40 45 46

If the A-99 graphite particles are aligned by the pressing operation and have a 3:1 anisotropy, the observed properties for heat-treated and nonheat-treated materials would be explained. Further testing would be required to resolve this question, but it is important to note that the usual assumption of equal resistance in both directions is invalid. Heat-treatment not only decreased the magnitude of the resistivity but also the anisotropy factor at high resin contents. Both features are important to the overall performance of fuel cell stacks. The temperature dependence of the resistivity was also evaluated for both heat-treated and nonheat-treated materials. Since most of the data were obtained at room temperature, the information in Figures 2.26 and 2.27 provided the means of estimating the resistivity at the fuel cell operating temperatures.

2.3 Bipolar and Cooling Plate Erosion

Some evidence of bipolar and cooling plate erosion was noted during the previous phase of this program. Since the scale-up of molded plates, there has been no evidence of erosion of molded plates. If, however, the molding resulted in porous sections along the plate edge, then regions are easily attacked by acid. When softened by acid corrosion, the plate does swell and is eroded. This type of erosion leads to blocked gas channels. Improved corrosion resistance and molding with no open porosity will prevent this effect.

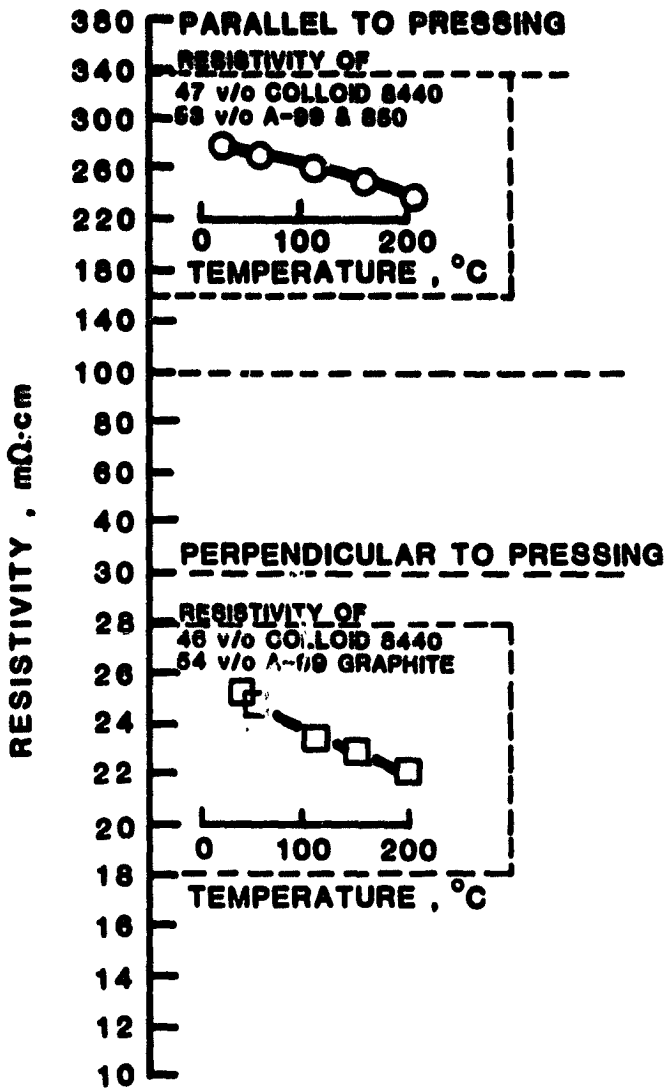

FIGURE 2.26 TEMPERATURE DEPENDENCE OF BULK RESISTIVITY FOR NONHEAT-TREATED MATERIALS

D1604

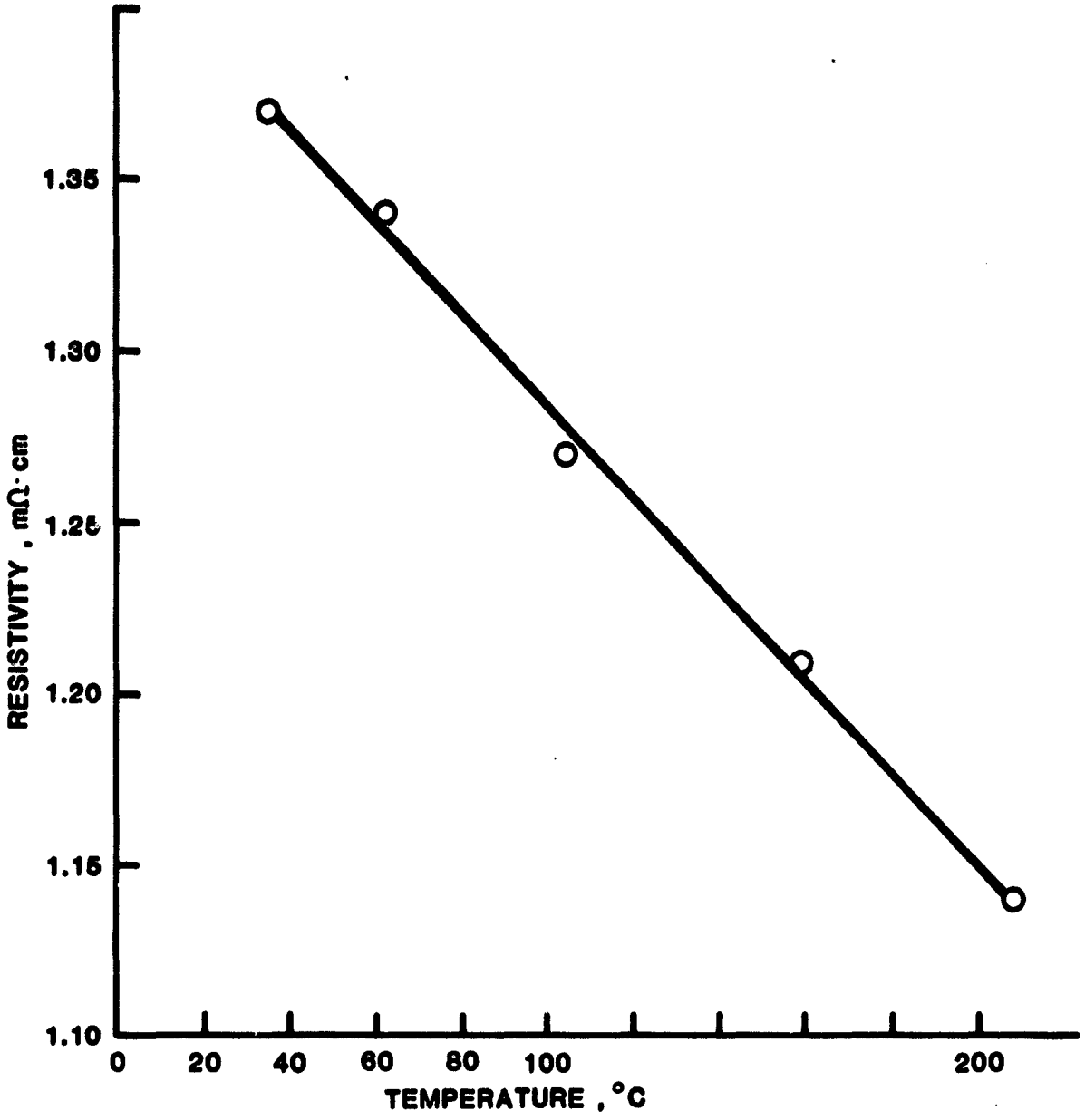

FIGURE 2.27 TEMPERATURE EFFECTS ON RESISTIVITY FOR HEAT-TREATED MATERIALS

TASK 3. ENDURANCE TESTING

The objective of this task was to investigate endurance related issues, such as acid loss and replenishment, the effect of wet-proofing and bipolar plate heat-treatment on cell life and the long-term corrosion behavior during cell operation. A limited number of experiments carried out to estimate the vapor pressure of acid yielded an order-of-magnitude estimate. The information was utilized in designing acid management for long-term runs. After initial testing, a set of twelve 350 cm^2 3-cell stacks were operated for up to 10,000 hours to study the component stability. The experience gained in the 350 cm^2 endurance tests was utilized to test 1200 cm^2 5-cell stacks for up to 5000 hours.

3.1 Acid Vapor Pressure

Vapor pressure data for the phosphorus species over phosphoric acid are extremely limited. Extrapolation of the high temperature measurements found in the literature produced an estimate of 0.46 ppm P_4O_{10} at 190°C. Calculations were made for the P_4O_{10}-H_2O system using ideal gas - nonideal liquid theory. These theories predicted very high values for the P_4O_{10} vapor concentration (Table 3.1). Experiments were performed in which the weight loss from 25 cm^2 cells and the condensation of exit vapors were measured. These experiments produced scattered data but they were in the range of 0.1 to 1.3 ppm P_4O_{10}. Additional data were obtained by evaluating the acid added to stacks during operation. The vapor concentration required to account for the acid additions was calculated to be approximately 0.4 ppm. Although a more accurate determination of the vapor concentration at various operating conditions is recommended, an estimate of the order-of-magnitude was obtained from this study.

TABLE 3.1

COMPARISON OF ACID LOSS DATA

(Temperature = 190°C, Air Atmosphere)

SOURCE	P_4O_{10} VAPOR, PPM	COMMENT
Theoretical Calc.*		
Van Laar Correlation	4.26	99.5% Acid
Margules Correlation	4.26	
Wilson Correlation	3.05	99.5% Acid
ERC Data		
Lab Expts.	0.1-1.3	99-106% Acid
Stack Data	0.25-0.4	99-106% Acid
Literature Data†		
Extrapolation	0.46	99-106% Acid

*Reid, R.C., Pravsnitz, J.M., and Sherwood, T.K., "The Properties of Gases and Liquids", Third Edition, McGraw Hill Book Co., 1976.

† Brown and Whitt, Ind. Eng. Chem., 44, 615 (1952)

3.2 Performance Stability

- Nonheat-Treated Bipolar Plates

On completion of the previous program, a 10,000 hour endurance test was anticipated for the best components that were available for Energy Research Corporation's 5 in. x 15 in. stacks. Prior to starting this long-term test, a stack was operated for several thousand hours at 150 mA/cm^2. There appeared to be no unusual effects due to the higher current density as shown in Figure 3.1.

The 10,000 hour test design as summarized in Tables 3.2 and 3.3 focuses on the performance of three matrices, two catalyst loadings and a resin/graphite composite bipolar plate. The three matrices were 1) phenolic fiber, 2) silicon carbide and, 3) ERC matrix, MAT-1. The MAT-1 is an ERC developed matrix which has a higher bubble pressure, enhanced acid transport properties and greater acid retention than either Kynol or silicon carbide matrices. Four stacks were assembled with each of the matrices. Electrodes with a lower platinum loading were also included in the test plan as outlined in Table 3.3. The stacks were assembled with two different platinum loadings, 0.8 mg/cm^2 and 0.6 mg/cm^2 (0.5 cathodes with 0.3 anodes and 0.4 cathodes with 0.2 anode). Thus, a total of 12 stacks were built and tested.

The performance of these stacks is summarized in Table 3.4. The overall performance trends for these stacks are plotted in Figure 3.2. An average performance for each matrix type is shown in this figure, because that is the most significant variable.

Several conclusions were drawn from this operating experience:

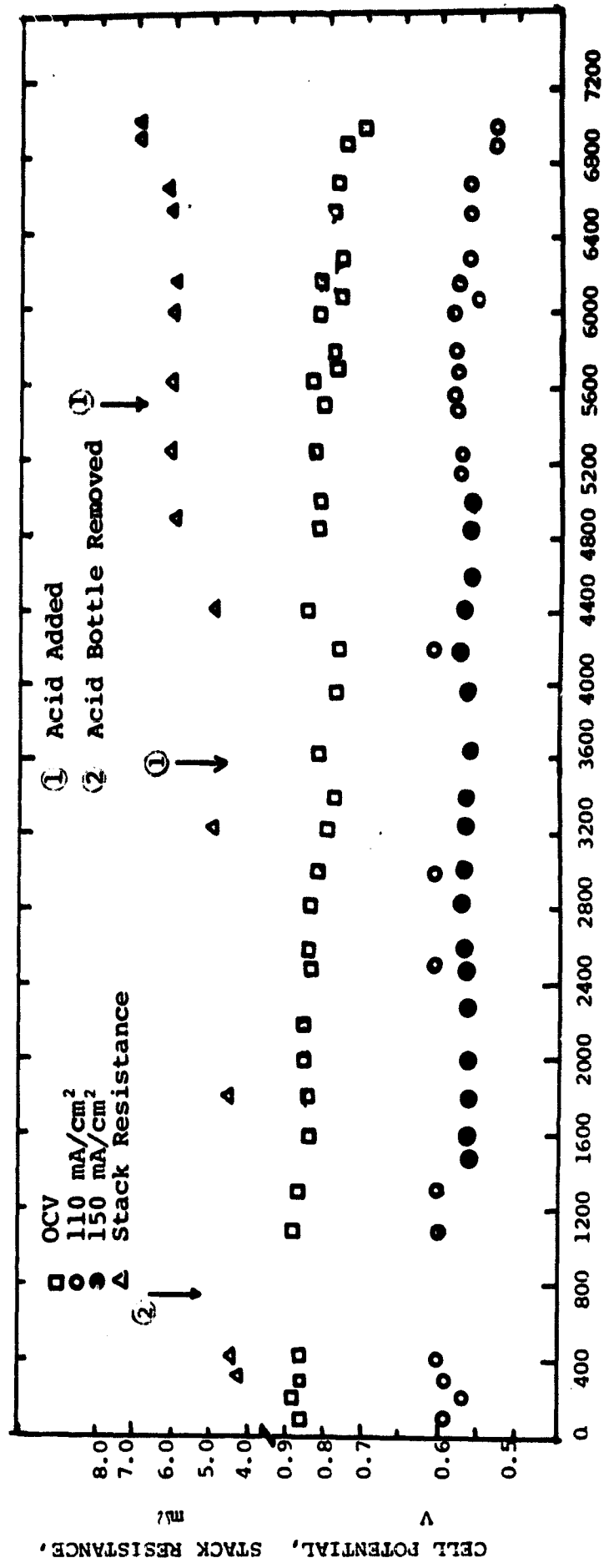

FIGURE 3.1 LIFEGRAPH OF STACK 349, SHOWING OPERATION AT TWO CURRENT DENSITIES

TABLE 3.2

LONG-TERM ENDURANCE TEST PLAN

	MATRIX					
	KYNOL		SILICON CARBIDE		MAT-1	
Total Cell Pt Loading, $mgPt/cm^2$	0.8	0.6	0.8	0.6	0.8	0.6
No. of 3-Cell Stacks	2	2	2	2	2	2

PURPOSE OF TEST VARIABLES

KYNOL - EVALUATE LONG TERM GENERATION OF POISONS BY DEGRADATION

SILICON CARBIDE - TEST ERC's METHOD OF PREPARATION

MAT-1 - EVALUATE LONG-TERM STABILITY AND ACID RETENTION

ELECTRODE LOADING - TEST VIABILITY OF LOW LOADING AND POTENTIALLY BE AN EARLY INDICATOR OF PROBLEMS IN OTHER CELLS

TABLE 3.3

ELECTRODES AND BIPOLAR PLATE DATA
For the 10,000 Hr Test

- ELECTRODES

  Type - Rolled Electrodes

  Composition - 40% PTFE

  60% ERC Platinum catalyst

  Anodes - 0.2 mg Pt/cm^2 and 0.3 mg Pt/cm^2

  Cathodes - 0.4 mg Pt/cm^2 and 0.5 mg Pt/cm^2

  Total Loading - 0.6 mg Pt/cm^2 and 0.8 mg Pt/cm^2

- BIPOLAR PLATE

  Composition - 33% Phenolic Resin from Colloid

  A-99 Graphite } From Asbury

  850 Graphite }

TABLE 3.4 SUMMARY OF PERFORMANCE FOR 10,000 HR. ENDURANCE STACKS (@ 100 mA/cm^2)

MATRIX TYPE	TOTAL Pt LOADING, mg/cm^2	STACK NO.	A PERF, V (OCV, V) At 500 Hrs.	AVG. PERF., V (OCV, V) At 2500 Hrs.	AVG. PERF., V (OCV, V) At 5000 Hrs.	AVG. PERF., V (OCV, V) At 7500 Hrs.	AVG. PERF., V (OCV, V) At 10,000 Hrs.
KYNOL	0.6	604	0.58 (0.84)	0.57 (0.81)	------ ------	------ ------	------ ------
		610	0.58 (0.82)	0.54 (0.82)	------ ------	------ ------	------ ------
	0.8	396	0.58 (0.83)	0.54 (0.82)	------ ------	------ ------	------ ------
		611	0.60 (0.86)	0.47 (0.72)	------ ------	------ ------	------ ------
SIC	0.6	605	0.61 (0.78)	0.61 (0.82)	0.56 (0.81)	0.55 (0.80)	------ ------
		607	0.63 (0.78)	0.61 (0.80)	0.60 (0.83)	------ ------	------ ------
	0.8	600	0.61 (0.77)	0.58 (0.79)	0.59 (0.80)	0.58 (0.83)	------ ------
		601	0.60 (0.77)	0.58 (0.79)	0.57 (0.83)	------ ------	------ ------
PAT-1	0.6	608	0.60 (0.81)	0.56 (0.80)	0.58 (0.82)	*@ 7220 Hrs. 0.46* (0.78)*	------ ------
		609	0.60 (0.82)	0.59 (0.81)	0.58 (0.84)	0.54 (0.82)	------ ------
	0.8	602	0.61 (0.79)	0.59 (0.78)	0.58 (0.78)	0.58 (0.79)	0.52 (0.75)
		603	0.61 (0.77)	0.58 (0.77)	0.61 (0.79)	0.60 (0.78)	0.57 (0.76)

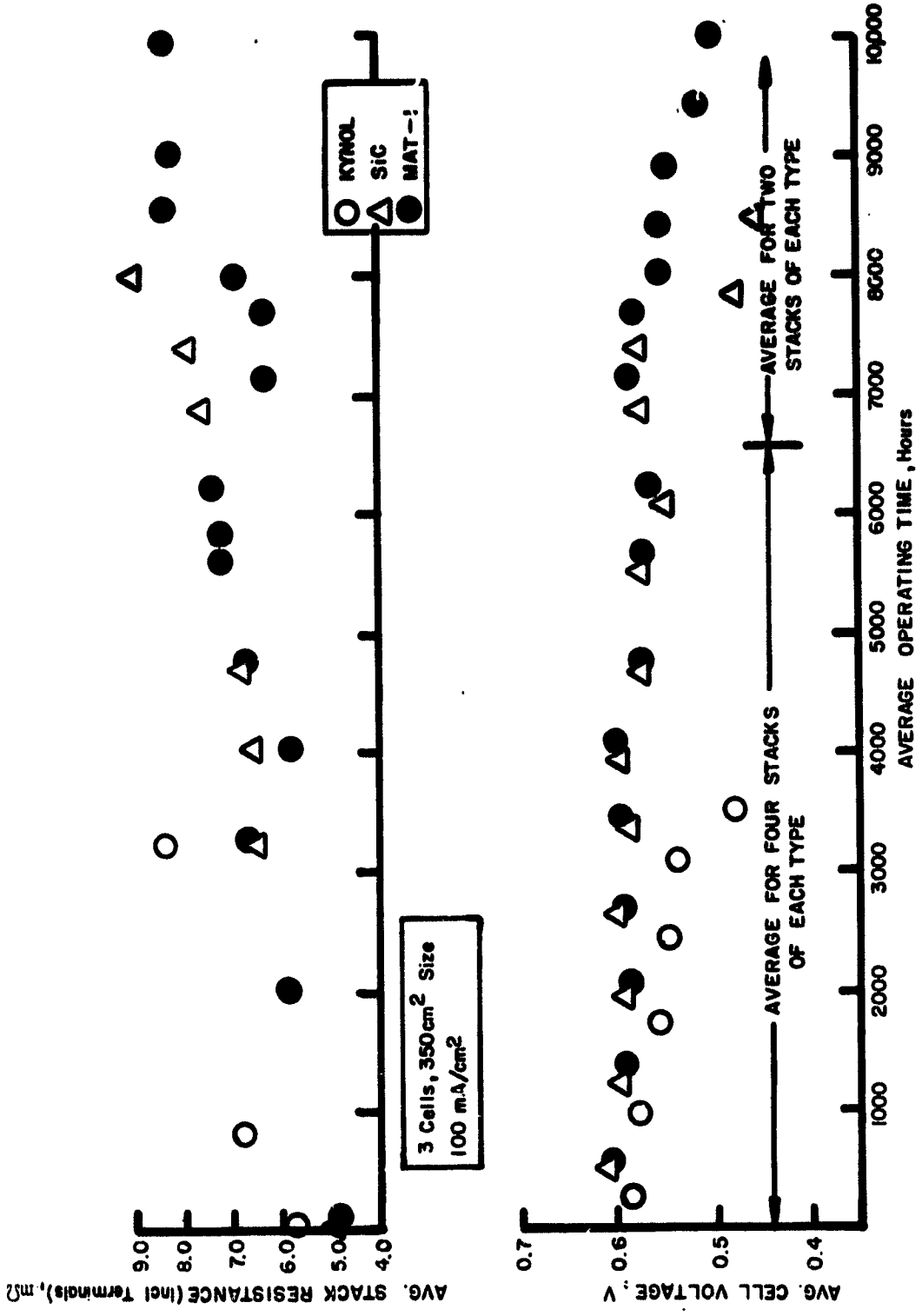

FIGURE 3.2 AVERAGE PERFORMANCE OF STACKS WITH THREE DIFFERENT MATRICES

D1317R

- Stack resistance increases and performance decreases as acid is lost from the stack.
- MAT-1 matrices are satisfactory for 10,000 hours and probably for 40,000 hours.
- Constant exposure of nonheat-treated bipolar plates to excess acid caused swelling, softening, and erosion. Limited additions of acid can control this degradation.
- The lifetime of Kynol stacks was limited by matrix degradation. SiC and MAT-1 stacks were limited by overexposure of the plate material in the acid fill channel which caused blockages that prevented further acid additions.
- Corrosion at plate edges which resulted in some blockage of reactant flow passages was the major factor limiting life for stacks assembled with non heat-treated plates and stable matrices. Proper acid management is very important for long-term stability of this type of stack.

Successful scale-up and development of the larger cell size (1200 cm^2) resulted in a 5,000 hour endurance test of three 5-cell stacks. These stacks contained 0.3 mg Pt/cm^2 anodes and 0.5 mg Pt/cm^2 cathodes and the MAT-1 matrix. Bipolar plates were the same composition as indicated in Table 3.3.

The performance is shown in Figure 3.3. The three nonheat-treated endurance stacks are compared to a stack containing heat-treated plates but otherwise identical to the three endurance stacks. Both types of stacks ran very well for the 5,000 hours. Limiting the acid additions have dramatically reduced the plate edge corrosion and channel blockage in nonheat-treated stacks.

- Heat-treated Bipolar Plates

Use of heat-treated bipolar plates not only improves the corrosion resistance but also the performance. A comparison of the stacks using nonheat-treated plate stacks with the heat-treated plate stack demonstrates the 70 mV to 90 mV improvement for at least 5,000 hours (see Figure 3.3). A summary of the

D1212AR1

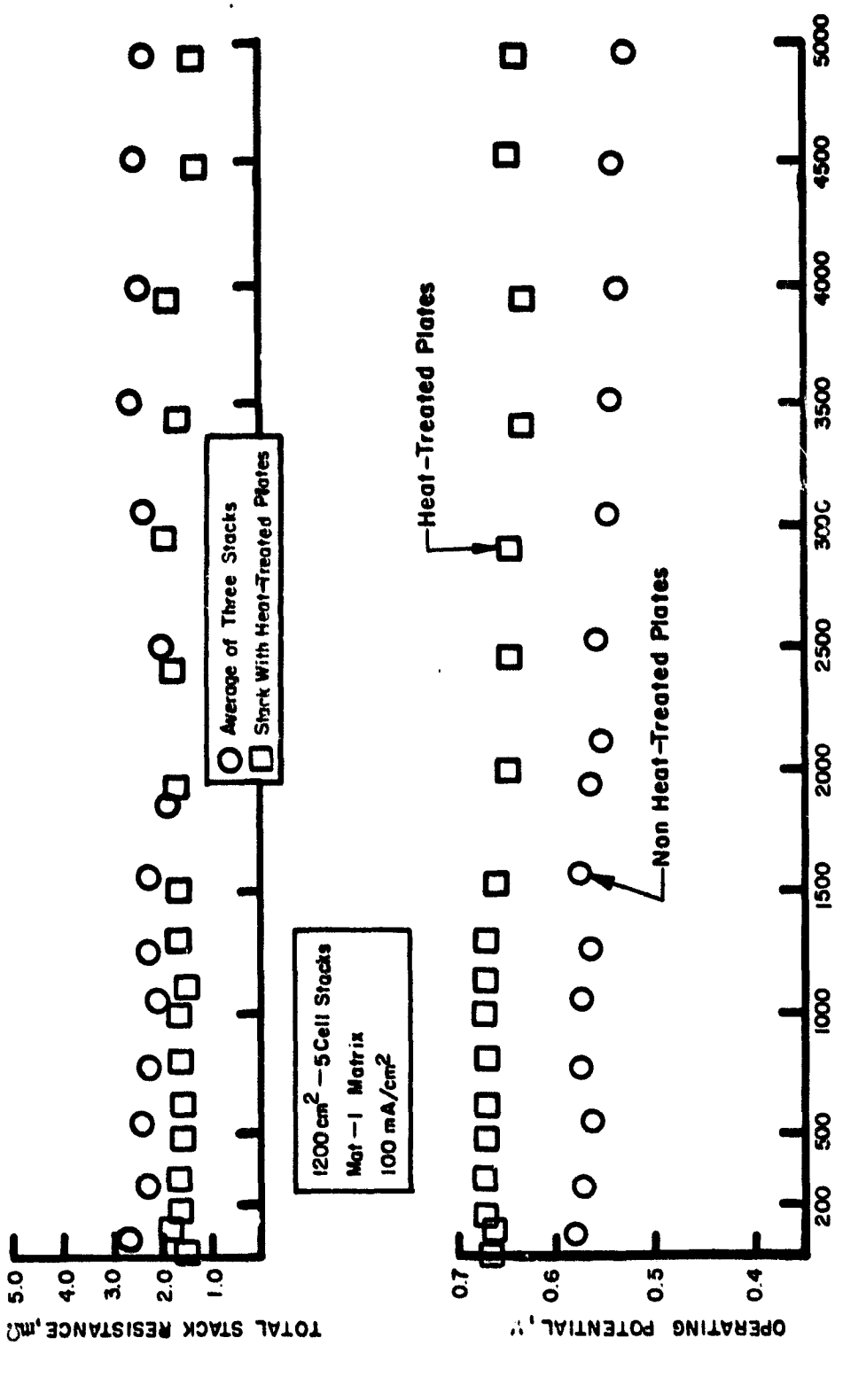

FIGURE 3.3 PERFORMANCE OF LONG-TERM STACKS
1200 cm^2 SIZE COMPONENTS

stacks built for this program which contain heat-treated plates is shown in Figure 3.4. It is evident from these data that the cathode loading can be reduced to 0.25 mg Pt/cm^2 and the anode loading to 0.12 mg Pt/cm^2 without changing the stability observed in other stacks.

The improvement observed for the heat-treated bipolar plate stacks is a result of improved electrical resistance and removal of an electrode poison. Although discussed previously in this report (Task 2), the changes in performance are quite dramatic. Further improvements by optimizing the heat-treatment and contact resistances are to be expected.

3.3 Post Test Analysis

When the 10,000 hour endurance test of 5 in. x 15 in. stacks was started, the acid addition and general maintenance procedures were adopted from previous experience running 25 cm^2 cells and 350 cm^2 stacks. From evaluation of the data and the visual observations at disassembly, it was apparent that the stacks were overexposed to acid and excessively subjected to maintenance. Maintenance includes a number of activities which were performed as needed. These included: replacing manifolds, cleaning all surfaces, changing heaters and hoses, tightening all hoses and adjusting the load. These procedures resulted in reactant gas channel blockage. Overexposure to acid hindered the ability to distribute the acid uniformly to each cell because of plate swelling and thus some cells would be somewhat starved of acid. The loss of acid finally results in crossleaks. The crossleaks lead to attempts at more acid addition which further exacerbates the problem. Continued overexposure of the cell to acid resulted in acid weeping in the reactant gas channels. This resulted in corrosion, swelling and erosion of the plate which also caused channel blockage. The ultimate effect is a decrease in performance due to crossleaks and reactant gas flow problems.

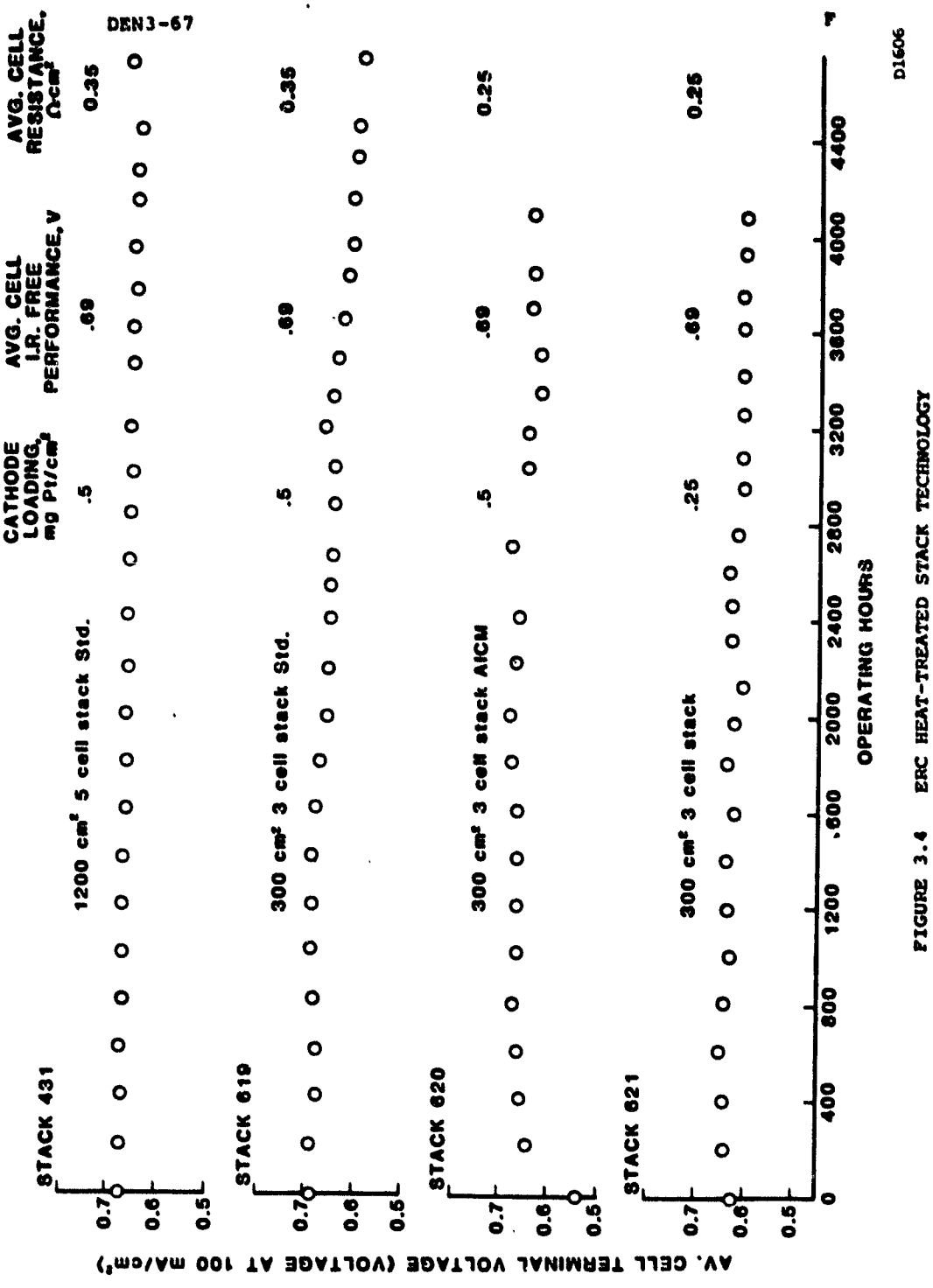

FIGURE 3.4 ERC HEAT-TREATED STACK TECHNOLOGY

The fundamental cause of the problems is plate corrosion and excessive acid addition. Prior to starting the 5,000 hour endurance test of 12 in. x 17 in. size stacks, the procedure was changed to restrict acid addition after the first 1,000 hours of operation even to the point of some small acid starvation. Maintenance was limited to one service check within the first 1,000 hrs. of operation. These stacks were not disassembled at the completion of 5,000 hours because of their steady operation. The general observation, however, is that the acid additions during the first 1,000 hours might be limited even further. Heat-treatment of the plates to improve corrosion resistance and limitations on acid addition should provide for a life of well over 10,000 hours. The results of the 10,000 hour (350 cm^2/cell) stack tests and the 5,000 hour (1200 cm^2/cell) stack tests reported in Task 3, provided definite guidelines for future stacks as follows:

a. Acid additions should be limited.

b. Backing paper crushing should be minimized.

c. Seal improvements would be advisable.

d. Acid management is critical to long-term life.

e. Material corrosion resistance is critical to long-term life.

f. Heat-treatment of plates eliminates poisoning from plates, improves electrical and thermal conduction significantly and improves corrosion resistance.

TASK 4. SHORT STACK TESTING

Twenty six short stacks with 1200 cm^2 components were built to verify components, stacking procedures and operating conditions. The development of these stacks required effort in the following areas prior to running the 5,000 hour endurance test described in Task 3:

a. Stack compression;

b. Prefilling of cell components with acid and acid additions during operation;

c. Qualification of full size MAT-1 matrices;

d. Qualification of full size rolled electrodes;

e. Current collector design.

Additional areas of interest that were studied include: 1) the performance at various current densities, 2) higher oxygen partial pressures, 3) simulated reformed fuel, and 4) higher temperatures.

4.1 Test Facility Construction

Test stands were constructed for atmospheric testing of 5-cell stacks (1200 cm^2/cell) over a range of temperatures and gas compositions. The test stand design is simple, reliable and easy to operate. A typical panel is shown in Figure 4.1.

4.2 Performance Verification and Mapping

Stack 427 embodied all of the full size components such as current collector post, acid prefilling and stack compression that were developed with the first 26 stacks. The performance shown in Figures 4.2 and 4.3 was typical of the nonheat-treated bipolar plate stacks. This provided the confidence that the 5,000 hour test in Task 3 would be successful.

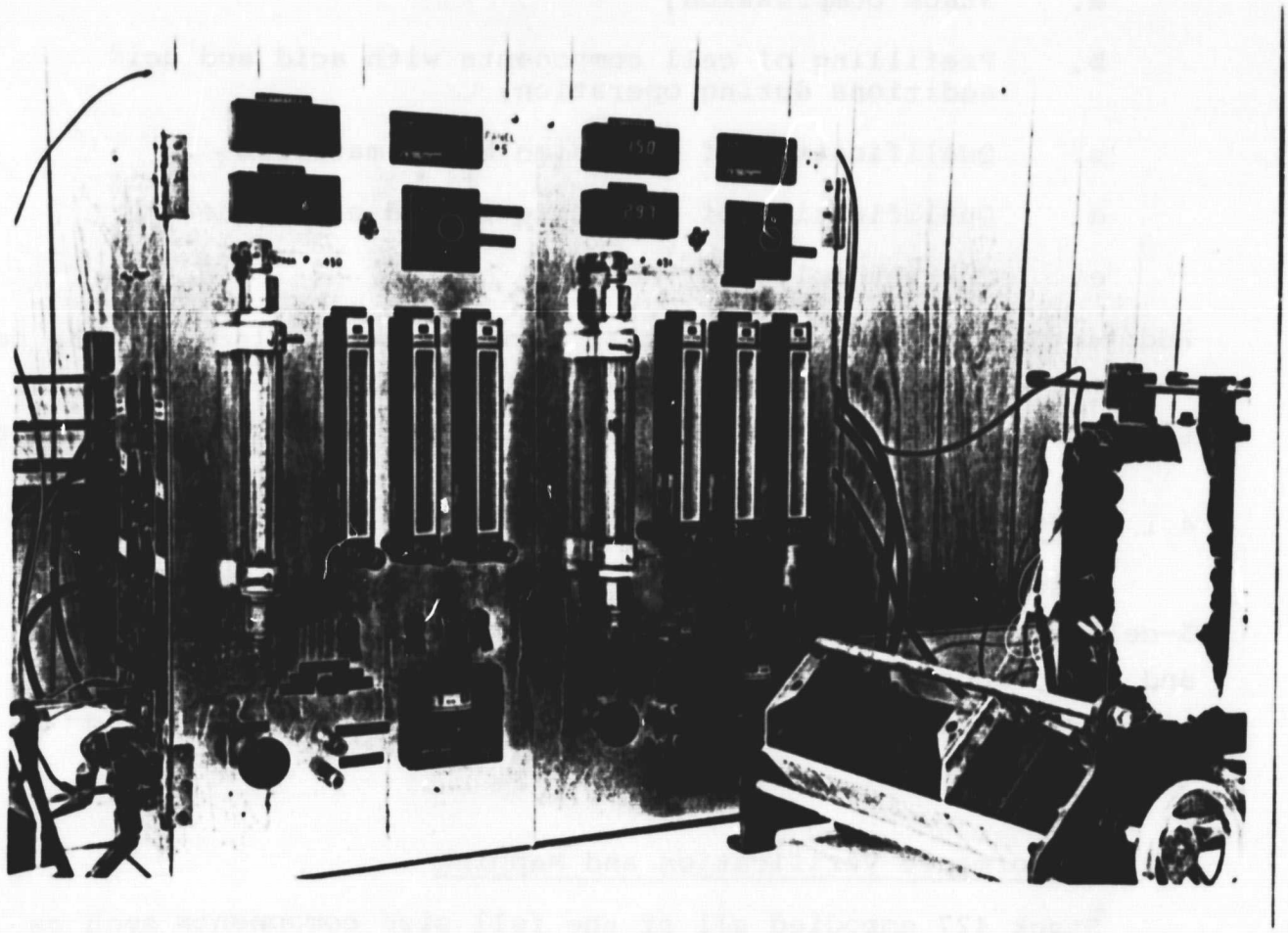

P0523

FIGURE 4.1 5-CELL STACK TEST STAND

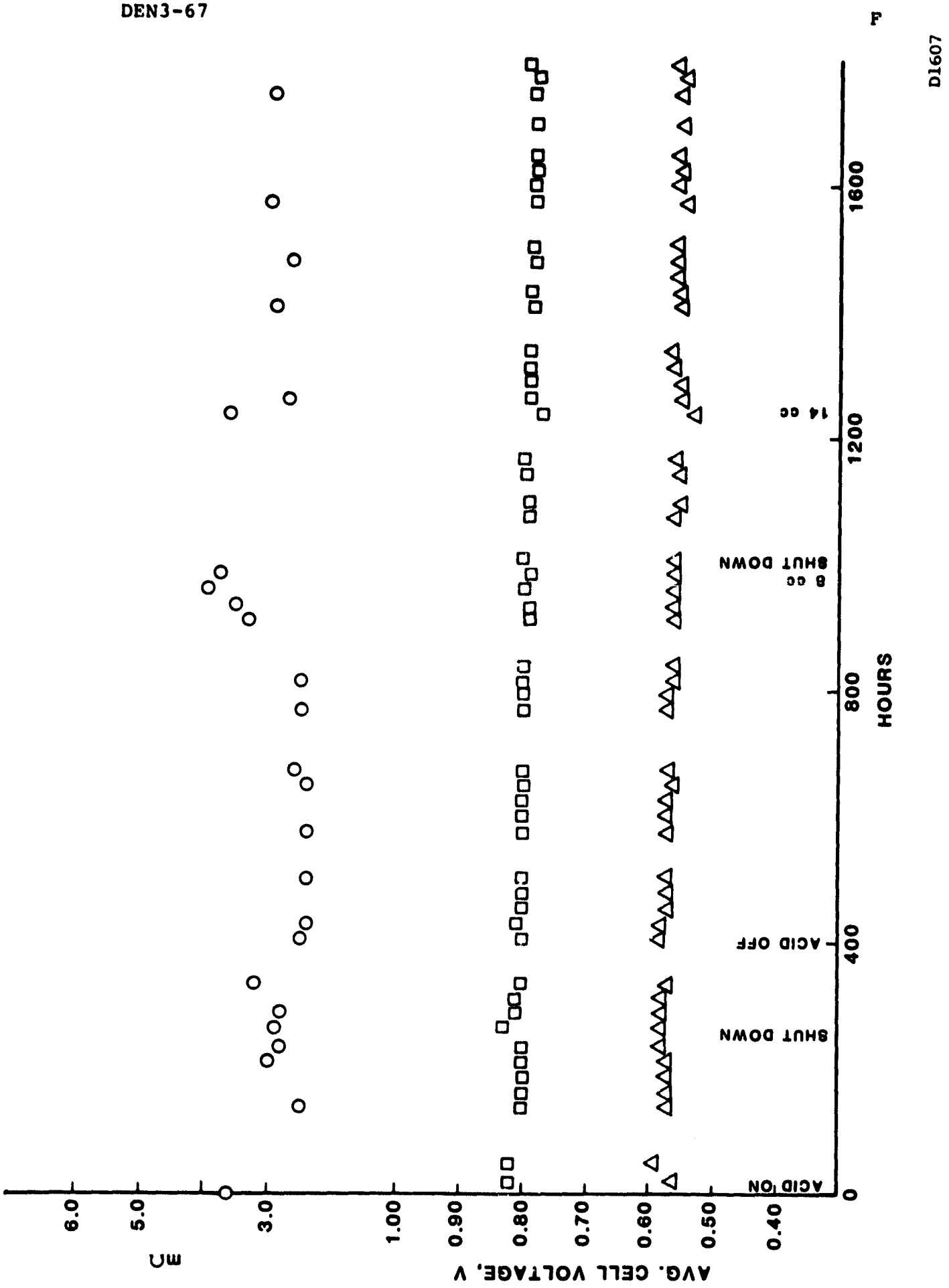

FIGURE 4.2 PERFORMANCE OF STACK NO. 427

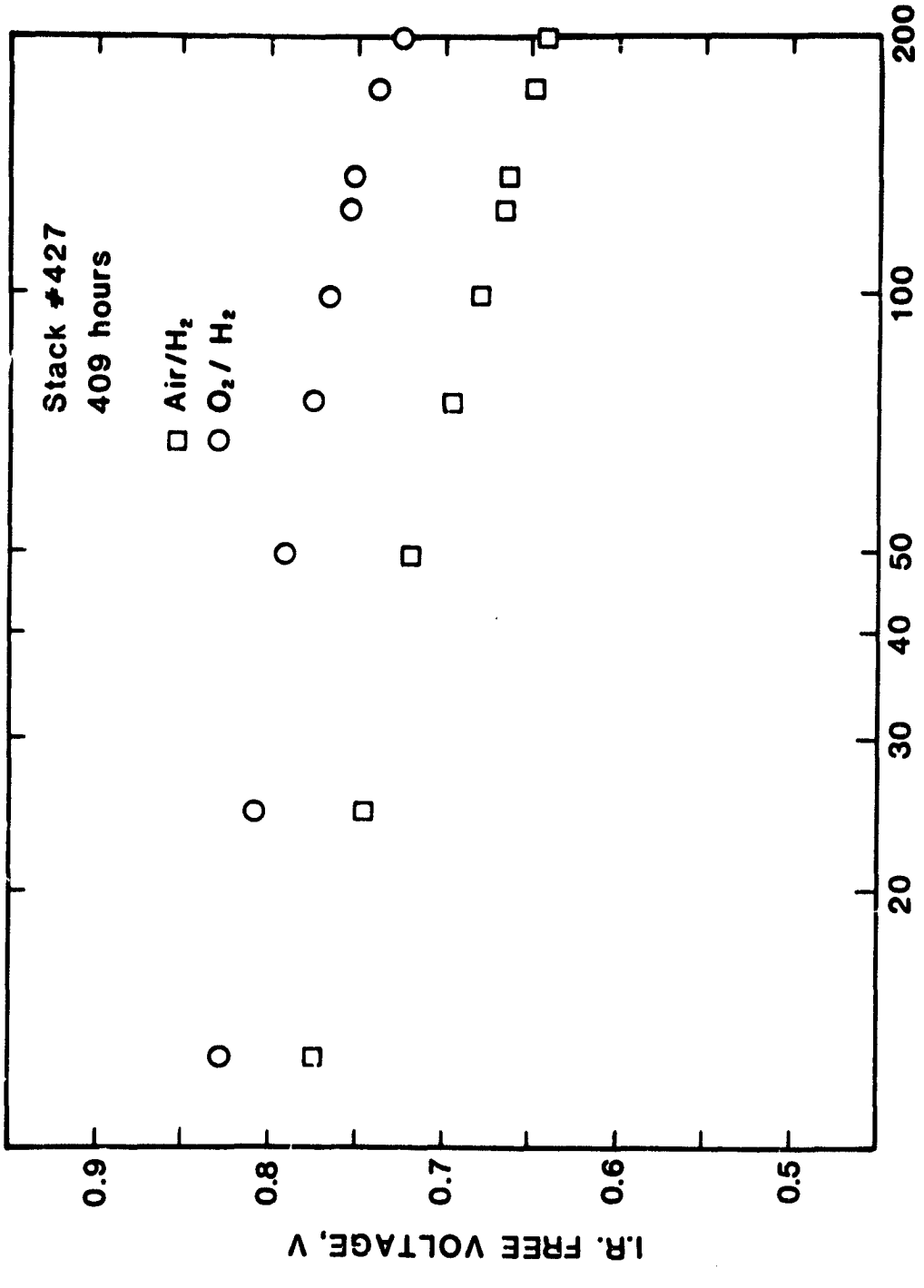

FIGURE 4.3 AVERAGE CELL PERFORMANCE

The three most important build and operation parameters are stack shimming, compression, and temperature. Stack shimming and compression is a trade-off between lowering the electrical contact resistance and crushing the backing paper. As mentioned in Tasks 1 and 2, the performance will increase as the resistance decreases but when the backing paper is crushed acid wets the material. When the material is wet enough, the gases have difficulty penetrating the electrode. This behavior also leads to undesirable corrosion of the paper and the bipolar plate. Stack shimming and compression was chosen so the backing did not crush but the resistance-compression curve as shown in Figure 4.4 had leveled out. Application of sufficient initial pressure eliminated any significant change during operation.

Rapid cost effective stack building was not possible using the long-term wicking procedures employed for experimental stacks. Prefilling of cell components was chosen as a solution to this problem. Assuming that it was necessary to fill the components completely before stack construction, the matrix and electrodes were exposed to acid for extended periods. After building a few stacks, it was evident that this procedure overfilled the material resulting in large quantitites of acid being squeezed out through the backing during stack compression.

Utilizing the acid pick-up calculations from Task 1 and a few stack builds, a controlled acid addition procedure was established. Combining the controlled acid additions prior to stack building and the controlled start-up conditions developed in Task 1 has resulted in a cost effective build and start procedure.

Prior to building Stack 427, full size electrodes and matrices were successfully tested in other 5-cell stacks which also served to test the prewetting procedures. The performance of the cells, when corrected for internal resistance, approached

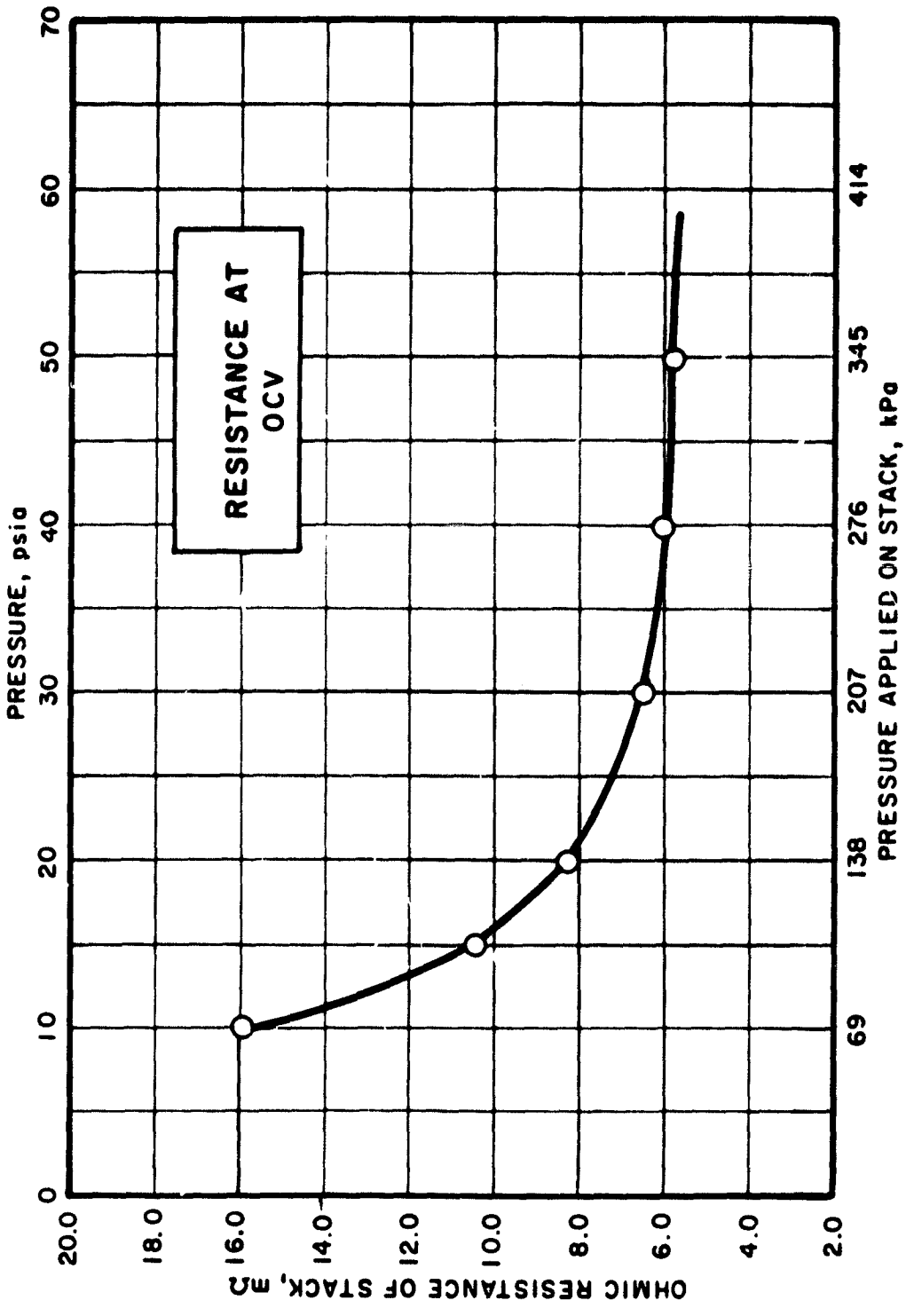

FIGURE 4.4

OHMIC RESISTANCE OF THE STACK AS A FUNCTION OF APPLIED PRESSURE

the values obtained in the small 25 cm^2 laboratory cells. This was considered sufficient qualification for the endurance tests.

Another important parameter in determining cell performance is the uniformity of cell temperature. Typical temperature maps of the 350 cm^2 and 1200 cm^2 cells are shown in Figures 4.5 and 4.6. These profiles are affected by insulation and heat removal processes in addition to preheating of the reactant gases. The performance at each temperature will be somewhat different. Increasing the overall stack temperature will modify the stack performance as indicated by Figure 4.7. These are only illustrative of the performance changes because the exact temperature profile will determine the performance change of any particular stack.

4.3 Off-Design Operating Conditions

The development of the heat-treated plates late in the program significantly increased the cell performance, so that further testing of stacks with nonheat-treated plates was not recommended. Additional variations of operating conditions were postponed until the heat-treated plate stacks were fully qualified.

4.4 Design and Construction Analysis

Modifications in stack design were made during the course of the program. The initial large area plate design did not include acid addition capabilities. This was found to be essential and was added to the plate by modifying the plate mold. This worked exceptionally well with all types of matrices tested.

Current collection was also identified as a weak point in construction. Initially a flat sheet of copper with extended tabs was used. This was changed to a flat sheet and a copper

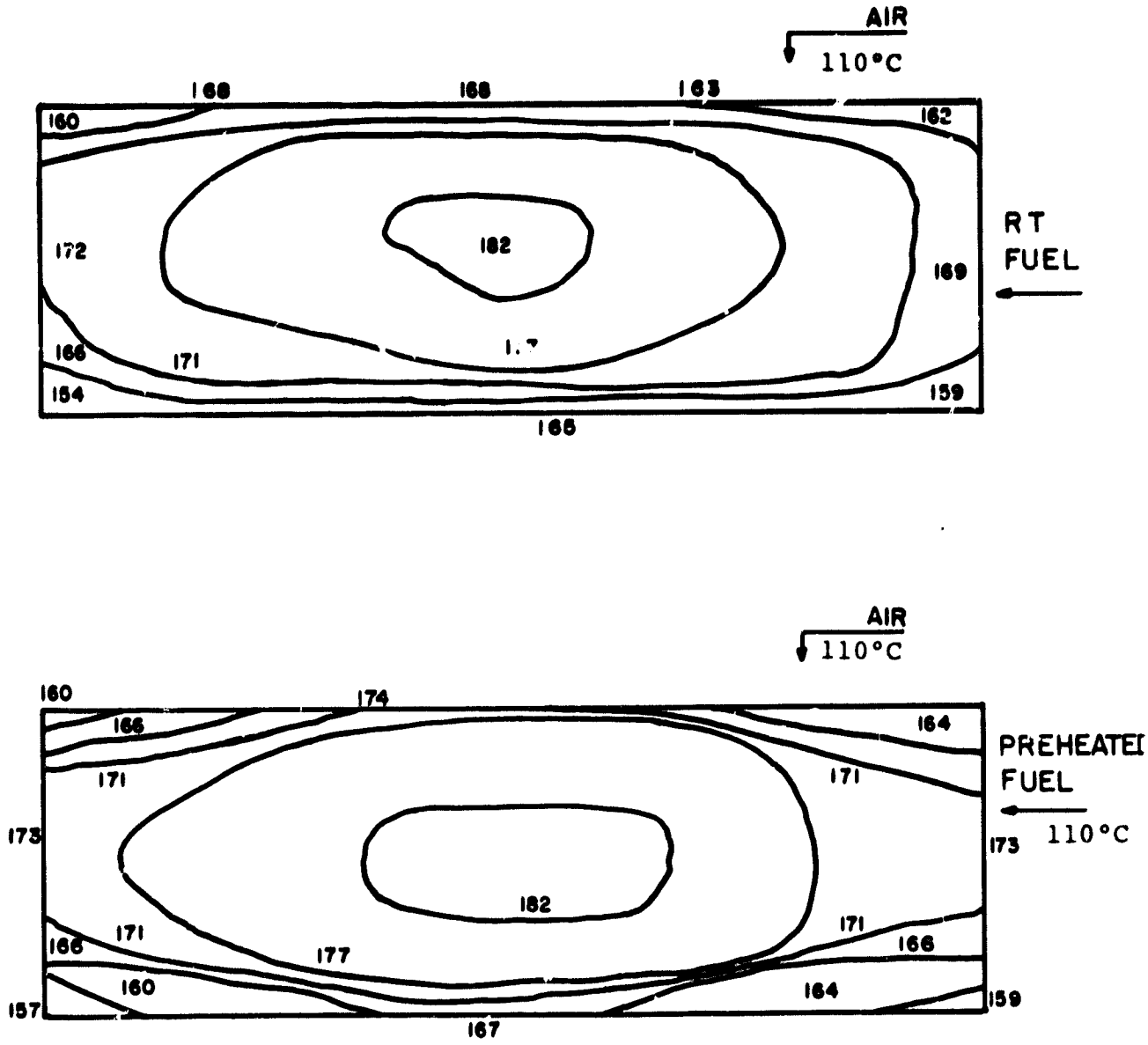

FIGURE 4.5 TEMPERATURE DISTRIBUTION FOR ROOM TEMPERATURE AND PREHEATED H_2 (Stack 381, Cell #2)

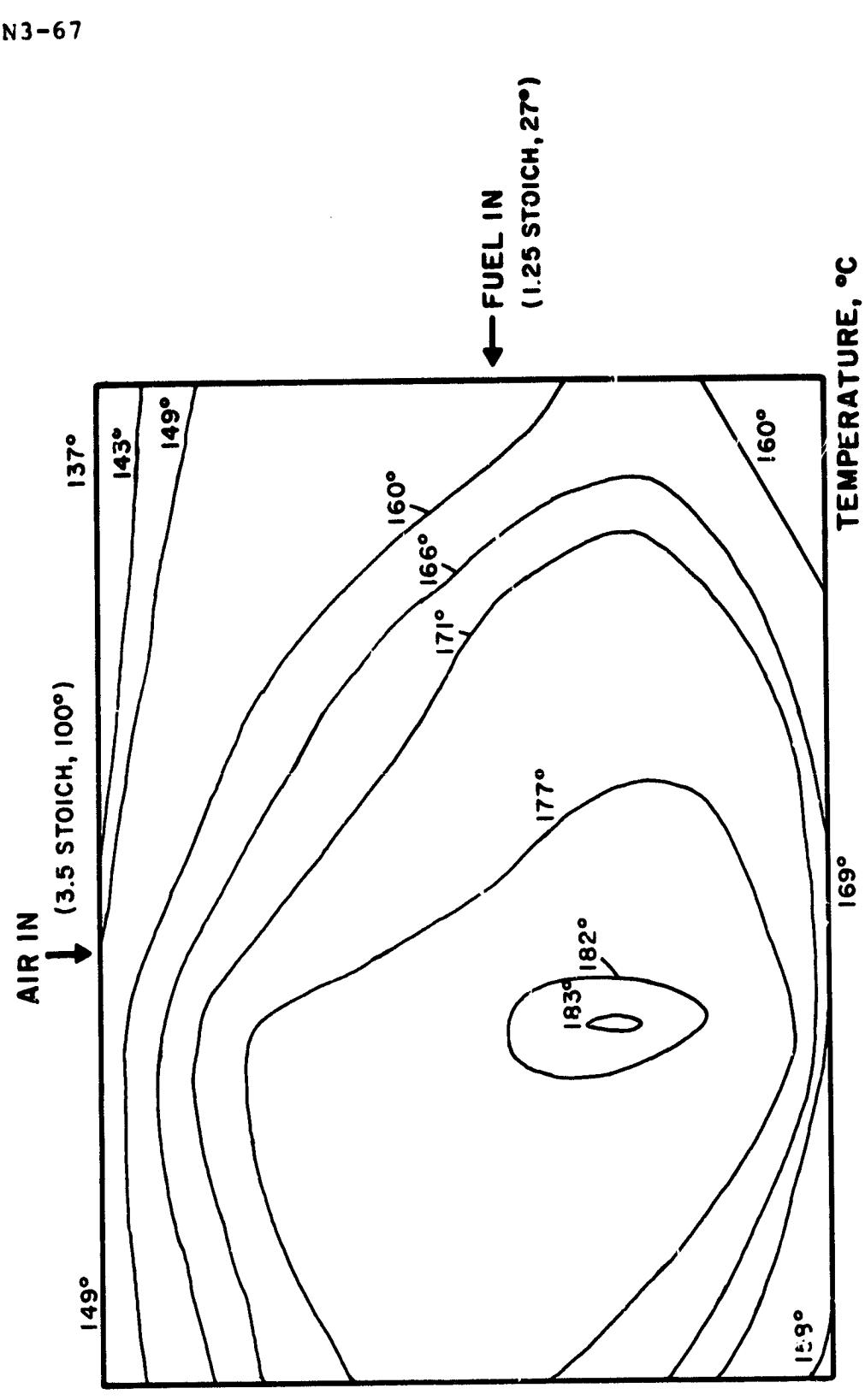

FIGURE 4.6

TEMPERATURE DISTRIBUTION OF CELL NO. 3 IN STACK 405

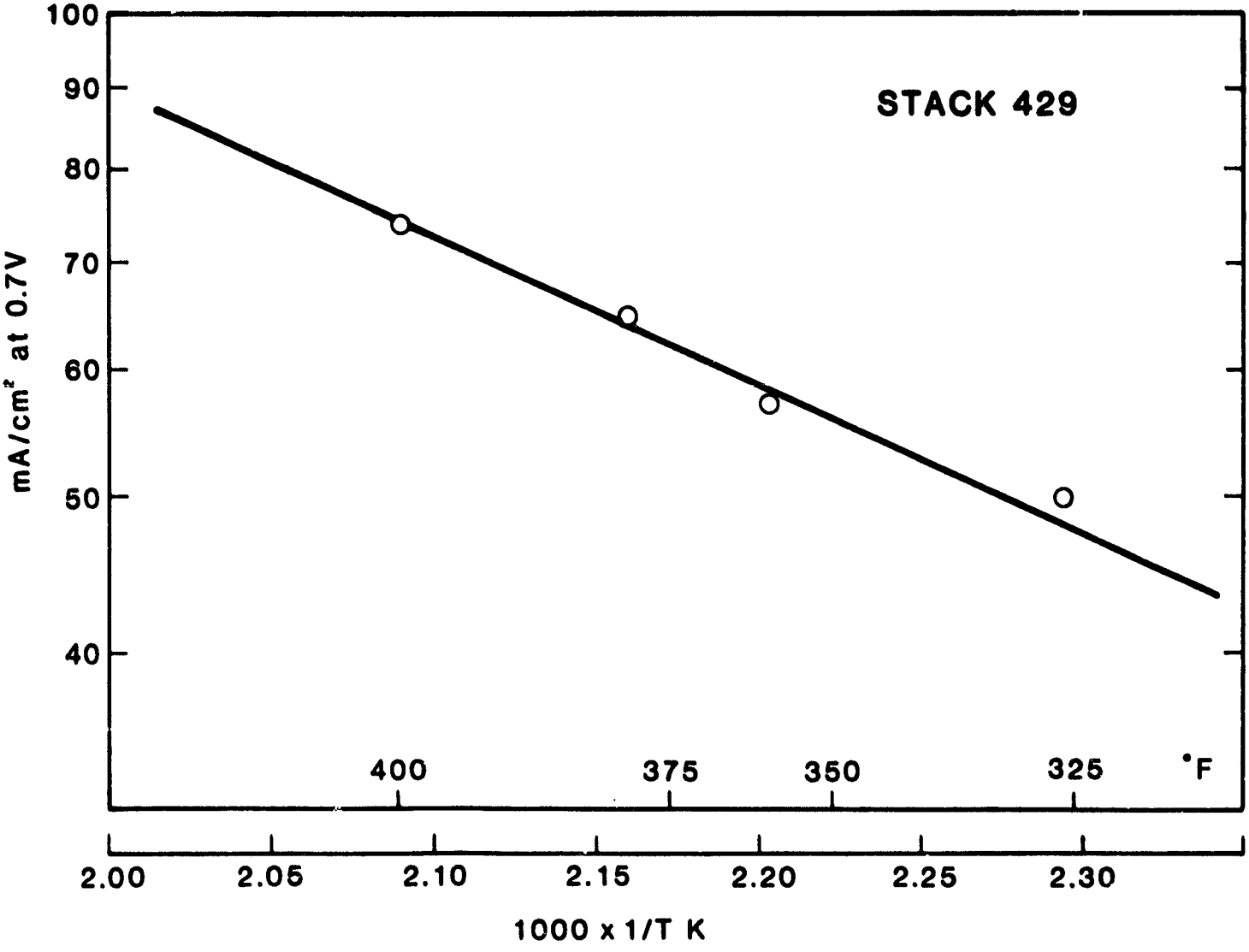

FIGURE 4.7 TEMPERATURE DEPENDENCE OF PERFORMANCE

post which itself was modified as indicated in Figure 4.8. This provided a more reliable contact which could be tightened as desired.

The compression and resistance of stacks were described previously as important parameters. One of the determining factors for this relationship is the edge seal shim thickness. This thickness was decreased to the point where the backing paper was not crushed and the contact resistance was not excessive. All modifications were made prior to starting the 5,000 hour endurance test in Task 3.

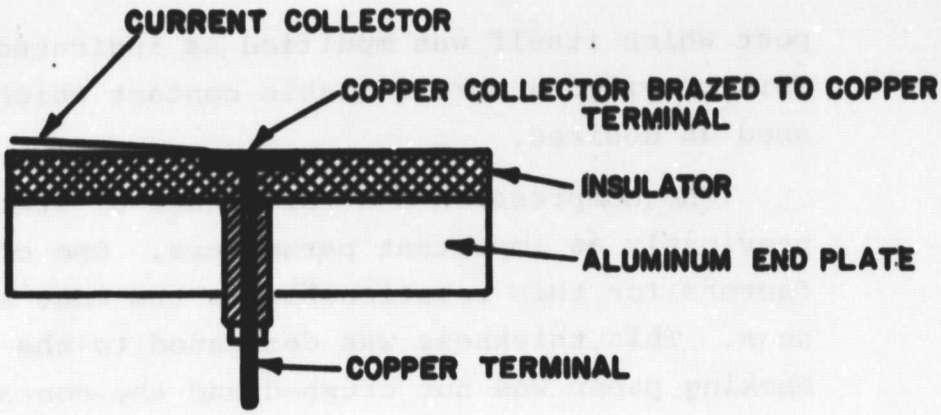

a. initial design

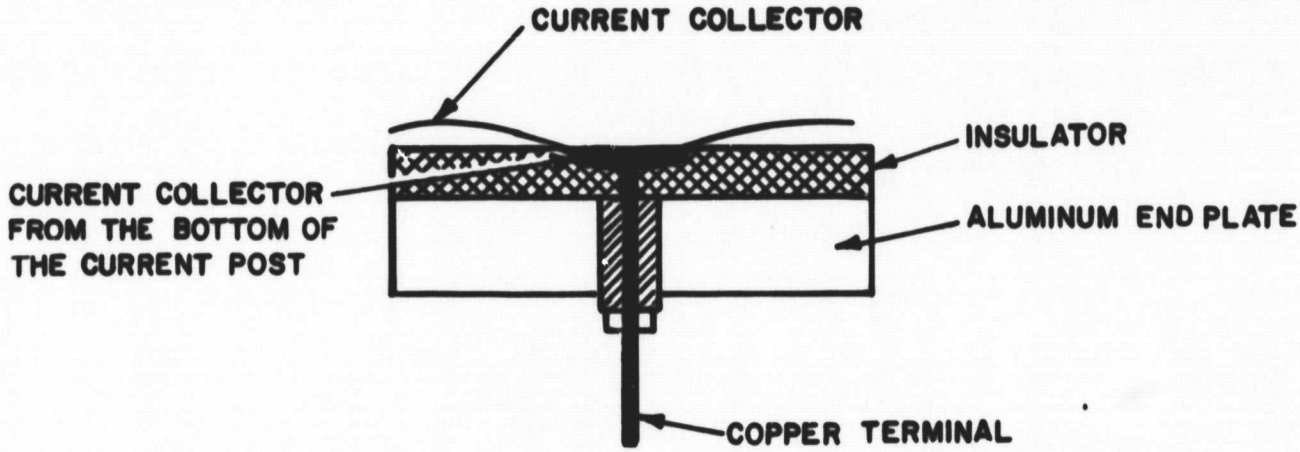

b. modified design

FIGURE 4.8 MODIFICATION OF COPPER TERMINAL DESIGN AT THE CENTER OF THE 1200 cm^2 STACK

TASK 5. LONG STACK TESTING

Stacks containing 23 cells (approximately 2 kW capacity) were used to define assembly procedures and to study the mechanical aspects of operating air cooled (DIGAS) fuel cells. The details of stack compression, seals and manifolds were derived from the 5-cell stacks fabricated under Task 4. The design of the DIGAS cooling plate as shown in Figure 5.1 was obtained from the previous phase of this contract and the assembly procedures were worked out using the 5-cell stacks of Task 4. As the technology of the 5-cell stacks changed and the changes tested, they were incorporated into the 23-cell stacks. Three stacks were built in this manner using the facility built under this contract.

5.1 Test Facility Design and Construction

Two test stands, capable of accommodating 2 kW stacks, were designed and built. Both were built to accommodate a fuel mixture from house supplies and one was equipped with a methane gas reforming system. The schematic diagram in Figure 5.2 shows the general manifolding of a stack and the turning vanes used for gas distribution. Panel layouts for the two test stands are shown in Figures 5.3 and 5.4. Each panel includes controls for anode gas mixing, stack heaters, and air preheaters. Cell voltages and temperatures are individually selected and displayed on a digital meter.

5.2 Stack Assembly Procedures

Figure 5.5 is a photograph of the first 23-cell stack (No. 408) which embodied the technology at the time. The straight tie bars for compression and copper current collectors with tabs were changed later.

The second 23-cell stack (No. 410) was redesigned with

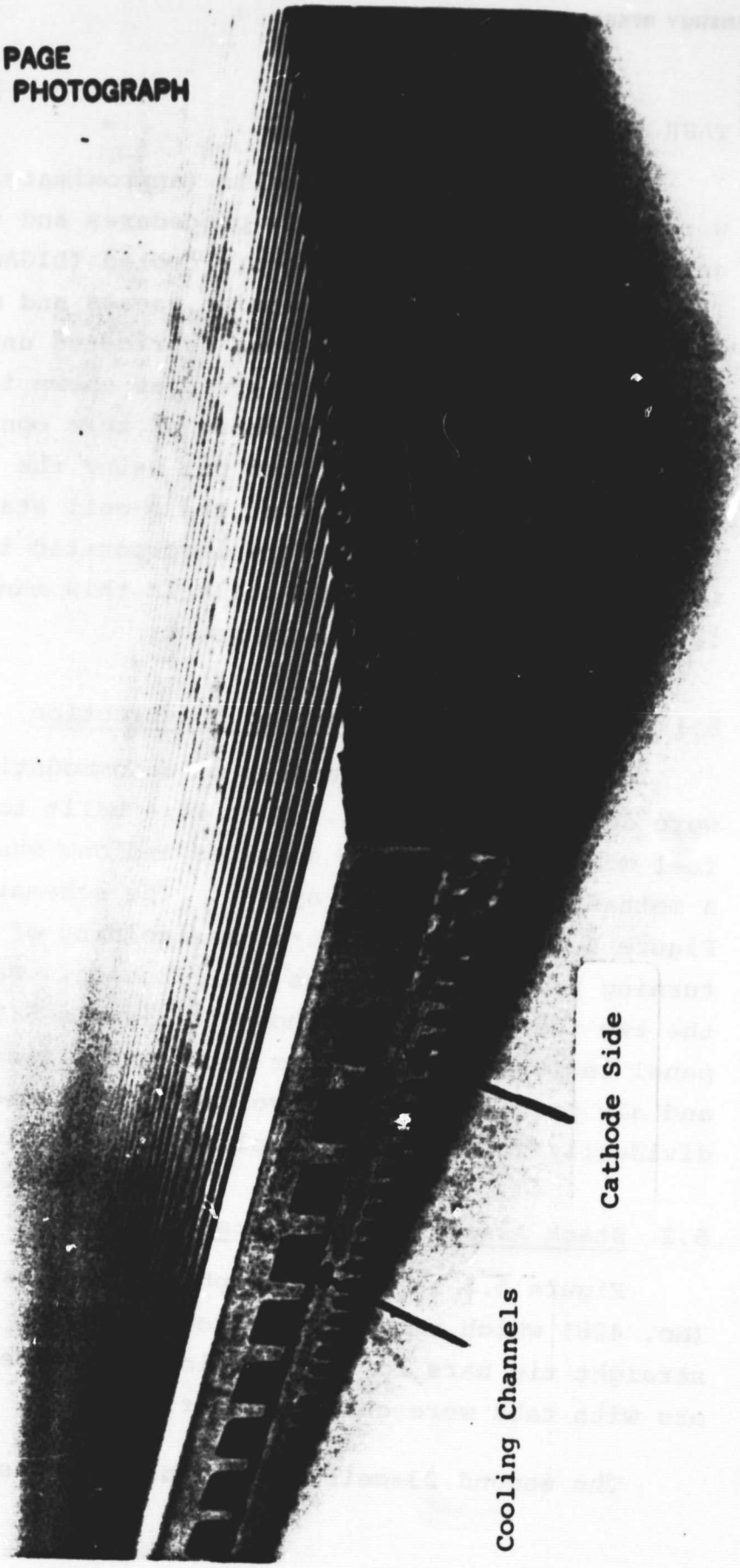

P0152

FIGURE 5.1 SINGLE COOLING PLATE ASSEMBLY OF A 1200 cm^2 STACK

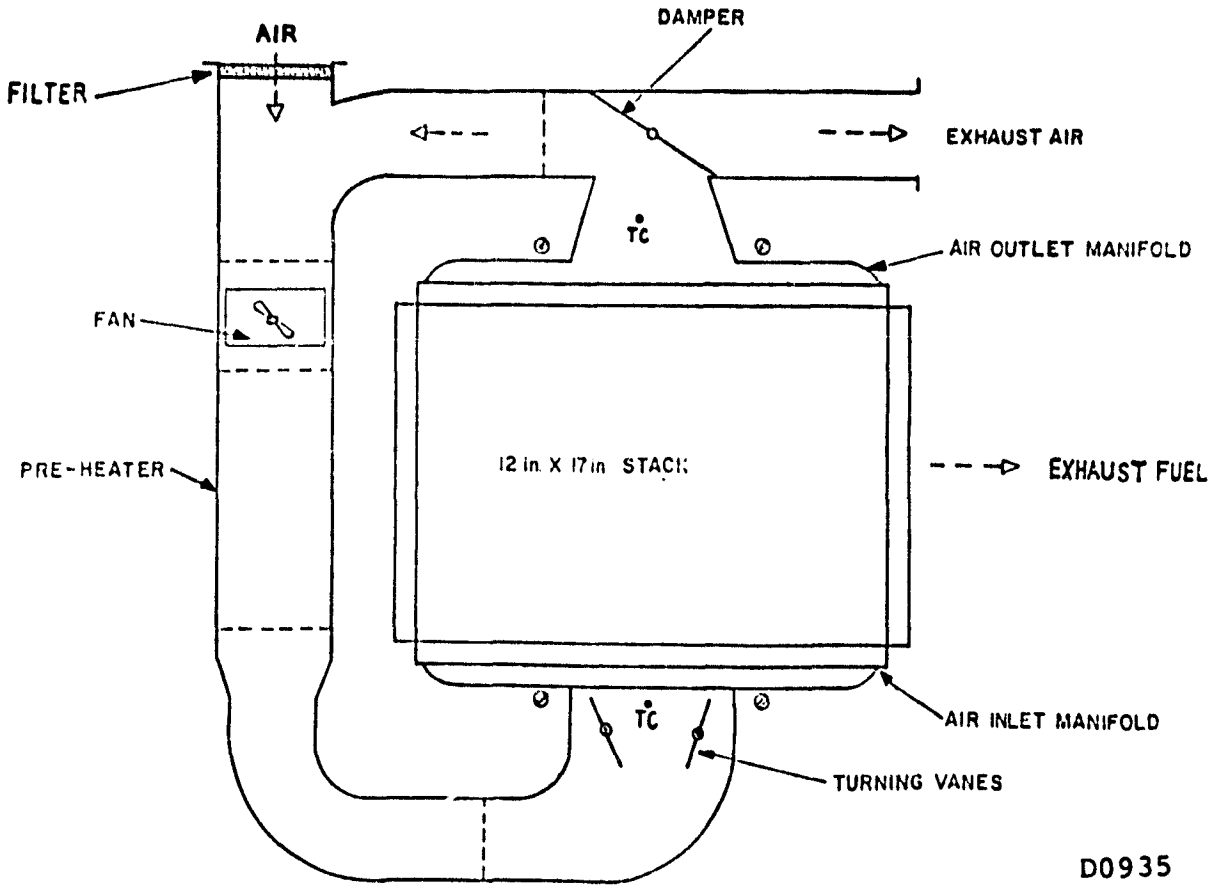

FIGURE 5.2 SCHEMATIC DIAGRAM OF A DIGAS COOLED STACK

ORIGINAL PAGE
BLACK AND WHITE PHOTOGRAPH

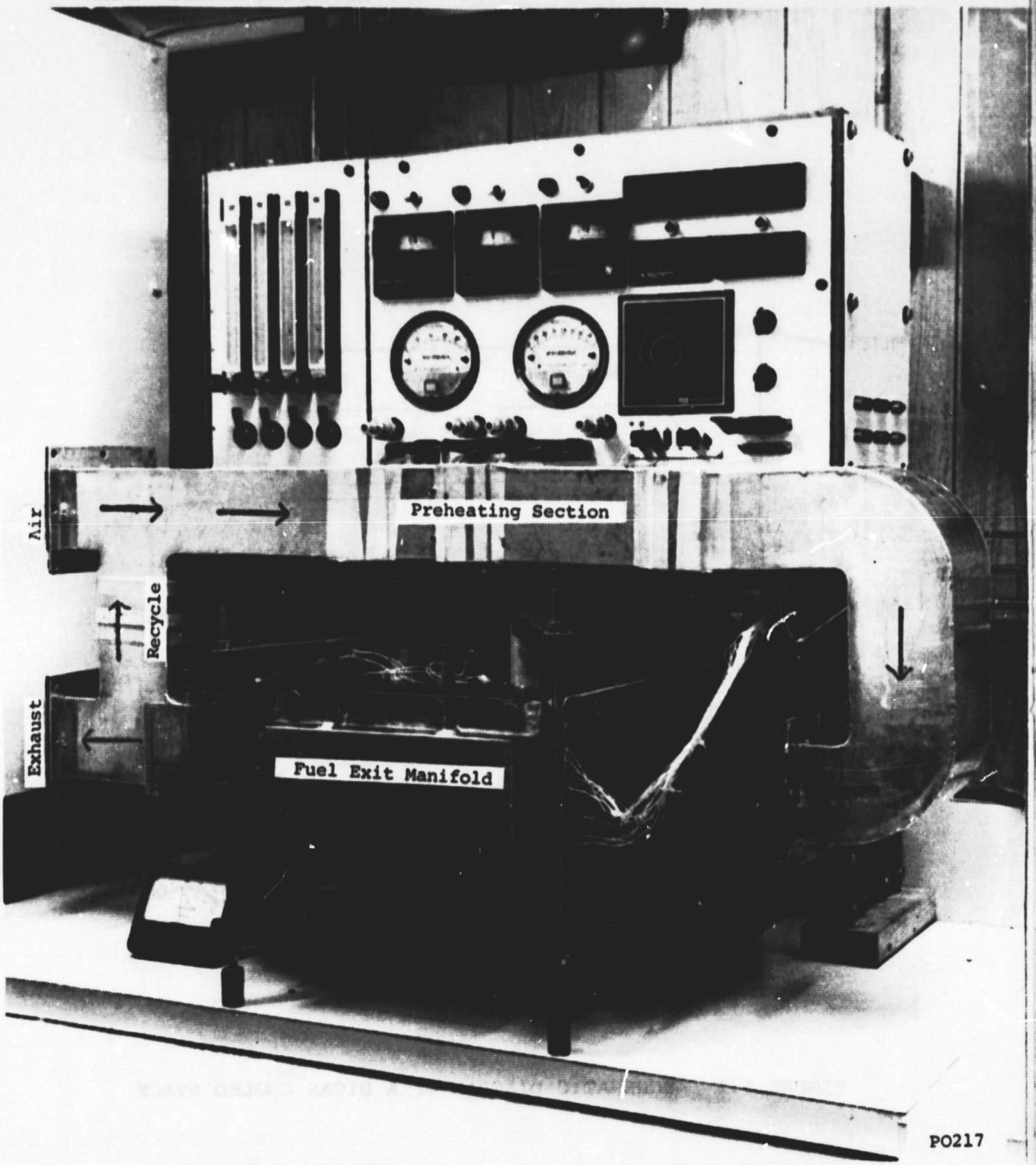

FIGURE 5.3 TWENTY-THREE CELL STACK BEING TESTED

ORIGINAL PAGE
BLACK AND WHITE PHOTOGRAPH

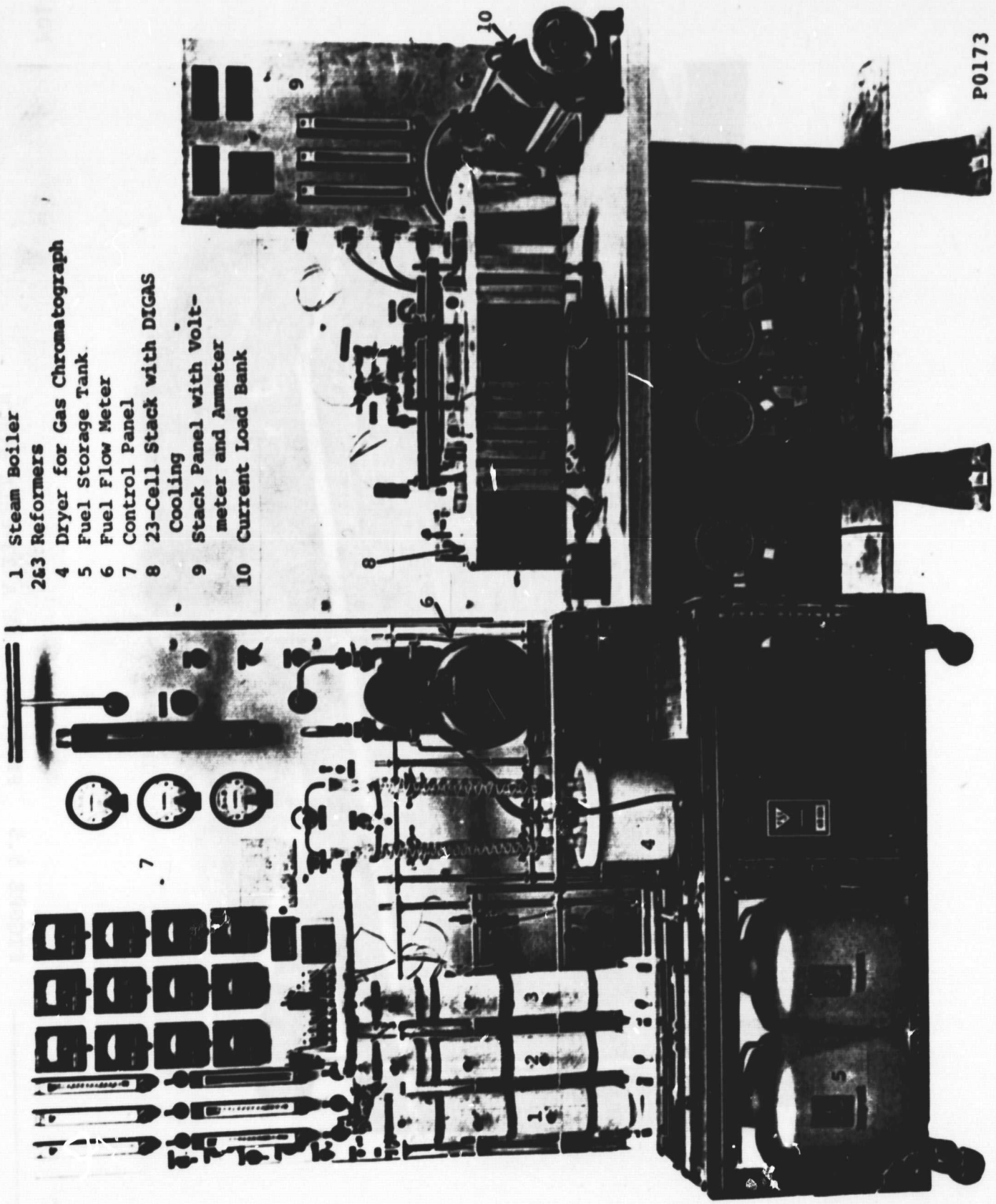

FIGURE 5.4 PHOTOGRAPH OF REFORMER AND 23-CELL STACK

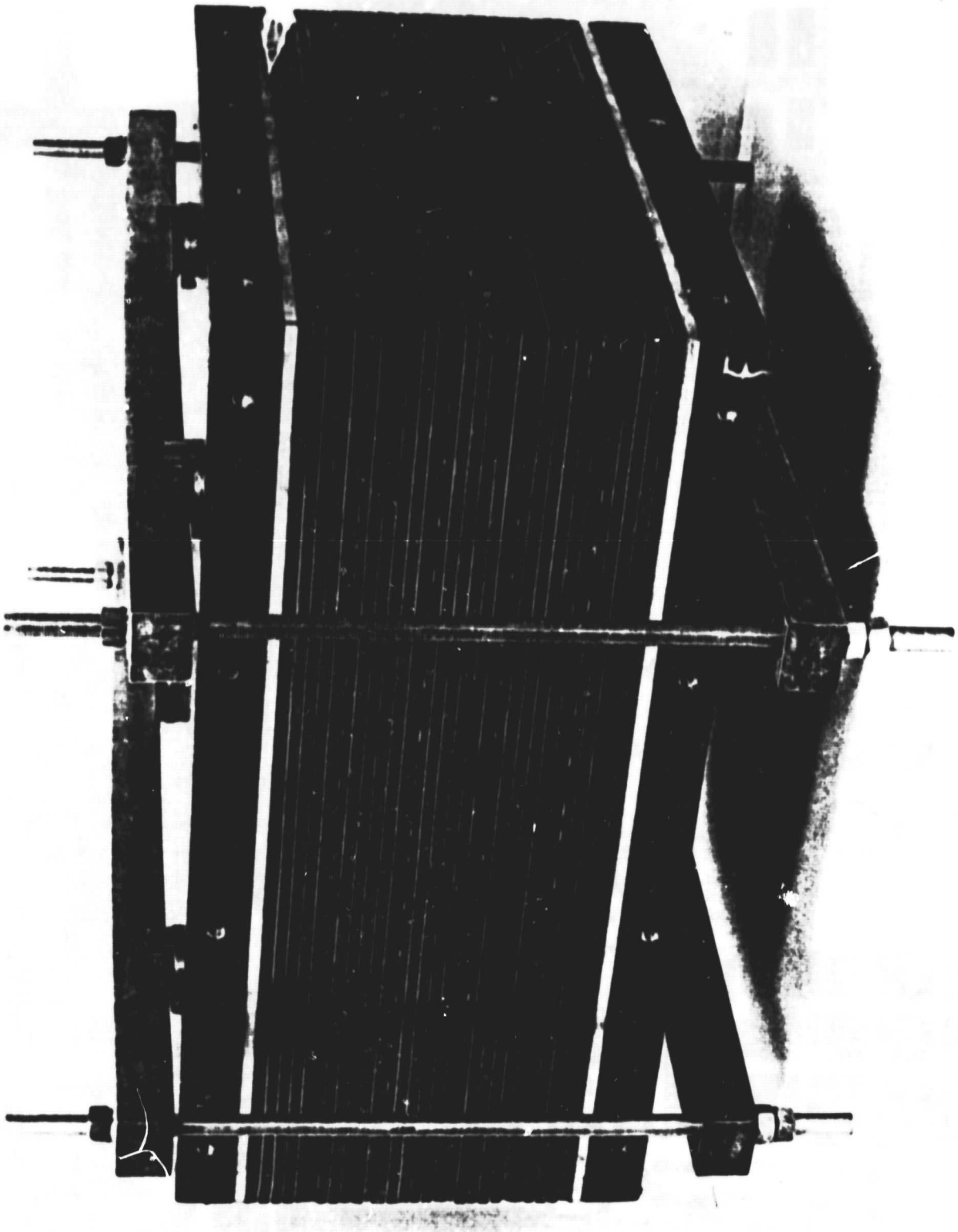

FIGURE 5.5 PHOTOGRAPH OF A 23-CELL STACK

modified compression bars, air ducts and manifolds as indicated in Figure 5.6. The parallel configuration of compression bars used in the first stack limited the air manifold depth and also made installation and removal of the manifold cumbersome.

The modified X-type compression bars allowed extension of the manifold to achieve a uniform air distribution. Air ducts were also redesigned to reduce flow resistance. In Stack 408, the exhaust air was turning 90 degrees immediately upon exiting the stack. The new design allowed an increased air flow rate (up 35%) from 1.34×10^6 to 1.81×10^6 cm^3/min (from 22 to 30 stoich) for the same blower. Recycling of up to 50% exhaust air could be achieved by this change without a significant performance decrease (previously 10% recycle was the maximum).

A specific startup procedure as outlined in Task 1 was instituted to reduce acid expansion in the cells. Prior to this procedure, cells had highly concentrated acid in the electrodes and matrices immediately after assembly. However, once the stack was operated the acid was diluted and eventually a considerable amount of acid expanded out from the cells. The optimal wicking and startup procedures were being pursued at the time of the second stack. Appropriate parameters were chosen and applied to this stack The wicking temperature for the first stack was 125°C and the stack was loaded immediately after OCV measurement at that temperature. This resulted in flooding of acid inside the stack (visual observation after taking manifolds apart). The wicking temperature for the second stack was reduced to 66°C and the stack was loaded at 30A when the temperature reached 150°C. This stack showed no such acid drippage in the manifolds.

The third 2 kW stack employed a procedure in which the components were prewet with acid prior to building. This

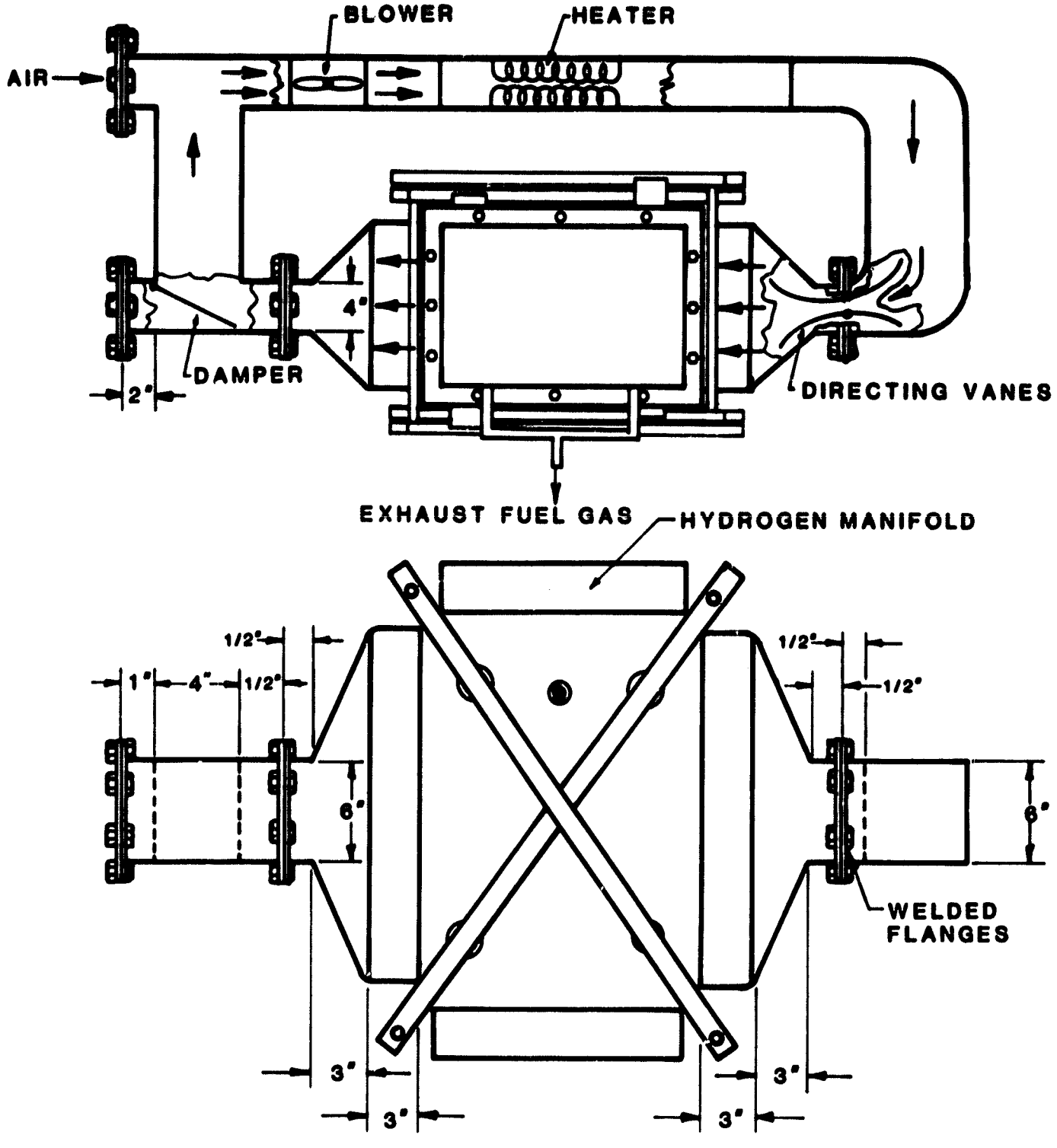

FIGURE 5.6 MODIFIED STACK CONFIGURATION

alleviated the necessity to wick all of the required acid into the stack prior to operation. Several additional features were incorporated in this stack after being tested in 5-cell stacks. It incorporated the MAT-1 matrix, the compression developed in Tasks 3 and 4. An acid fill channel in the bipolar plate provided the possibility of acid addition during operation. A discussion of the performance of this stack is provided in Section 5.3. Overall, the stack performed well for a nonheat-treated bipolar plate stack. The features embodied in this stack were also incorporated in the 5,000 hour 5-cell endurance stacks which performed well for the planned test period and beyond.

5.3 Performance Verification and Testing

At various stages of the technology development, 23-cell stacks were constructed which utilized the best features that had been tested in 5-cell stacks. The first 23-cell stack achieved an average terminal voltage of 0.53V/cell at 162°C and 100 mA/cm^2. The stack resistance was 29 mΩ which was higher than the 20 mΩ anticipated based on 5-cell results. This contributed to the low performance. The average IR-free voltage of 0.68V/cell at 100 mA/cm^2 was typical. Problems with acid inventory control, however, resulted in performance fluctuations. This was overcome in later stacks by providing an acid fill channel in the bipolar plate. This stack, however, did provide a test of the DIGAS concept with ERC molded plates. Temperature profiles and air velocity measurements were used to characterize this stack.

Temperature profiles in the air inlet and outlet of the DIGAS cooled stack showed the average temperature rise for air was 45°C in the cathode channels and 40°C in the cooling channels. The hottest spot (190°C) was observed at the middle section of the air outlet, while outer cells near the compression

plates showed 178°C.

Figure 5.7 shows air flow distributions in cell and cooling channels. The air velocities were measured by an anemometer while running the stack. The air flow appeared to be more uniform in the cooling channels than in the cell channels. This flow nonuniformity was attributed to some channel blockage by acid drops. For this measurement, the total air flow rate was 1918 liters per minute at 118°C (equivalent to 2? stoich air).

Figure 5.8 summarizes ERC testing of the second 23-cell stack (#408). Peak performance at 100 mA/cm^2 was 580 mV/cell. This slowly decreased as the acid in the matrix and electrodes was depleted. Cell running conditions before and after acid depletion are illustrated in Figure 5.8. As the acid is lost, OCV and performance on load drops rapidly. After replenishment of acid, the initial performance was regained. For the third stack, acid wicking channels were built into the bipolar plates to replensih acid while the stack was running.

The air temperature profiles in the stack (refer to Figure 5.9) were uniform and the overall process air and cooling air temperature rise was only 30 to 36°C. The improved temperature gradients on the air side compared to the previous stack (No. 408) are attributed to improved stack manifolding. The fuel side also showed a very uniform temperature distribution.

The third 23-cell (#425) stack ran more that 160 hours with 33 daily stop-starts. Performance increased initially but then decreased as time went on. The stack performance is summarized in Figure 5.10 and Table 5.1. This rise and fall in performance is characteristic of the bipolar plate poisoning identified during this program. It was eliminated by heat-treatment of the bipolar plate. Extrapolating the decreasing voltage portion of the performance curve to zero time gives a voltage of 15.2 V (0.66V/cell). A voltage of 0.68V/cell was achieved

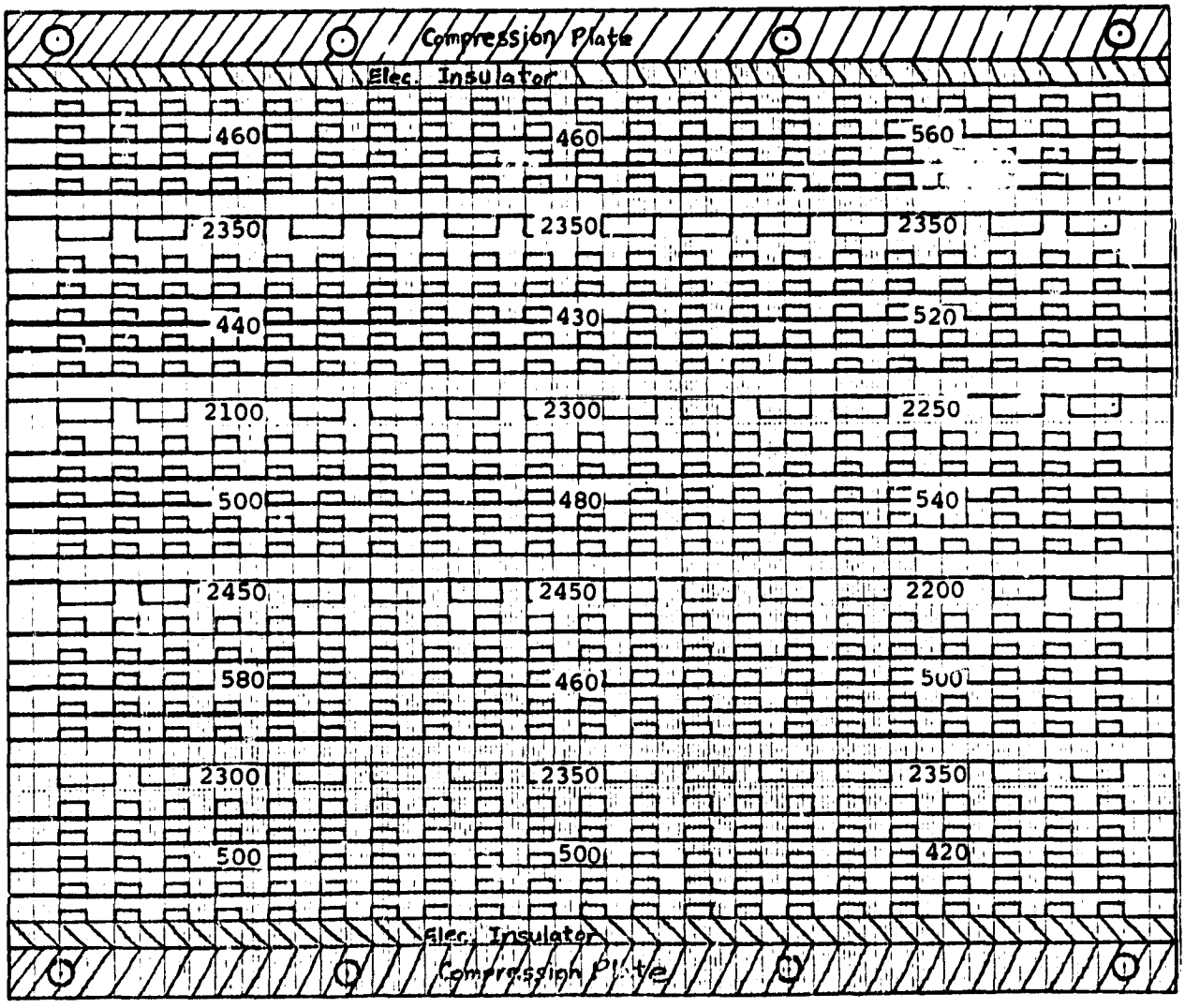

D0934

FIGURE 5.7 AIR VELOCITY DISTRIBUTION THROUGH CELL AND COOLING CHANNELS

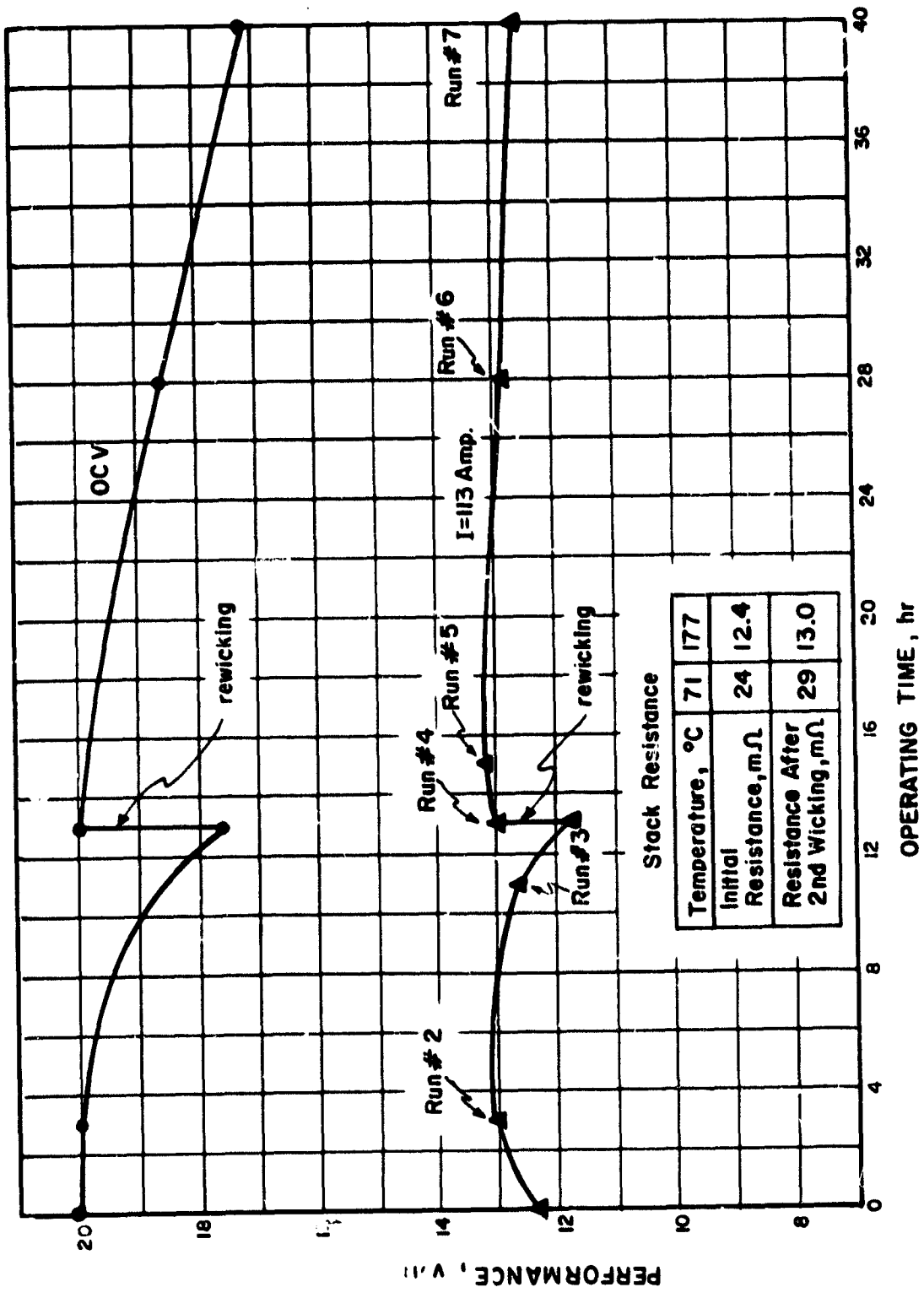

FIGURE 5.8 LIFEGRAPH OF THE SECOND 23-CELL STACK

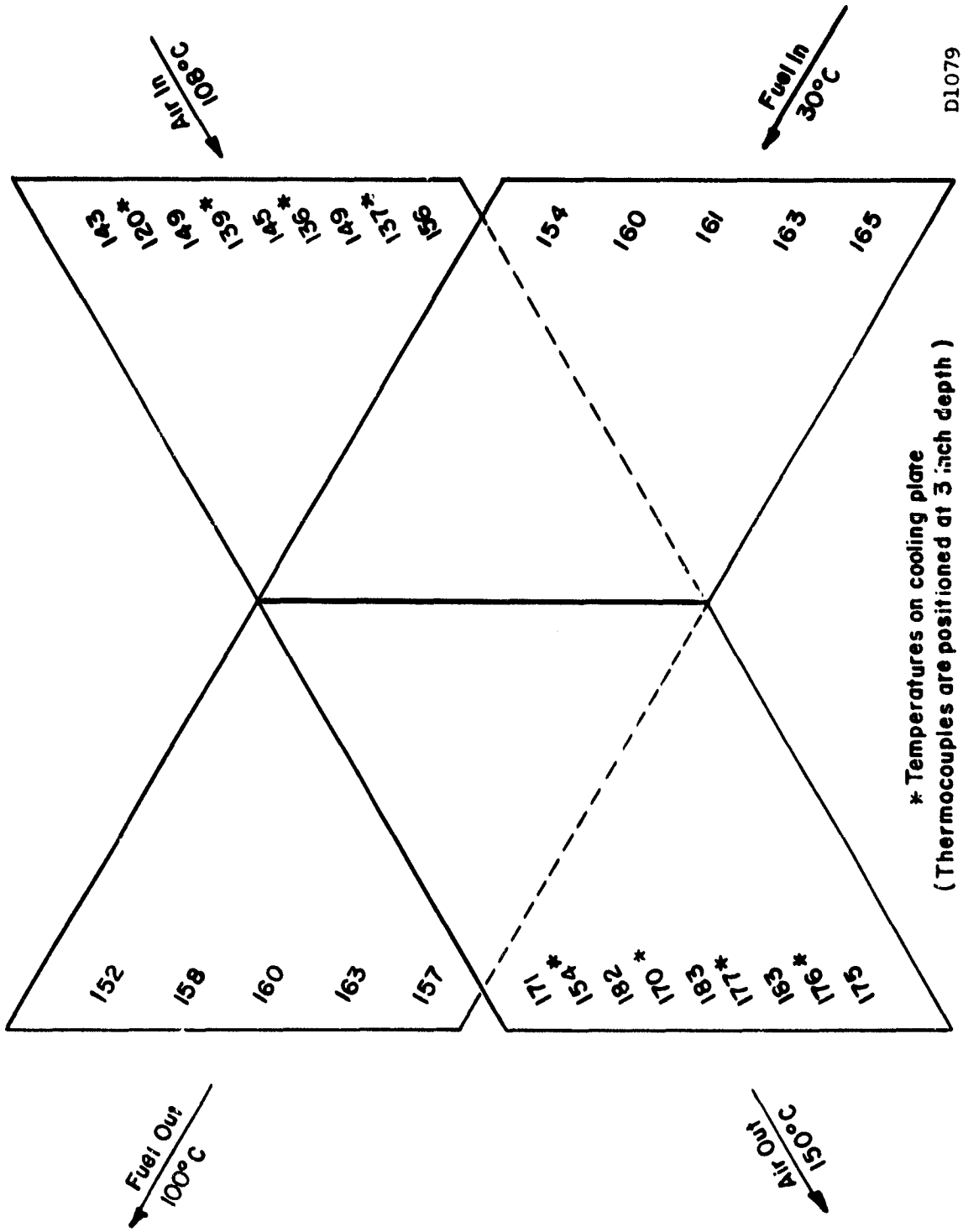

FIGURE 5.9 TEMPERATURE PROFILES ON CENTER PLANES OF THE SECOND STACK (Measured at E = 12.90V and I = 112A)

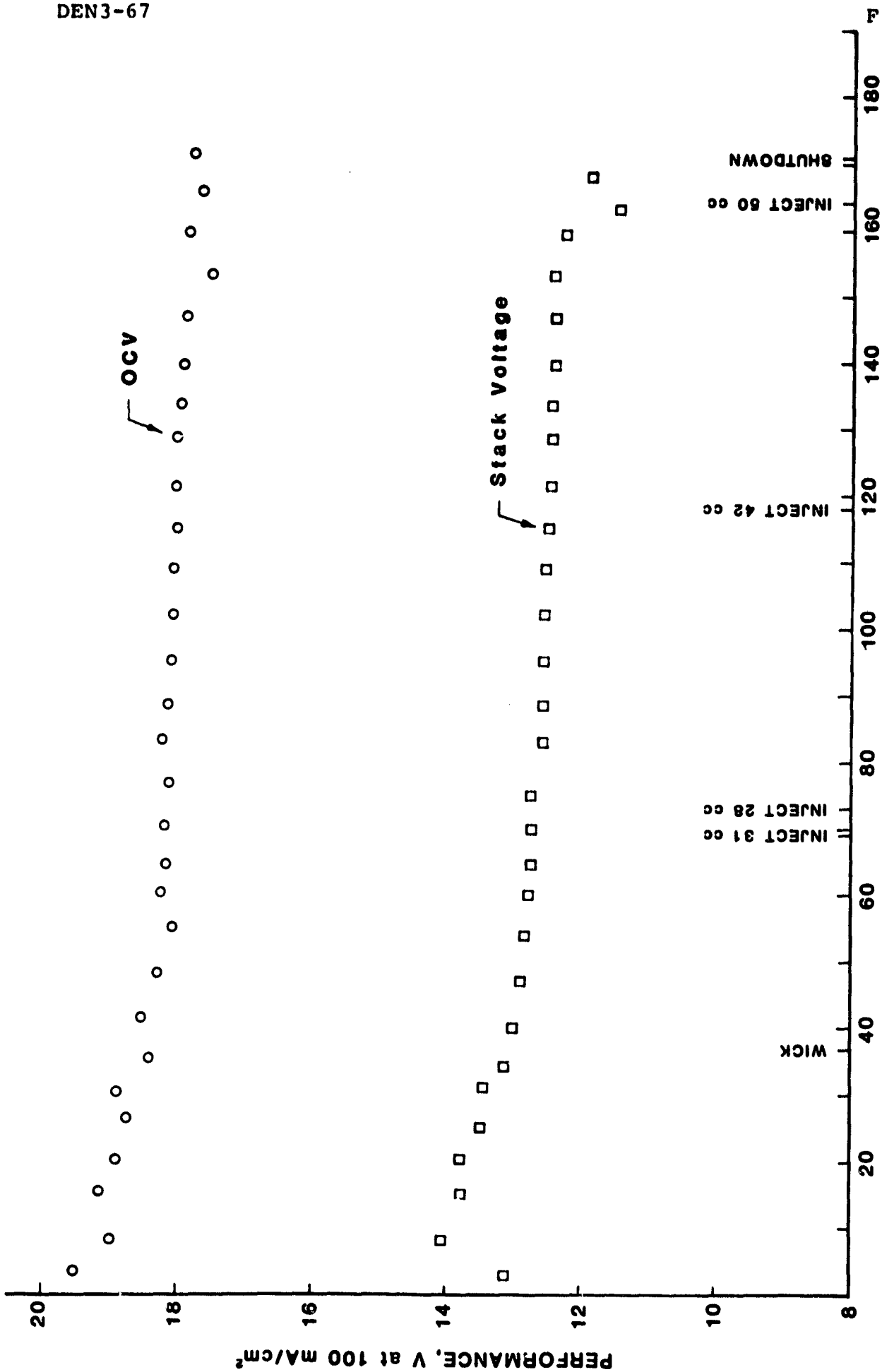

FIGURE 5.10 PERFORMANCE OF THE THIRD 23-CELL STACK

TABLE 5.1 SUMMARY OF INDIVIDUAL CELL PERFORMANCES (STACK NO. 425)

(Daily On/Off Running)

Cell No.	OCV, V		PERFORMANCE @ 100 mA/cm^2, V	
	1st Day	2nd Day	1st Day	2nd Day
1	0.86	0.80	0.56	0.55
2	0.86	0.87	0.58	0.64
3	0.86	0.85	0.58	0.62
4	0.86	0.84	0.57	0.62
5	0.86	0.83	0.57	0.62
6	0.86	0.84	0.57	0.62
7	0.82	0.81	0.58	0.62
8	0.87	0.84	0.58	0.63
9	0.86	0.84	0.58	0.63
10	0.85	0.84	0.55	0.61
11	0.85	0.83	0.54	0.60
12	0.84	0.82	0.56	0.61
13	0.84	0.81	0.57	0.62
14	0.81	0.80	0.54	0.60
15	0.83	0.80	0.57	0.62
16	0.87	0.82	0.58	0.62
17	0.87	0.83	0.58	0.62
18	0.84	0.82	0.57	0.62
19	0.85	0.82	0.59	0.63
20	0.88	0.76	0.58	0.60
21	0.83	0.81	0.58	0.61
22	0.89	0.84	0.58	0.61
23	0.86	0.83	0.56	0.58
Total	19.52	18.95	13.12	14.10

in 5-cell stacks that used the heat-treated bipolar plates.

The steam reformer built during this program was tested for performance with propane and methane fuel at various space velocities. For propane fuel, a space velocity of 355 hr^{-1} showed a trace of unconverted propane in the reformed product at 516°C. Comparison of the experimental product compositions with equilibrium calculations at the reformer exit temperatures showed the reformer was close to equilibrium operation. To produce the hydrogen required for a 23-cell stack, the propane space velocity in the present reactor was 455 hr^{-1} and at this space velocity, a reforming temperature of 649°C was expected for 100% fuel conversion.

Tests with methane also revealed a close approach to equilibrium. When coupled with the 23-cell stack, the voltage drop was consistent with the expected change caused by carbon monoxide. Additional work in this area was deemphasized.

APPENDIX A

SUMMARY OF STACKS BUILT FOR DEN3-67

SUMMARY OF STACK TESTING

STACK NUMBER	TEST PURPOSE	NUMBER OF CELLS	CELL SIZE, in.	HOURS OPERATED (11-17-81)	PEAK PERF., V @ 100 mA/cm²	PEAK OCV, V
346	SiC Matrix	3	5 x 15	145	.620	.787
347	Kynol Matrix	3	5 x 15	4042	.610	.889
348	No Tantalum	3	5 x 15	2780	.591	.833
349	Kynol Matrix	3	5 x 15	7626	.606	.857
350	C Plate with Anode Recess	3	5 x 15	5	.456 @ 20A	.663
351	SiC Matrix	3	5 x 15	2106	.600	.771
352	Kynol Matrix	3	5 x 15	4009	.590	.853
353	Horizontal	3	5 x 15	240	.596	.753
354	Double Kynol Matrix	3	5 x 15	1045	.593	.813
355	High Current Density	3	5 x 15	408	.580	.712
356	High Current Density	3	5 x 15	2068	.620	.751
357	Reamed Electrodes	3	5 x 15	2998	.593	.830
358	Horizontal	3	5 x 15	1404	.610	.810
359	Horizontal	3	5 x 15	96	.576	.737
360	Compression Studies	3	5 x 15	17	.506	.720
361	Compression and Wicking Studies	3	5 x 15	23	.556	.803
362	Dry Room Wick/Std. to T/E Content Test	3	5 x 15	947	.580	.780
363	Wicking	3	5 x 15	3261	.556	.827
364	Compression and Wicking	3	5 x 15	20	.526	.801
365	Compression and Wicking	3	5 x 15	16	.580	.830
366	Endurance	3	5 x 15	2878	.583	.827
367	Endurance	3	5 x 15	1902	.593	.830
368	NC Machining and Gasketing of Plates #1 and #2	3	5 x 15	2977	.583	.837
369	Wicking	3	5 x 15	2313	.590	.840
370	C Plate Assembly	3	5 x 15	174	.580	.850
371	C Plate Assembly	3	5 x 15	66	.603	.863
372	C Plate Assembly	3	5 x 15	87	.603	.880
373	C Plate Assembly	3	5 x 15	44	.593	.873
374	C Plate Assembly	3	5 x 15	76	.612	.868
375	C Plate/Compression	3	5 x 15	6	.597	.873
376	Compression/Resistance	3	5 x 15	4	.571	.877
377	Wet Assembly w/Acid Channel	3	5 x 15	121	.620	.797
378	H_3PO_4 Spread on Matrix	3	5 x 15	29	.606	.877
379	Sheetmold Electrodes	3	5 x 15	8634	.620	.833
380	Endurance	3	5 x 15	9516	.626	.843
381	Wet Assembly	3	5 x 15	3096	.623	.800
382	Matrix Thickness	3	5 x 15	46	.546	.670
383	Endurance	3	5 x 15	68	.500	.850
384	Sheetmold Electrodes	3	5 x 15	2294	.606	.887
385	Endurance	3	5 x 15	1460	.591	.760
386	New Kynol Process	3	5 x 15	277	.510	.846
387	New Current Collectors	3	5 x 15	2112	.600	.830
388	Resintered Electrodes	3	5 x 15	1229	.557	.850
389	Kurahe Backing Paper	3	5 x 15	1392	.573	.867
390	Prefill Components with Higher Conc. Acid	3	5 x 15	1221	.610	.780
391	SiC Coated Sheetmold Electrodes	3	5 x 15	3856	.620	.750
392	FEP Variations in Anode Backing	3	5 x 15	622	.590	.853
393	FEP Variations	3	5 x 15	200	.587	.867
394	FEP Variations	3	5 x 15	571	.600	.860
395	Endurance	3	5 x 15	2427	.590	.860
396	Endurance	3	5 x 15	3726	.603	.880
397	Endurance	3	5 x 15	12	.587	.723
398	Endurance	3	5 x 15	1420	.580	.747
399	Endurance	3	5 x 15	45	.583	.867
600	Endurance	3	5 x 15	4418	.607	.840
601	Endurance	3	5 x 15	6369	.613	.847
602	Endurance	3	5 x 15	10171	.617	.847
603	Endurance	3	5 x 15	10979	.617	.797
604	Endurance	3	5 x 15	1902	.587	.870
605	Endurance	3	5 x 15	7614	.620	.820
606	Reduce Stack Resistance	3	5 x 15	1236	.600	.870
607	Endurance	3	5 x 15	6090	.627	.833
608	Endurance	3	5 x 15	7228	.607	.840
609	Endurance	3	5 x 15	8366	.613	.837
610	Endurance	3	5 x 15	3176	.587	.823
611	Endurance	3	5 x 15	2578	.606	.863
612	Endurance	3	5 x 15	1218	.573	.743
613	Endurance	3	5 x 15	1078	.600	.847
614	Varcum without #50	3	5 x 15	1477	.607	.877
615	Low Bicarb Rolled .5-.6 Cathodes	3	5 x 15	35	.550	.840
616	Endurance/Varcum w/o #50	3	5 x 15	3389	.597	.870
617	25% Colloid	3	5 x 15	2698	.623	.817
618	32% Varcum	3	5 x 15	2710	.610	.786
619	Heat Treated	3	5 x 15 H.T.	6075	.690	.860
620	Heat Treated, AICM	3	5 x 15 H.T.	11635	.683	.870
621	Heat Treated/Low Load	3	5 x 15 H.T.	11921	.656	.810
401	Scale Up	5	12 x 17	26	.570	.818
402	Scale Up	5	12 x 17	140	.572	.880
403	Scale Up	5	12 x 17	151	.536	.912
404	Scale Up	5	12 x 17	253	.558 @ 122A 116A=100 mA/cm²	.797
405	Scale Up	5	12 x 17	490	.579 @ 122A	.911
406	Improved Scale Up	5	12 x 17	1397	.530	.894
407	Acid Channel	5	12 x 17	1243	.590	.900
408	2 kW Technology	23	12 x 17	35	.562	.811
409	Sheetmold Electrode	5	12 x 17	56	.580	.876
410	2 kW Technology	23	12 x 17	55	.572	.867
411	Performance Verification	5	12 x 17	124	.580	.880
412	Sheetmold	5	12 x 17	55	.606	.800
413	Sheetmold/Wet Assembly	5	12 x 17	69	.614	.842
414	C;C; Plates w/Reservoir/3 K Kynol	5	12 x 17	768	.550	.890
415	C;C; Plates/Sheetmold	5	12 x 17	2997	.588	.896
416	C;C; Plates Rolled Electrode	5	12 x 17	2364	.570	.918
417	Anode Backing Single Dip FEP	5	12 x 17	1753	.560	.861
418	Wickability Test	5	12 x 17	(480)	672 @ 24A	.744
419	Wickability Test	2	12 x 17	(432)	No Gases & No Load	
420	Compression Test	5	12 x 17	----	No Gases & No Load	
421	MAT-1 Dry Assembly Wicking Test	5	12 x 17	50	.518	.668
422	MAT-1 Dry Assembly Wicking Test	5	12 x 17	395	.594	.832
423	MAT-1 Wet Assembly, Restart	5	12 x 17	1721/335	.570	.822
424	Sheetmold MAT-1 Pseudo Wet Assembly	5	12 x 17	2695	.546	.904
425	2 kW Technology	23	12 x 17	170	.557	.830
426	MAT-1 Dry Assembly Wicking Test	5	12 x 17	----	No Gases & No Load	
427	MAT-1 w/Holes in Acid Channel Region	5	12 x 17	2159	.622	.888
428	Endurance	5	12 x 17	8594	.618	.804
429	Endurance	5	12 x 17	8699	.584	.824
430	Endurance	5	12 x 17	8615	.634	.880
431	Heat Treated/Endurance	5	12 x 17 H.T.	12420	.680	.900